Numerical simulations of multiple arms star polymer translocation in the presence of constraints

Mesay Tilahun Abebe

Dissertation Submitted to the Graduate Programs
In Partial Fulfillment of the Requirements
For the Degree of Doctor of Philosophy in Physics

College of Natural and Computational Sciences
Department of Physics
Addis Ababa University
Addis Ababa, Ethiopia

Addis Ababa University
School of Graduate Studies
College of Natural and Computational Sciences
Department of Physics

The undersigned hereby certify that they have read and recommend to the School of Graduate Studies for acceptance a thesis entitled "**Numerical simulations of multiple arms star polymer translocation in the presence of constraints**" by **Mesay Tilahun Abebe** in partial fulfillment of the requirements for the degree of **Doctor of Philosophy in Physics**.

Dated: November 2020

Approved by the Examination Committee:

	Name	Signature	Date
Advisor:	Dr. Tatek Yergou	_____	_____
Internal Examiner:	Dr. Lemi Demeyu	_____	_____
External Examiner:	Prof. Mesfin Tsige	_____	_____
Chairman:	Dr. Teshome Senbeta	_____	_____

ADDIS ABABA UNIVERSITY

Date: **November 2020**

Author: **Mesay Tilahun Abebe**

Title: **Numerical simulations of multiple arms star polymer translocation in the presence of constraints**

Department: **Physics**

Degree: **Ph.D.** Convocation: **November** Year: **2020**

Signature of Author

For my families who have unlimited potential but can not attend the higher education

Table of contents

List of Figures

List of Tables

List of publications

A. Journal publications

1. Mesay Tilahun and Yergou B. Yergou, End-pulled translocation of a star polymer out of a confining cylindrical cavity, Macromol. Theory Simul. 2020. Submitted.

2. Mesay Tilahun and Tatek Yergou, A 2D Monte Carlo simulation of three and four arms star polymers. To be submitted.

3. Mesay Tilahun and Tatek Yergou, Unforced translocation of star polymer through a nanopore. To be submitted.

4. Mesay Tilahun and Tatek Yergou, Langevin dynamics simulation of star polymer translocation into a circular nanochannel. To be submitted.

B. Conference talks

1. Investigation of statics and dynamics properties of three and four arms star polymer with a 2D Monte Carlo simulation, Ethiopian Physical Society 11^{th} Annual National Conference, Dire Dawa University, Dire Dawa, Ethiopia, February 2017.

2. Star polymer translocation in the presence of constraint: Langevin dynamics simulation, Ethiopian Physical Society 14^{th} Annual National Conference, Arba Minch University, Arba Minch, Ethiopia, February 2020.

C. Posters

1. Driven translocation of a star polymer from a confined cylindrical cavity with a finite volume, American Physical Society March Meeting, Los Angeles, California, USA, March 2018.

2. Effects of the functionality on the dynamics of multiple arms star polymer translocation under a pulling force, XXXI International Union for Pure and Applied Physics (IUPAP) International Conference on Computational Physics, The Chinese University of Hong Kong, Hong Kong SAR, July 2019.

3. Multiple arms star polymer translocation from a cylindrical cavity subject to a pulling force, American Physical Society March Meeting, Denver, Colorado, USA, March 2020.

Acknowledgments

On the way to perform this research paper, I have received much encouragement and support from different people. Above all, I would be happy to praise my Almighty God, who enabled me to succeed in my work. I am hugely thankful to my advisor, Dr. Tatek Yergou, who gave an opportunity of graduate study under him, for his constructive advice and critical comments all the time of this work. And my sincerest thanks go to Dr. Mulugeta Bekele and Dr. Lemi Demeyu for their insightful comments during the period of Ph.D. progress reports.

I am most grateful to my wife, Ema, and sweet daughter, Edil, for their endless wishes to my success, and extensive moral throughout my study and my son (Keab) for the happiness, he has brought us. I would express my appreciation to my family, Iya, Mignote, Abayo, Father, Abu, Dil, Ayich, Mabi, Mito, Emu, Mimi, Kecho, and Bish for their contribution and supports to my work. Special thanks also extend to my colleagues Mehari Bayou and Andualem Zenebe, who are sharing their experience in computational skills.

My indebted thanks also go to the statistical and computational physics groups, particularly Fikre Jida and Seyfan Kelil, all staffs members of Addis Ababa Science and Technology University (AASTU) Physics Department, Marcos or Tikusus Group, Sholas or Molachaws Group, and all other staff members of the School of Indiana (SOI), especially Mr. Anteneh Getachew (vice manager of SOI) and Mr. Zelalem Tesfaye (manager of SOI), for their valuable encouragement.

Finally, I would like to thank the International Science Program (ISP), Uppsala University, Sweden, for providing work station computer facilities to perform our simulation tasks and funding to attend an international conference and Addis Ababa University for allocating the research budgets. Also, I want to thank AASTU for covering the sponsorship expenses to pursuing my study.

Abstract

Star polymers are branched macromolecules that each f-linear polymeric arms emerging radially from or chemically connected to the branching point, and which can itself be polymeric. Using an efficient algorithm of Monte Carlo (MC) and Langevin Dynamics (LD) simulations, we study the dynamics of star polymers translocation in the presence of constraints. In this work, star polymers are modeled by a coarse-grained approach, that is, a bead-spring model in which polymers are treated at the monomer level rather than at the atomic level. By carrying out extensive simulation in terms of different parameters such as star polymer functionality, the total mass of the chain, the magnitude of the pulling force, and dimensions of the constraints, we provide an in-depth description of the translocation process. Our simulations were done by using the molecular dynamics package ESPResSo, an extensible simulation package for research on soft matter.

In the first part of the dissertation, we carried out a two-dimensional (2D) MC simulation of three and four arms star polymers. We have considered two different cases: one is the free diffusion of star polymers without using constraints, and the other is the unforced translocation of the polymer through a nanopore where the common point is initially located at the center of the pore. These tasks are done with computer simulation using the bond fluctuation algorithm. In the first case, we determine both the radius of gyration and the self-diffusion coefficient. The mean radius of gyration exhibits a power scaling dependence on the total number of monomers, N, and functionality, where the

exponent is found to be nearly 0.75. We also find that the self-diffusion coefficient, D, displays a scaling relation in terms of N as $D \sim N^{-1}$, corresponding to the Rouse-type model. As a second case, we analyze the kinetics of star-branched polymers translocation in the absence of a driving force, focusing on the influence of N upon the translocation time, τ. Our simulation results satisfy the scaling law $\tau \sim N^{\alpha}$ with the scaling exponent $\alpha = 1 + 2\nu$, where $\nu \equiv \nu_{2D} = 0.75$ is the Flory exponent in 2D.

In the second part of the dissertation, the unforced translocation of star polymers through a nanopore has been studied using a three-dimensional (3D) LD simulation, in which case, the central bead is initially placed just inside the pore. Star polymers of various functionalities are considered with the total mass of the chain kept constant. In the absence of a nanopore, the gyration radius of star polymers in terms of f is evaluated. We observe that the gyration radius, R_g, decreases systematically as the functionality increases. Our results also confirm the scaling law $R_g f^{-1/2} \sim (N f^{-1/2})^{\nu}$, where the Flory scaling exponent is $\nu \equiv \nu_{3D} = 0.6$ in 3D. Here the results of the average exit time distributions display narrow, highly peaked, and symmetric profiles for smaller f; whereas, the distributions become wider and asymmetric with a long tail when f increases. Moreover, the impact of both the system temperature and coefficient of friction on the translocation dynamics is presented.

Besides, the dynamics of forced translocation of star-shaped polymers into a circular nano-scaled pore is investigated via a 3D Langevin Dynamics approach. For forced translocation, the branched-chain is initially placed in an open volume, and also the end monomer of the leading arm is located inside a nanopore. The magnitude of a pulling force, F, is applied directly at the end of the chain, which considerably affects the process of translocation. Such a single-force setup mimics typical experimental situations in a new sequencing technique based on a combination of magnetic and optical tweezers for controlling the DNA motion. The effect of star's functionality upon the translocation time

with constant molecular weight has been investigated for a given nanopore diameter. We reveal that the dependence of mean exit time on the number of arms is non-monotonic. The minimum mean escape time is also obtained at $f = 5$. Further, we explore the scaling predictions of the polymer mass and the pulling force for various channel lengths, L, with $L/N < 1$. In the limit of a strong driving force, the escape time illustrates a power-law behavior as a function of N. In this regime, the scaling exponent for $\tau \sim N^{\alpha}$ is $\alpha = 2$. Our results also verify that the exit time decays with the pulling force as $\tau \sim F^{-1}$.

Furthermore, a 3D Langevin Dynamics computer simulation is used to investigate the dynamics of star polymer translocation out of a confined cylindrical cavity, where the cylinder is connected to the wall with a circular nanopore along the tube axis. The translocation is performed by applying an external pulling force that is exerted only on the first monomer of the leading arm. In the present study, we have considered star polymers of different masses and functionalities. In this context, it is quite interesting to understand the role of the polymer's functionality with constant mass but varying functionality. We find that the exit time first decreases with f until a critical functionality f_c, and then increases with f. We have also found that the translocation dynamics are significantly affected by the pore radius. For larger pores, the translocation time decreases as f increases, while for smaller pores, the exit time shows non-monotonic features with a minimum value closer to f_c. On the other side, our results display a scaling behavior $\tau \sim N^2$ under a strong pulling force, but $\tau \sim F^{-1}$ for a given N. Besides, we examine the variations of τ on the tube dimensions, as well as the aspect ratio, a, defined to be the ratio of the tube length to cavity diameter. These outcomes do not confirm the scaling law dependence in the regime of a strong driving force.

Chapter 1

General introduction

Polymers are the most vital group of materials. Polymer molecules comprise of several atoms connected by bonds (that is, covalent), which results in the level of macromolecules [1]. Polymers are found in nature and also synthesized in laboratories and industries around the world. Polymers that are naturally found in nature are known as biopolymers. They can be grouped into three, including nucleic acids, proteins, and carbohydrates (polysaccharides). These biopolymers have monomeric units, such as nucleotides, amino acids, and simple sugars (monosaccharides), respectively. The above three categories of biopolymers are all crucial in various biological processes. DNA and RNA are excellent examples of biopolymers of nucleic acids. DNA is responsible for the storage of genetic code, and RNA is responsible for the translation of genetic information into proteins. A specific example of a carbohydrate biopolymer is cellulose. It is used as the structural constitutes of cell walls.

Engineering polymers, however, are usually synthetic polymers. Currently, one of the rapidly growing polymeric materials in the industries is plastics. Also, the macromolecular structure of artificial polymers gives biocompatibility and enables them to perform various biomimetic works that cannot be done by other synthetic polymers, including drug delivery, use as grafts for arteries and veins, and use in articial tendons, ligaments, and joints [1].

Regarding the general kinds of polymerization processes used to build polymers, on

their conformation and characteristics, there are different possible kinds of polymers. Usually, the difference in polymers features comes from how the atoms and chains are linked together in space. Recent advances in polymerization and efficient coupling techniques have enabled the simple synthesis of complex polymer conformations with controlled dimensions and the number of arms [2]. For instance, star-shaped polymers comprise many linear chains joined at a common origin with numerous chain-end arms. Hence star polymers resemble more closely the hard-sphere approach instead of linear polymers, especially when their functionality increases. Consequently, molecules with spherical shapes are expected to have smaller hydrodynamic volumes and radius of gyration, which leads to a lower viscosity.

The main feature of star-shaped polymers, differentiating them from the linear analogs of identical masses, is their compact structure and the multiple functionalities that are useful for many applications in life sciences and nanotechnologies. Owing to this attribute imparts for the use in viscosity index modiers, coating materials, adhesives, and occulating systems, motor oil additives, dispersants, potential drug delivery agents, thermoplastic elastomers, surfactants, and lubricants [1–5]. Because of some star-shaped polymers are non-toxic, they have prospects in monitored release applications (large numbers of functional groups in a considerably small volume could be used to immobilize enzymes). Besides, the latest gel-like star polymer has promising values in deposing cholesterol and providing medication to tumors [5].

Since the hopeful contributions and its vital role in biological processes to sequencing and diagnostic technologies, the study of polymer propagation across a pore or channel has stayed an active topic for the last couple of decades [6]. The translocation of polymeric materials via a nanometric pore or channel is of substantial relevance to several biological phenomena. These events include DNA and RNA translocation via nuclear pores, protein transport across membrane channels, DNA packaging into viral capsids, gene swapping,

viral DNA injection into host cells, and the uptake of specific oligonucleotides by membrane proteins [6–16]. The polymer translocation is also vital in technological utilizations, such as fast DNA sequencing, gene treatment, and monitored drug delivery [16].

Most of the previous studies have been focused on the translocation of linear polymers through pores or channels. In contrast, the translocation mechanism of polymers with star topology has been observed in fewer studies. Under strong constraint, the topology of polymer plays a notable role in its physical features. For instance, human astrovirus is a source of diarrhea, which has a peculiar star-shaped appearance [16]. Biological star polymers made of DNA also exist, particularly three-arms and four-arms. Currently, synthetic star polymers with a specified number of arms have also been manufactured [17]. Recent experiments by H. Ge *et al.* on the ultra-filtration of star-branched polymers of various functionalities and arm lengths revealed that the rate of critical flow considerably depends on the total number of arms and the forwarding arms across the channel during the translocation process [18]. For such applications where the translocation is in a free open volume through a pore or channel, it may be desirable to control the range of conformations accessible to the polymer at the start of translocation. For instance, it has been suggested that the technology-limiting wide distribution of translocation times generally observed for DNA is very large due to the initial arrangement of DNA conformations [19]. Thus, the transport of polymers through a nanopore from a confining cavity also has an impressive contribution to diagnostic and sequencing technology [19].

Most importantly, the impacts of confinement are investigated by finding relationships and dependencies among system characteristics and the degree as well as the type of confinement. Knowing the influences that confinement has on polymeric materials and how the properties change with the kind of confinement is an essential task to accomplish. The motivation behind examining polymeric confinement is that both natural and artificial polymers are usually directed to this confinement. Also, several examples of restricted polymers are of biological importance. Some relevant applications of this research into

confined polymers include single DNA molecule manipulations in nanostructures [20], DNA translocation through nano-scaled pores [21,22], chromosome organization and segregation in bacteria [23], and viral capsids for DNA packaging [24]. Moreover, star-shaped polymers have been applied to eukaryotic cells for mitochondrial DNA [25].

Apart from studying how confinement affects the properties of the polymeric materials, we can be considered the dynamics of the polymer systems. The observation of the change of a given system characteristic with time is called dynamics. Therefore, understanding the basic principle of dynamics is quite significant because it provides a concept of how constraint affects the polymer and also how the system evolves with time. A dynamics calculation is done by calculating the property of interest at even time intervals over a range of time. The relaxation or unfolding time is the most common parameter that can be measured in the event of confined polymers. When a polymer is subject to strong confinement, the polymer can form a fold or bend. Such a polymer arrangement can be considered as entropically unfavorable in contrast to a relaxed elongated conformation. Entropy is related to the number of accessible arrangements for the polymer. The unrelaxed (folded) polymer has less available arrangements than a relaxed (unfolded) polymer, which implies the folded polymer attains a lower system disorder than the unfolded polymer. Since a system will always evolve in a direction that increases entropy, the folded polymer configuration in unfavorable, and the system will naturally evolve to the unfolded state. Unfolding is defined as the transition from a folded structure to a relaxed one. As a result, unfolding time is the time it requires the polymeric material to relax.

In addition to the biological and technological importance, polymer translocation is of significant concern in polymer sciences, namely, physics and chemistry [26]. To permits the motion of polymer into a pore, which is considerably smaller than its size (or radius of gyration), the chain has to consider an elongated structure, that is to say, entropically unfavorable. A localized driving force can be observed in different ways since the entropic barrier enforced by a restricted region is commonly occurred [27]. Hence, the

most common types of translocation processes can be called as pore-driven, end-pulled, and unbiased setups [28]. The pore-driven translocation is facilitated by applying an electric field or the potential difference bias among the two terminals of the layer, which takes action on the beads in the middle of the pore. Translocation of polymeric materials via a pore subject to an electric field is implemented to a cheaper analytical instrument that we call gel electrophoresis. It is employed for identifying and separating polymers according to their structure [17]. As for the second type, end-pulled translocation, the polymer is driven across a pore under an external pulling force that acts only on the end monomer (found in the middle of a pore). Translocation of polymers under such a force has been proposed to reduce and manage the propagation process, which is essential for the suitable identication of the nucleotides (monomeric units of the nucleic acid) in DNA sequencing [28, 29]. In the operation of single molecules, the movement of polymer is usually managed by optical tweezers [28, 29]. This idea gives the reason to investigate the translocation in which the first bead only encounters a pulling force. Besides, new sequencing procedures based on the integration of magnetic and optical tweezers for managing DNA transport has been notified. Therefore it's of noticeable concern to theoretically examine the polymer translocation with the aid of a pulling force [29]. In the last case (unbiased or natural translocation), the central monomer is fixed inside a pore, but the other beads are occupied a free space in the *cis*-side and *trans*-side. This approach is more natural in the computation to ensure the efficient polymers translocation in which the first bead cannot cross back out of the pore. In the study of free translocation, the experimental confirmation is based on the view of pure osmotic flow, which draws the DNA to the nanometric pore.

Analytical and experimental perception of biological aspects needs modeling and simulations at the scales of various time and length. One can set up the system by incorporating all particle interactions, which requires enormous computational effort. The other

option is to conduct the simulation (using either molecular dynamics or Monte Carlo approach) at larger scales, which incorporates the powerful interactions among the combined units or groups of beads. In a coarse-grained approach, polymers are considered at the monomer level rather than analyzing the atomic level, as stated earlier. The selection of this procedure is motivated by its capacity to be utilized to a big collection of polymers since it does not take into account the specific chemical compositions.

The main focus of this dissertation is to understand how multiple arms of star polymer moves across different geometrical constraints in the absence or presence of a driving force. Accordingly, the simulations of polymers translocation in the existence of constraints are carried out using the coarse-grained Langevin dynamics and Monte Carlo techniques. Typically, we are concentrated on the most simplified systems where the dynamics of f-arms star-shaped polymers translocation is affected by the chains topology, the total number of monomers, the driving force, and the dimensions of the constraints. Also, we implemented concepts and techniques in polymer physics to explain these biological systems. In LD computer simulation, the equation of motion is integrated using the velocity Verlet integrator with a Langevin thermostat [30]. The trajectory integration is performed by using the exible molecular dynamics (MD) computer simulation package for the soft matter what is called ESPResSo (noted earlier) [30]. Regarding the MC simulation, we have used the bond fluctuation model. In this approach, we begin with the branched polymers of the desired chain length. A monomer is taken and displaced to its nearest neighbor position using the self-avoiding principle. The move is simplistic and local, which is similar to a growth algorithm at any extended step; if the selected position is previously possessed by a monomer, then we reject the entire move and begin the whole process again. Concerning the bond fluctuation algorithm, however, the lengths of the bond are altered continuously [31].

The rest of the dissertation is well-organized as follows. Chapter 2 introduces the background theory of polymers and the theoretical scaling predictions as well. In chapter

3, we start with a description of the model used for the polymer, specific details about the simulation technique, and other computational details. Chapters 4, 5, 6, and 7 present an overview of the results, a detailed explanation of the simulation results, and comparing the results with the theoretical scaling predictions. The last chapter ends with a brief summary, closing remarks, and suggestions for future outlook.

Chapter 2

Background theory

In this chapter, the theory associating with this dissertation is presented in detail. It includes an introduction to polymer physics, followed by a brief overview of the theoretical framework of star polymers. The derivation that describes the statics and dynamics properties of the star-shaped polymers as a function of system parameter is also included. We, therefore, briefly review several factors used in the process of polymers translocation.

2.1 A primer to polymer physics

Much of human being history has been affected by the accessibility of materials. Polymers that can be used by humans and have been found naturally are called biopolymers, for a hundred years without recognizing the polymeric materials as macro-molecules [32]. Natural rubber was functional for several centuries before it had been known as a polymeric material. Staudinger (in 1920) suggested the macromolecular hypothesis as polymers are macro-molecules that consisting of basic units of covalent bond called monomers [32]. Even though this proposed idea was initially encountered with strong opposition, its gradual recognition at the time 1920s allowed significant progress within the field. Carothers (by 1929) had produced various types of polymers with clearly defined structures, and therefore the Polymer era was born [32].

2.1.1 Polymer chemical structures

A polymer is formed from a large group of molecules with regularly repeated chemical units of the same kind, or probably of various types, connected end-to-end, or sometimes in more complicated approaches, to set up a chain molecule [32,33]. Polymeric materials have a very high molecular mass with long-chain molecules that are chemically connected, which covers in the hundreds of thousands. Consequently, the word 'macromolecules' is mostly used to refer to the polymers. The means of connecting the monomer units within a chemical reaction to produce huge chains is called polymerization. Different physical characteristics of polymeric systems are determined considerably by the extent of polymerization of high-order molecular materials. For instance, as the beads are joined together, both boiling and melting points of the polymers vary [32]. Oligomer as a type of macromolecules contains only a smaller molecular weight, which includes the number of monomers below twenty. While polymeric materials that contain monomers ranging between twenty and ten billion are known as linear polymers, typically, the longest straight chain is a chromosome [32].

A homo-polymeric system is a form of polymer that contains only the same types of monomer. The chain-like molecules have a simplified structure with the sample of:

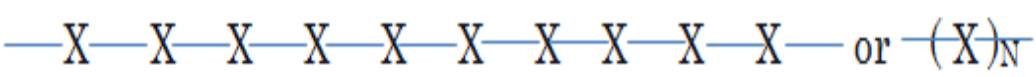

Figure 2.1: The simplified sample structure of chain-like molecules.

where N is the total number of monomers and X is the mono-functional units such as hydrogen (H), methyl (CH_3), Chlorine (Cl), and C_6H_5 (phenyl) with the corresponding polymers polyethylene, polypropylene, poly(vinyl chloride), and polystyrene, respectively [33]. The polyethylene in the form of a simplified linear-chain structure is designated as:

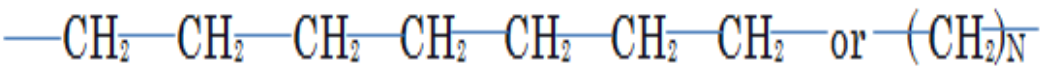

Figure 2.2: The simplified linear-chain structure of the polyethylene.

where N is equal to twenty thousands $(20,000)$. Next, copolymers are macromolecules containing two distinct types of beads. As shown in Fig. (2.3), copolymers can be graft, alternating, random, or block (that is, diblock, triblock, and multiblock), based on the order in which their beads are joined together.

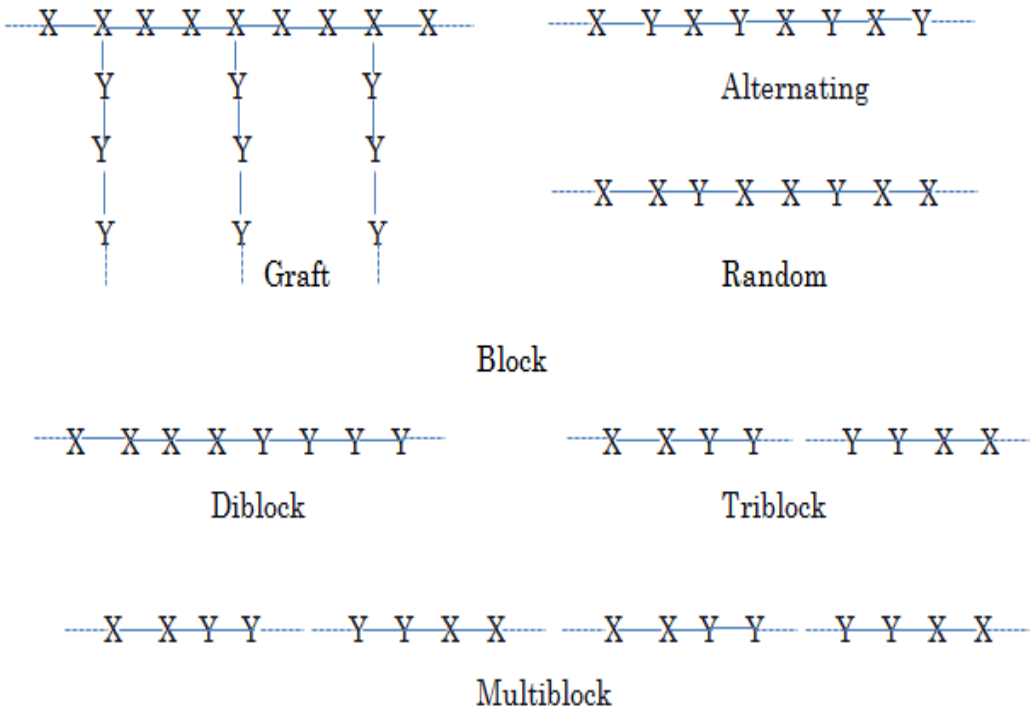

Figure 2.3: Different types of copolymers: graft, alternating, random, or block (diblock, triblock, or multiblock).

Furthermore, terpolymers are another sort of polymer that consists of three different types of monomeric units. There are two types of terpolymers, such as random and ABC triblock, as depicted in Fig. (2.4). Also, heteropolymers are macromolecules that can be formed by mixing various kinds of monomers and merged into a single-chain with

peculiar properties. Most of the synthetic polymers are heteropolymers. One example of a heteropolymer is DNA, which includes four (4) distinct types of monomers that we call nucleotides. But, natural proteins are also heteropolymers, which contains twenty (20) distinct sorts of monomers, the so-called amino acids.

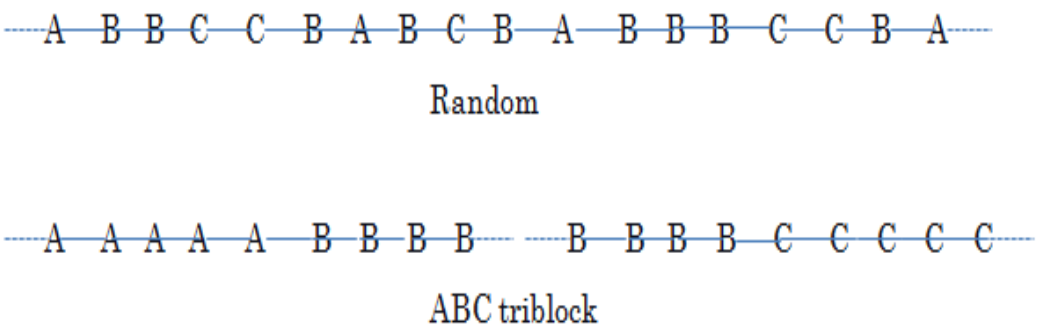

Figure 2.4: The representations of chemical structures of terpolymers: Random and ABC triblock.

2.1.2 Polymer architectures

Polymer architecture is another aspect of polymer systems that control its characteristics. Polymer architectures can be comb, dendrimer, ladder, star-shaped, randomly branched, H-branched, ring, or linear [32], as sketched in Fig. (2.5).

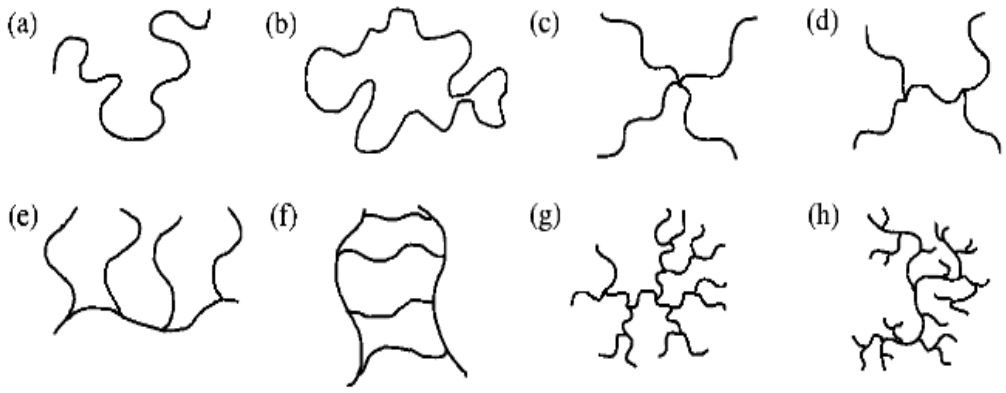

Figure 2.5: Representations of various forms of polymer architectures: linear (a), ring (b), star-shaped (c), H-branched (d), comb (e), ladder (f), dendrimer (g), and randomly branched (h).

A polymer network is an enormous extent of crosslinking that can give rise to a macroscopic molecule, as depicted in Fig. (2.6).

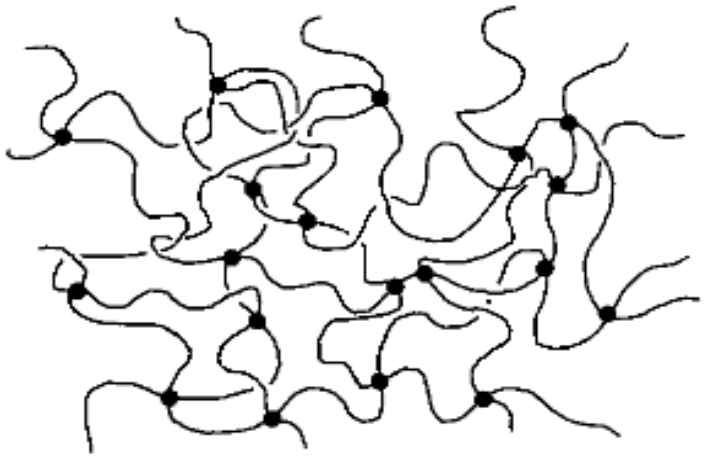

Figure 2.6: The simplified structure represents the polymer network. Note that the dots indicate the cross-links.

Since the middle of the 1990s, the discipline of the chemical study of the polymer has noticed the critical development of numerous procedures to carry out a manageable radical polymerization. One notable effort within the area of polymer conformation focuses on the synthesis of clearly defined high-molecular materials with precisely controlled structure by including site-specific branching (central) points and functionalities. Polymers have the non-linear (branched) architectures based on the functionality, the number, and relative order of the central points within the system. These can be further categorized as randomly branched, molecular brushes/graft, dendrimers, hyperbranched, gels, and star-shaped polymers [34]. Typically, from the beginning to the end of this work, we have been concentrated on dealing with star-shaped branched polymers. Single-star polymers with an identical total polymer mass but multiple functionalities enable us to recognize the impact of conformation on the translocation dynamics. Regarding the selection of beads and the type of the central unit of the chains without touching the level of polymerization, they provide enormous flexibility [35].

2.1.3 Models of polymer chain

By performing computer simulations using coarse-grained models rather than the skeletal chain model, we can predict how various physical parameters depend on the chain size, polymer concentration, and so forth. Fig. (2.7) illustrates the three distinct kinds of polymer models: the model of a bead-stick, the model of a bead-spring, and the model of a pearl-necklace. In the model of bead-stick approaches, the entire chain

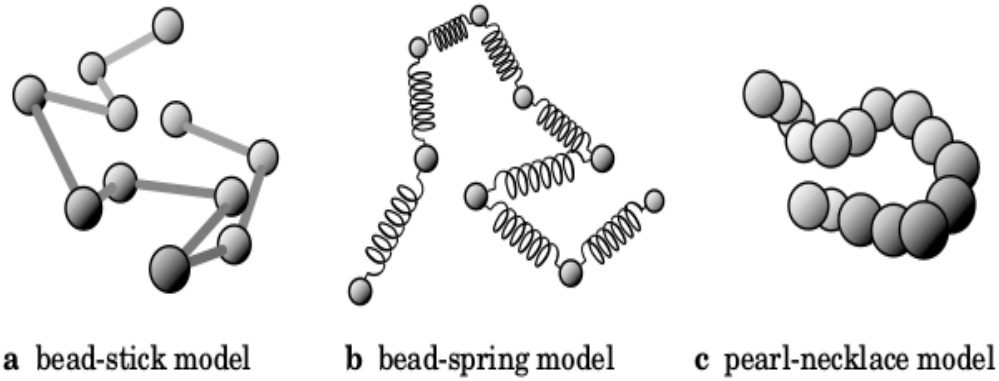

Figure 2.7: The scheme is displaying the three different types of polymer models within a continuous space.

comprises monomers that represent the core unit (including more atoms) and sticks that connect adjacent beads. Then, the model is a version of the coarse-grained approach. A couple of bead-stick is known as a segment, which represents the smallest part of the chain. A monomer diameter and the stick thickness might be any positive value. If the diameter of a bead is zero, then the segment is simply a stick. Also, the angle among two nearby sticks can be restricted or let it free, or the dihedral angle of a stick about the next neighboring stick can be limited [36]. In the model of bead-spring, the entire chain is characterized by a set of beads linked by springs. Each spring has a zero-length of stability. Also, this model appropriately describes the motion of various sections of the chain. Here, spring is representing the segment in which a monomer on its end [36]. In the model of pearl-necklace, the pearls (or beads) are regularly in touch with the two neighboring monomers; it is equivalent to a model of bead-stick, where the length of the

stick corresponding to the diameter of a monomer. The diameter of a bead is always non-negative. The bond and dihedral angles could be restricted, as in the case of the bead-stick model [36].

2.2 Basics of star polymer

2.2.1 Introduction

In 1948, Paul Flory and John Schaefgen were investigated star-branched polymers for the first time while analyzing multi-chain polymeric material. They chemically synthesized polyamides (star-shaped in configuration) in which the repeating units of amino acids connected by amide bonds [37], as displayed in Fig. (2.8). Morton and work-

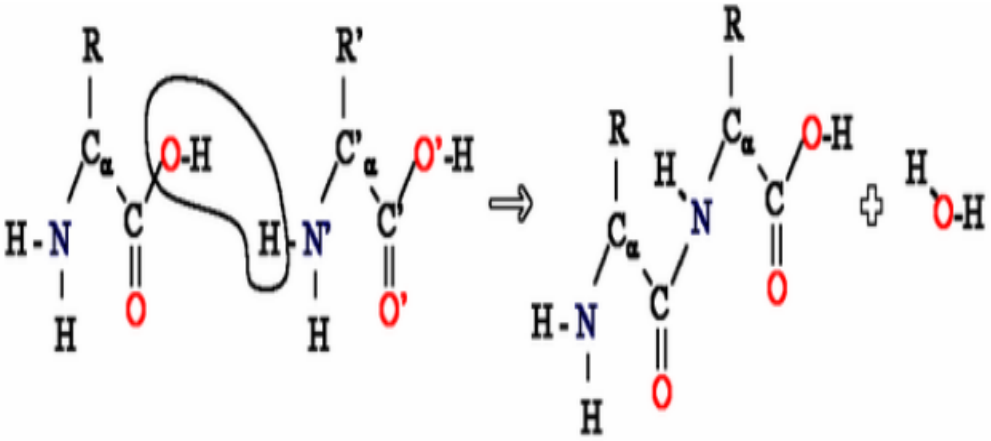

Figure 2.8: Representation of star-shaped polyamides with repeated monomeric units of amino acids.

mates (in 1962 or fourteen years later) synthesized 4-arms star polystyrenes (PS) by taking advantage of the living nature of anionic polymerization method [38]. Wenger and Orofine (in 1963) were investigated 3-arms star PS using benzene tri(chloromethyl) as a linking means [39]. Mayer was prepared four-arms star-shaped diblock and triblock copolymers (isoprene and styrene) using $C_{10}H_{10}Cl_4$ (that is, 1,2,4,5-tetra(chloromethyl) benzene) [40]. However, it was quite difficult to extend the functionality of star-branched

polymers beyond $f = 6$ with the aid of the derivatives of chloromethyl benzene. Rempp and Decker were the foremost scholars to show the effectiveness of divinylbenzene (DVB) as a linking means by getting ready and describing PS star-branched polymers with functionality ranging between 6 and 15 [41]. However, the DVB technique was introduced by Milkovich, and this method didn't provide clear evidence that the branched chains were prepared [42]. Thus, the DVB approach doesn't permit one to predict the functionality of the branched chains and give ways for polymers with a uniform number of arms [43]. In conclusion, the other linking agent (multifunctional chlorosilane compounds) became the ultimate solution to the above problems [44].

Star-branched polymers are consisting of the most simplistic form of branching, which leads to rises in the interest of many scholars. Star macromolecules are designated by a single branching point. Besides, they also have at least three flexible arms, where each arm length has a total number of beads N_{arm} [45, 46]. These are attached to a common center by one of their ends. The number of arms is denoted as f that we called the functionality of star polymers. For the first and second functionalities ($f = 1, 2$), branched stars resemble linear chains and exhibit highly aspherical conformations [47]. For star polymers ($f \geq 3$) with the given total polymer mass, enabling the long branched-chains in the system significantly decreases the chain dimensions (or sizes) and intensifies the distribution of segment density. Cotton and Daoud have introduced the conformational statistics of a single-star polymer in a non-concentrated solution using the usual blob model [48] and further updated under the operation of Birshtein and his collaborators [49, 50]. The star is characterized by the same center shells of blobs using the Daoud-Cotton approach [48]. The number of arms of such a branched polymer plays a significant role, that is, the more the functionality, resulting in the more the sphericity shape of the chain as well. Therefore, the stars exhibit stiffer and spherical similar to a soft colloid as the functionality increases.

Star-branched polymeric setups are generally categorized into the following two classes:

regular star-branched polymers with the same arm segments and asymmetric (also called mikto-arm) star-branched polymers with various arm segments, as presented in Figures (2.9a) and (2.9b)), respectively. The regular star-branched chains are consisting of block copolymers or homopolymers [51]. Star polymers with varying arms (mikto-arm star polymers) have got a prominent concern in their characteristic of phase separation [51]. Consequently, the conformations of multiple arms star-shaped polymers can be served as the bridge two sections of soft matter polymers and colloids, which have extensive archives and signicant applications of industry [52–54].

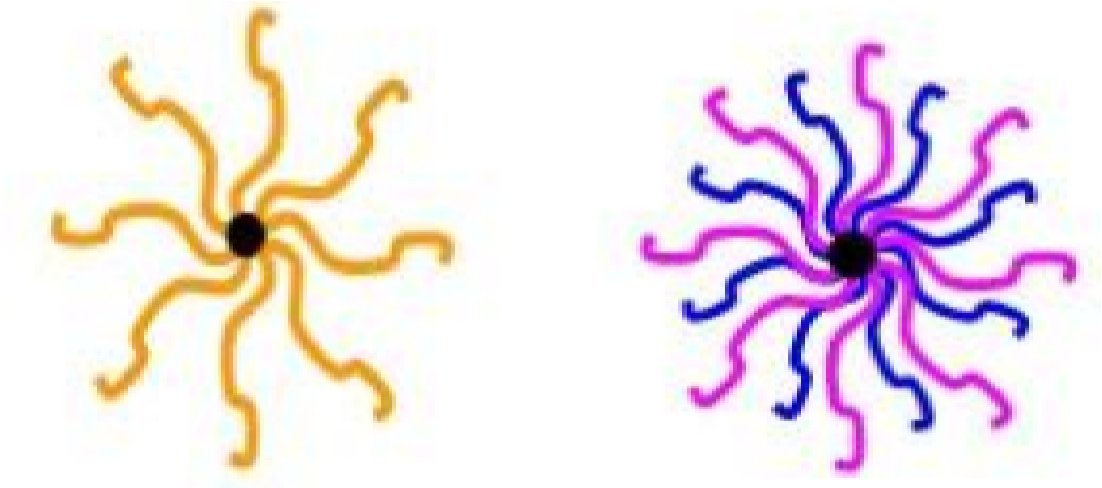

(a) (b)

Figure 2.9: Schematic representation of star-branched polymers with regular (a) and asymmetric (b) arms.

2.2.2 Synthesis of star polymer

A. Arm-first method

In the arm-first method, mono-functional living chains with understood characteristics are utilized as precursors in the chemical reaction. This method is also called as the arm-in or convergent. As shown in Figure (2.10), to produce star polymer, the active site at the head of the chain can be reacted with a reactive multi-functional polymer core unit,

the so-called a linking means that has two vinyl groups (divinylbenzene) [55]. In this approach, the outcome of a star-shaped polymer consists of the chain with homogeneous groups. In contrast, heterogeneous star polymers can also be produced easily using the convergent method. Besides, there is a statistical distribution in the proportion of arm types within every monomer [55]. Consequently, the arm-in way of synthesis is the most important synthesis of star-branched polymers due to each reaction step can be easily controlled and evaluated. Also, the number of arms and the core bead can be separated and identified before a chemical reaction [55]. Therefore, the functionality of a star polymer can then be precisely and directly measured.

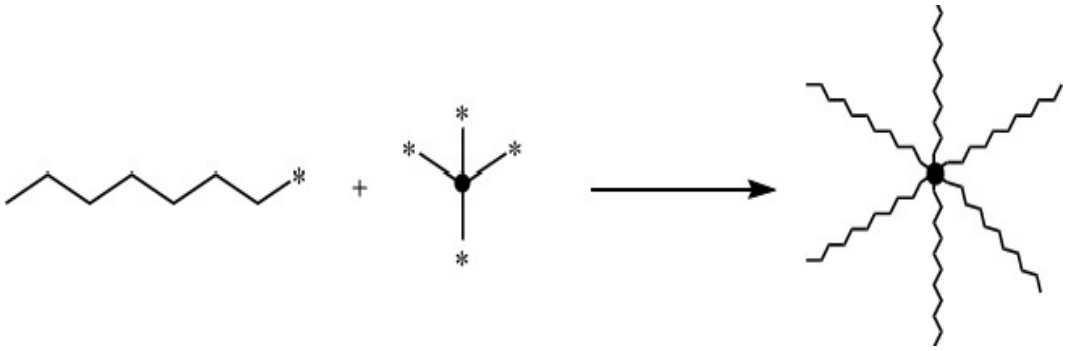

Figure 2.10: Illustration of star polymer synthesis via the arm-in approach.

B. Core-first method

The core-first approach is sometimes also called the divergent or arm-out method. In this method, a multi-functional central core unit serves as the initiator at the same time for multiple arms [56]. In the synthesis of star-branched polymers using the arm-out method, the polymer functionalities are growing from the central core unit, including various reactive sites (see Figure (2.11)). The arm-out approach is more complicated than the arm-in method, finding a proper and stable core unit is tough, and identifying the synthesized branched-chain is call [56]. Due to the composition of star-shaped polymers with a well-defined functionality and core unit architecture, the functionality of star polymers in the arm-out synthesis method is commonly limited to amounts far

smaller than possible within the arm-in approach. Here, heterogeneous star polymers can also be produced under extremely high control over the conformation of the outcome, which implements via the reactive localities for orthogonal polymerization reactions [56].

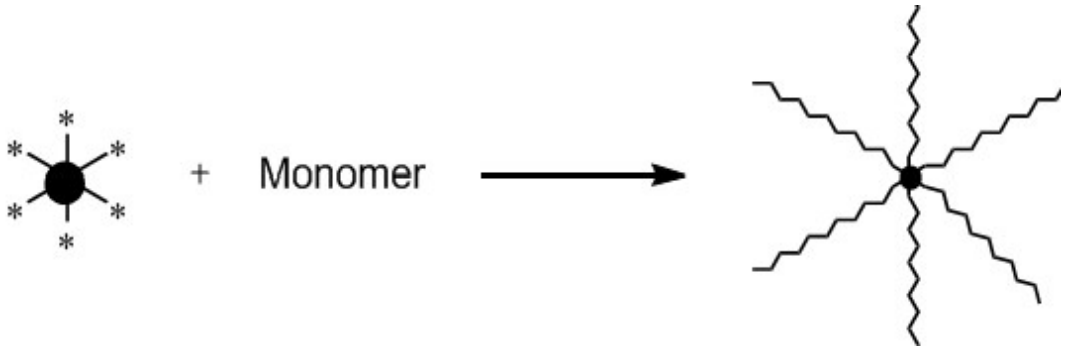

Figure 2.11: Representation of star polymer synthesis via the arm-out approach.

C. Coupling-onto method

The coupling-onto approach for the synthesis of a star-shaped polymer can also be recognized as the arm-in method with the rise of the polymer functionality separate from the preparation of the central core unit, as displayed in Figure (2.12). Here, the pre-

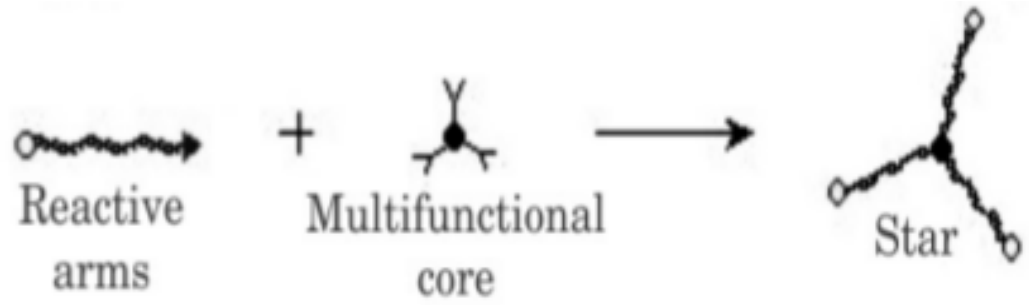

Figure 2.12: Schematic illustration of star-shaped synthesis suing coupling-onto approach.

synthesized functionalities of the polymer are attached to the common origin under a tidy and effective coupling reaction [57]. This technique enables remarkably high control of the arrangement of both the functionalities and the central core unit. However, the attachment of the chain functionalities is arbitrary that decreases control of all-inclusive

structures in the heterogeneous star-shaped polymer synthesis in contrast to the arm-in approach [57].

Star polymers obtained by the above three synthesis methods, such as arm-in, arm-out, and the coupling-onto, have a broad organization of the number of arms (or functionality) due to the impact of the reaction situations. Various techniques are employed for finding the functionality; however, among them is comparing the molar masses determined for star-shaped polymer and the arm precursor [1]. Hence, the functionality of the chain is represented by [1]:

$$f = \frac{M_s(1 - W_c)}{M_a}, \tag{2.2.1}$$

where M_s represents the molar mass for star polymer, W_c denotes the weight fraction of a central core unit, and M_a signifies the molar mass for the arm of the chain. This technique can only be applied for branched polymers with the first-generation of arms from branching indices (g_g), which equals the ratio of the square of gyration radii of the star (R^2_{gs}) and linear (R^2_{gl}) chains with similar molar masses (M) and determined independently [1]. Thus,

$$g_g = \frac{R^2_{gs}}{R^2_{gl}} \tag{2.2.2}$$

2.2.3 Characteristics and applications of star polymer

A. Rheology

Molecular dynamics and rheological features of polymeric materials are affected by polymer structure and have been the issue of extensive analytical and experimental studies [58]. Here, the main quantities to consider are the arm's molecular weight, the star's functionality, and the size of the central core. For star polymers with smaller functionality, the central core unit is considered as a branching point of the chain that does not change the molecular dynamics of the polymer arms. In other words, star polymers that have Gaussian coil structure and stress relaxation are not dependent on the functionality [2].

However, for star polymers with higher functionality and considerable size of a core unit, the polymers embrace a core-shell structure, and the impact of the core unit needs to be recognized for the rheological perspective [2].

B. Thermal properties

The structure of polymers also affects the thermal features of such materials. The following parameters are examples of thermal characteristics of polymers: temperature of glass transition (T_g), the temperature of crystallization (T_c), decomposition temperature (T_d), melting temperature (T_m), and crystallinity [59]. For star polymers with a small core unit and a lower functionality, thermal traits are remarkably tempered by the chain arms because of the insignificance of the central unit mass fraction. For star polymers prepared under the arm-in approach with a larger core size and the higher functionality, the impact of the core unit on the thermal characteristics is amplified itself by causing uneven distribution of segmental mobility and structure of the chain arms from the core unit to the ends of the arm monomers, leading to the higher density of the chain and more extended chains around the central point [59]. Star polymers usually have noticeably lower T_g, T_c, T_d, and T_m as well as reduced crystallinity as compared with linear polymers of similar molecular weights [2, 4].

C. Nanostructured thin films

Star polymers that contain various chemical elements within a single-star, their conformation can undergo microphase separation in the form of bulk. Consequently, the structure of the branched-chain has led to self-organized morphologies and nanostructures [60]. Star-shaped copolymers with different types of arms and similar arms block copolymers originating from the central core unit, heterogeneous polymers, and homogeneous star block copolymers, respectively, are branched polymers that most commonly considered for such processes of assembly [61]. During the establishment of bulk nanostructured

assemblies, the advantage of working with different arm star-branched polymers is the ease in which they build 3D periodic rather than 2D conformations. It has something to do with the fact that the composition of polymers with various types of arms connected to a branching point, resulting in a borderline between separated polymer phases, which drives the conformation into a 3D arrangement [61].

D. Interfacial stabilizing agents

Lately, star-branched polymers emerge as novel agents of interfacial stabilizing for the use in emulsion droplets. Remarkably, multiple arms of core networked star-shaped polymers and a densely networked core unit have proved to be efficient and adaptable surfactants for various oily (water-in-oil) and water-soaked (oil-in-water) emulsion systems [62]. Bearing in mind that such polymers have the dimensions quiet smaller than long-established Pickering agents and are flexible polymeric chains (that is, not hard spheres) originating from the networked core unit, which can be quickly damaged. This idea raises the question in regards to they are serving as particle-like (Pickering stabilizers) or rather like a molecule traditional unsymmetric surfactants) [63]. Therefore, core networked star-shaped polymers may introduce an emerging area of stabilizing agents that relate surfactant-like and particle-like modes, which may provide new prospects for particular applications. For instance, stimuli-responsive is one of the tremendous applications that enable switching among the stable and unstable states of emulsion [2].

E. Gene delivery

Gene therapy contributes to a novel way for the handing of genetic complications, for example, cancer, blindness, hemophilia, Parkinson's disease, diabetes, and cystic fibrosis [64, 65]. The delivery of genetic components, including micro-RNA, plasmid-DNA, sh-RNA, and si-RNA, into the cells is crucial for genetic therapy [66, 67]. These genetic

elements, mainly si-RNA and DNA, are hydrophilic and charged negatively, and consequently, their way via hydrophobic layers with charged negatively are considerably hard to achieve. Additionally, the encapsulation of such molecules enhances the demand for the delivery of successful trans-membrane as these nucleic acids are possibly degraded just by enzymes before arriving at the center (nucleus) [67]. Nucleic acids may be coated in branched macromolecules is called vectors, which divides into viral and non-viral vectors [66]. Viral carriers (retroviruses, adenoviruses as well as adeno-associated viruses) were employed as transporters of genes. However, there are several limitations: restrict their clinical applications, potentially protected reply to the transfection vectors, massive production cost, restriction in the dimension, and quantity of genetic materials [66, 67].

F. Drug encapsulation

Employing well-designed polymeric materials have been focused over the past decades in the field of nanotechnology and biotechnology to prepare valuable encapsulation instruments for drug molecules [68]. Commonly, those encapsulation machines have a core-shell arrangement that non-water-soluble units can be efficiently placed in the center of hydrophobic surrounded by a stabilizing shell of hydrophilic. Apart from the fact that polymeric micelles formed from straight-chain block copolymers, star-shaped polymers have been widely tempered to create delivery carriers for drug molecules because of their peculiar architectural and chemical characteristics [69].

G. Drug delivery

Since star polymers may contribute to sustained, managed, and focused drug delivery, they have been considered as drug carriers [2]. Using the arm-in approach, the encapsulation of doxorubicin in star-branched chains illustrated by Boyer and Davis, in the existence of vinyl benzyl aldehyde and cross-linker [70]. The star-shaped chains that could pile up by the intensified retention and permeability influences in the tumor

were shown by Davis and his collaborators [71]. The synthesis of branched chains (star polymers) under the arm-in returnable addition-fragmentation transfer means of polymerization was investigated by the scholars for the biological fortune of poly [(oligo-ethylene glycol) acrylate]. As contrasted to the corresponding micelle systems, the core unit of star-shaped polymers have been encapsulated with various substances, which considers their release outlines that depict fewer burst defects. These substances are listed as follows: small molecules, dyes, and model drugs, which contain 5-Fluorouracil, progesterone, doxorubicin, furosemide, hydrochlorothiazide, etoposide, and paclitaxel [2].

H. Imaging

The act of therapy is significantly conducted by molecular imaging. It is possible to obtain an upgraded understanding of cell migration and the disease status by pursuing the biodistribution and focusing the capacity of a drug delivery mechanism in the living body [72]. Using the procedures of clinical diagnostic, imaging assists in assessing an unhealthy situation before the beginning of therapy, provided that relying upon imaging agents to identify specific sorts of tissue [72]. The features of star-branched chains with a large number of arms make them suited as contrast means, in the ways of vitro diagnostic as well as fluorescent probes [2].

I. Other industrial applications

In comparison to the linear chain, the conformation of star-shaped polymer allowed a better performance or acceptable features toward the given applications. For instance, a star polymer with the functionality ranging between 9–13 (Lubrizol) is synthesized by convertible addition-fragmentation chain shift polymerization techniques as a principal component of their engine fuel viscosity improving lubricant Asteric [2]. Also, a more selective low-temperature fluidity outcome is contributed by the star modifiers, which leads to better fuel economy and effectiveness. Star polymers as modifiers of viscosity are

used in Kraton performance chains in the range of outcomes to promote different tasks: deliver increased outflow capability, a smooth finish, and a high gloss the subsequent application. With the aid of anionic polymerization, their typical chain conformations like poly(isoprene) and polystyrene copolymers are synthesized [2]. The applications of Kraton MD6953 and G1750 (forms of star polymers) can be specified as follows: the role in cosmetics as gelling means or modifiers of viscosity for film development and promoted filler loading, as forming compounds for shoemaking, and also as elements of sealant, coatings, and adhesive [2].

2.3 Dimension of star polymer

Here, we will study how to assess the size or the dimension of star polymer for both real and ideal chains. Figure (2.13) outlines the difference between the real chain (b) and the ideal chain (a) for a threaded approach in two dimensions. The structure of the chain is nearly the same except for a small portion where two sections of the chain get close, as designated by circles with a broken line. The crossover is not observed in the real chain, but it is allowed in the ideal chain.

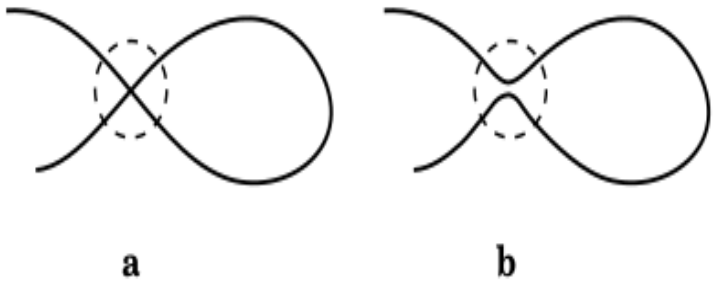

Figure 2.13: Representation of an ideal chain (a) and a real chain (b) in a two-dimensional lattice.

2.3.1 Dimension of the ideal chain

First, let us determine the dimension (that is, gyration radius R_g) of a linear polymer in the case where the chain is ideal. The radius of gyration squared, R_g^2 , is the second moment near the chain center of mass. $\langle R_g^2 \rangle$ is defined as the average distance squared between the monomers and the chain center of mass (see Fig. (2.14)).

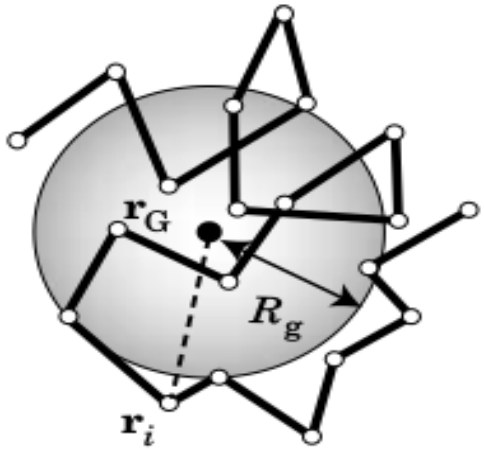

Figure 2.14: Schematic depiction of the bead-stick model that describes the chain center of mass $\mathbf{r}_G$ and the gyration radius.

The chain center of mass is expressed as:

$$\mathbf{r}_G = \frac{1}{N+1} \sum_{i=0}^{N} \mathbf{r}_i \tag{2.3.1}$$

where we suppose that the beads have the same molecular weight, and they are joined by massless bonds. Next, the mean-square radius of gyration over the possible conformations for polymers and other fluctuating objects in free space is [36]:

$$\langle R_g^2 \rangle = \left\langle \frac{1}{N+1} \sum_{i=0}^{N} (\mathbf{r}_i - \mathbf{r}_G)^2 \right\rangle = \frac{1}{N+1} \sum_{i=0}^{N} \langle (\mathbf{r}_i - \mathbf{r}_G)^2 \rangle, \tag{2.3.2}$$

where the averaging and summation can be interchanged.

We can also apply the average distance squared between two beads to get R_g instead of determining r_G first and then the average distance squared between r_G and each bead. Due to the summation regarding i and j is another averaging, we can state that $\langle R_g^{2\rangle}$ is half of the average distance squared between two beads on the entire chain (see Fig.

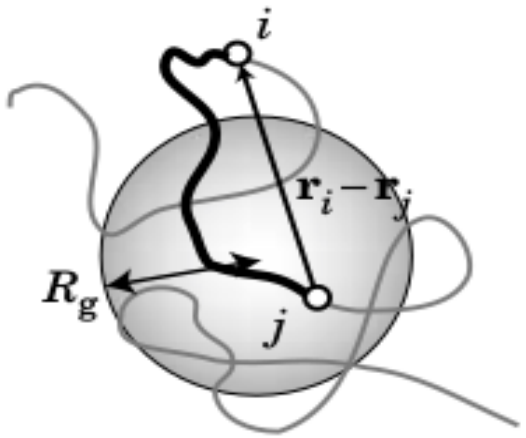

Figure 2.15: Illustration of the average distance squared between two monomers i and j is twice as long as $\langle R_g^2 \rangle$.

(2.15)) [36].

The following identity is necessary to drive the equation, leading to [36]:

$$\begin{aligned}
\sum_{i,j=0}^{N} (\mathbf{r}_i - \mathbf{r}_j)^2 &= \sum_{i,j=0}^{N} [(\mathbf{r}_i - \mathbf{r}_G) - (\mathbf{r}_j - \mathbf{r}_G)]^2 \\
&= \sum_{i,j=0}^{N} (\mathbf{r}_i - \mathbf{r}_G)^2 - 2 \sum_{i,j=0}^{N} (\mathbf{r}_i - \mathbf{r}_G) \cdot (\mathbf{r}_j - \mathbf{r}_G) + \sum_{i,j=0}^{N} (\mathbf{r}_j - \mathbf{r}_G)^2 \\
&= 2(N+1) \sum_{i=0}^{N} (\mathbf{r}_i - \mathbf{r}_G)^2 - 2 \sum_{i,j=0}^{N} (\mathbf{r}_i - \mathbf{r}_G) \cdot (\mathbf{r}_j - \mathbf{r}_G) \\
&= 2(N+1) \sum_{i=0}^{N} (\mathbf{r}_i - \mathbf{r}_G)^2, \qquad (2.3.3)
\end{aligned}$$

where Equation (2.3.1) was used. This transformation doesn't consider any particular model of the polymer [36]. Eq. (2.3.4) be applied, therefore, to any chain structure. Then,

$$\sum_{i=0}^{N} (\mathbf{r}_i - \mathbf{r}_G)^2 = \frac{1}{2(N+1)} \sum_{i,j=0}^{N} (\mathbf{r}_i - \mathbf{r}_j)^2 \qquad (2.3.4)$$

For any structure, inserting Eq. (2.3.4) into Eq. (2.3.2), and doing some rearrangements we get:

$$\langle R_g^2 \rangle = \frac{1}{2} \left\langle \frac{1}{(N+1)^2} \sum_{i,j=0}^{N} (\mathbf{r}_i - \mathbf{r}_j)^2 \right\rangle = \frac{1}{2(N+1)^2} \sum_{i,j=0}^{N} \langle (\mathbf{r}_i - \mathbf{r}_j)^2 \rangle \qquad (2.3.5)$$

Again, let us consider $\mathbf{r}_{ij}$ is the position vector of the j^{th} bead ($j = 0, 1, ..., N_{arm}$) on the chain's i^{th} arm ($i = 1, 2, ..., f$), as depicted in Fig. (2.16) [36]. The central unit is at r_{i0}.

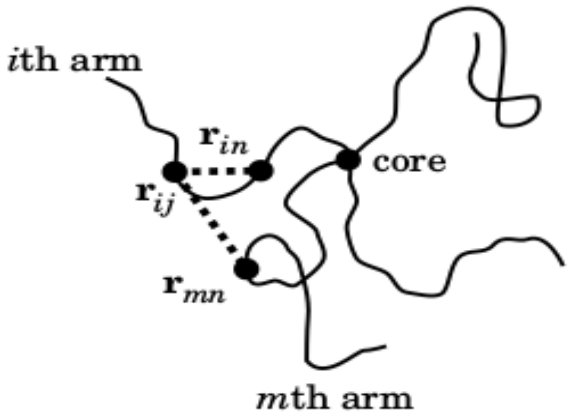

Figure 2.16: Diagrammatic representation of two beads can be on a single-arm (same arm) or two different arms.

Using Eq. (2.3.5), the average radius of gyration squared for star polymer, R^2_{gs} is written as [36]:

$$\langle R^2_{gs} \rangle = \frac{1}{2N^2_{arm} f^2} \sum_{i,m=1}^{f} \sum_{j,n=1}^{N_{arm}} \langle (\mathbf{r}_{ij} - \mathbf{r}_{mn})^2 \rangle \tag{2.3.6}$$

where the central unit is excluded in the sum. The average monomer distance squared is determined for beads on a single-arm and those on two different arms independently (see Figure (2.16)) [36]:

$$\begin{aligned}
\sum_{i,m=1}^{f} \sum_{j,n=1}^{N_{arm}} \langle (\mathbf{r}_{ij} - \mathbf{r}_{mn})^2 \rangle &= \sum_{i=1}^{f} \sum_{j,n=1}^{N_{arm}} \langle (\mathbf{r}_{ij} - \mathbf{r}_{in})^2 \rangle + \sum_{i \neq m}^{f} \sum_{j,n=1}^{N_{arm}} \langle (\mathbf{r}_{ij} - \mathbf{r}_{mn})^2 \rangle \\
&= \sum_{i=1}^{f} \sum_{j,n=1}^{N_{arm}} |j - n| b^2 + \sum_{i \neq m}^{f} \sum_{j,n=1}^{N_{arm}} |j + n| b^2 \\
&= b^2 \left[f \sum_{j,n=1}^{N_{arm}} |j - n| + f(f+1) \sum_{j,n=1}^{N_{arm}} |j + n| \right] \\
&= \frac{1}{3} b^2 f N_{arm} (N_{arm} + 1)(3 f N_{arm} - 2 N_{arm} - 1)
\end{aligned} \tag{2.3.7}$$

Equating Equations (2.3.6) and (2.3.7), we get:

$$\langle R_{gs}^2 \rangle = \frac{b^2(N_{arm}+1)}{6fN_{arm}}(3fN_{arm} - 2N_{arm} - 1) \cong b^2 \frac{N}{f}\left(\frac{1}{2} - \frac{1}{3f}\right) \tag{2.3.8}$$

where $N_{arm} \gg 1$ and $N = fN_{arm}$ were applied. For linear chain ($f = 2$), the average radius of gyration squared is $\langle R_{gl}^2 \rangle = b^2 N/6$. Thus, the parameter of branching g_g for multiple arms star polymer is given by:

$$g_g = \frac{\langle R_{gs}^2 \rangle}{\langle R_{gl}^2 \rangle} = \frac{1}{f}\left(3 - \frac{2}{f}\right) \tag{2.3.9}$$

where the total polymer mass of the two chains is the same, and $g_g \leq 1$.

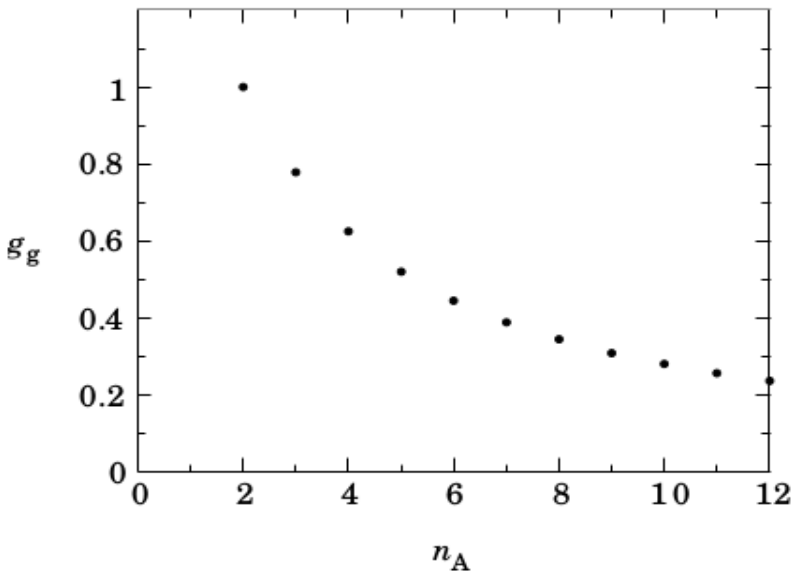

Figure 2.17: The plot of the branching parameter of $f-$arms star polymer as a function of the chain's total number of arms, $f = n_A$. As the functionality increases, the chain becomes more compact, and therefore the branching parameter decreases.

2.3.2 Dimension of real chain

In the case of a real chain, two beads can't hold the same space at the same time, and this is known as the effect of excluded volume. In a star-shaped polymer, many theories are elaborated by statistical mechanics. These theories are ranging from self-consistent

reduction of intramolecular interactions [73] to renormalization ensemble methods [74]. But, Flory theory was a crucial step in the background of significant phenomena, notably, in recognizing the rising of power-laws and the part of dimensionality. As stated by Flory theory, the free energy $F(R,N)$ of a star-branched chain with the aid of the effect of excluded volume is written as [75]:

$$F(R,N) = F_{ent}(R,N) + F_{int}(R,N) \tag{2.3.10}$$

where $F_{ent}(R,N)$ is the entropic flexibility of the polymer, and $F_{int}(R,N)$ is to the pair-wise interactions among the beads. For a single chain, the contribution of the entropic term to the free energy can be determined from the probability distribution function which supports Gaussian statistics:

$$P(R,N) = \left(\frac{3}{2\pi N b^2}\right)^{3/2} exp\Big[-\frac{3}{2}\frac{R^2}{Nb^2}\Big] \tag{2.3.11}$$

where b is the size of a bead, and the entropic term contributions to the free energy is given by:

$$S(R,N) = \kappa_B\ logP(R,N) = S(0,N) - \frac{3\kappa_B R^2}{2Nb^2}, \tag{2.3.12}$$

where κ_B is the Boltzmann constant and $S(0,N) = \frac{3}{2}\kappa_B log\Big[\frac{3}{2}\pi N b^2\Big]$. Since the free energy of a chain is written as $F(R,N) = E(R,N) - TS(R,N)$, the entropic energy because of swelling of a chain can take the form ($\kappa_B T \equiv 1$):

$$F_{ent}(R,N) = \frac{R^2}{Nb^2} \tag{2.3.13}$$

where T is the system temperature, and E is the interaction energy among the beads and the solvent molecules. The entropic energy for f-arms star polymer is defined by:

$$F_{ent}(R,N) = fR^2/Nb^2 \tag{2.3.14}$$

By using a viral expansion with volume $V \approx R^3$ and the number density of monomers in the pervaded volume of the chain $c_n = N/V \approx N/R^3$, the energetic contribution to the

free energy density (that is, free energy per volume F_{int}/V) can be described as:

$$\frac{F_{int}(R,N)}{V} \approx \kappa_B T\left[c_n + \nu_{exc}c_n^2 + \omega c_n^3 + ...\right] \approx \kappa_B T\left[\frac{N}{R^3} + \nu_{exc}\frac{N^2}{R^6} + \omega\frac{N^3}{R^9} + ...\right], \quad (2.3.15)$$

where the first summand (c_n) is the ideal gas contribution, the factor ν_{exc} (c_n^2 term) is proportional to the effect of excluded volume, and the factor w (c_n^3 term) is related to the coefficient of the three-body interaction $\omega \approx b^6$. The repulsive characteristics of between bead-bead interactions enlarge the chain, provided that the polymer is in a good solvent. Under such conditions, the 3-body interaction term isn't relevant, the size (equilibrium) of the polymer is often determined by just considering the entropic, and the repulsive effect of excluded volume interaction terms. Consequently, the excluded volume effect v_{exc} of each couple of beads times the couple number of monomer $(fN)^2$ per unit of accessible volume $V = R^3$ is proportional to the repulsion energy, that is:

$$F_{int}(R,N) = v_{exc}(fN)^2/R^3, \quad (2.3.16)$$

here ν_{exc} is associated with the factor of the 2^{nd} virial term. Hence, the free energy of the entire system results in the form:

$$F(R,N) = fR^2/b^2N + v_{exc}(fN)^2/R^3 \quad (2.3.17)$$

To determine the free energy of the entire system at the minimum level, we can apply:

$$\frac{\partial F(R,N)}{\partial R} = 0 \quad \Rightarrow \quad 2fR/b^2N - v_{exc}3(fN)^2R^{-4} = 0 \quad \Rightarrow \quad R^5 = 3/2v_{exc}b^2fN^5$$

As the excluded volume rises, a crossover to a higher stretching is predicted with the star-shaped chain radius, which scales as:

$$R \sim f^{1/5}N^{3/5} \quad (2.3.18)$$

This expression leads to the scaling behavior for the size (dimension) of star polymer [76]:

$$R \sim f^{\frac{1-\nu}{2}}N^{\nu}, \quad (2.3.19)$$

where the Flory exponent $\nu = 3/5$ in 3D, and also the exponent $(1-\nu)/2$ equals to $1/5$. Accordingly, Flory theory predicts the scaling behavior for the size of a linear chain as:

$$R \sim N^{\nu}, \tag{2.3.20}$$

where the number of arms in the chain is ignored, and the Flory exponent ν is expressed as:

$$\nu = \frac{3}{d+2}, \tag{2.3.21}$$

provided that d is the dimension in which the polymer resides. Also, the scaling exponent for real chains is assigned to be $\nu = 3/4$ and $\nu = 3/5$ in two and three dimensions, respectively. Next, we will examine how to evaluate the size of star polymer by finding the mean gyration radius and mean center-to-end distance of the polymer.

A. The gyration radius of star polymer

The first quantity that describes the average size of the star polymer is the gyration radius. Since a star polymer comprises of N beads in which each homogeneous arm connected to a single-core unit, it is convenient to define the position center of mass r_{cm}:

$$r_{cm} = \frac{1}{N}\sum_{i=1}^{N} r_i, \tag{2.3.22}$$

where the beads have equal mass and also joined by massless bonds, and r_i is the position of the i^{th} monomers. Then, the gyration radius squared is given by:

$$\langle R_g^2 \rangle = \left\langle \frac{1}{N}\sum_{i=1}^{N} (r_i - r_{cm})^2 \right\rangle = \frac{1}{N}\sum_{i=1}^{N} \langle (r_i - r_{cm})^2 \rangle, \tag{2.3.23}$$

where the place of summation and averaging can be interchanged.

B. The center to end distance

The distance from the core unit to the end is the second parameter, that is, used to measures the dimension of star polymer. Since star polymer has at least three functionalities, we can consider one of these functionalities to determine the distance between

the central unit and the end monomer. The distance between the position of the central monomer (r_c) and the end monomer of one of the targeted functionalities (r_i) of the chain R_{ce} is given by:

$$R_{ce} = r_c - r_i, \tag{2.3.24}$$

where R_{ce} is varying along each arm of the chain configuration. Although the chain ends are not significantly faced outward and therefore R_{ce} doesn't always span the largest dimension of the chain, its average length may be a good measure for the all-inclusive chain dimension. The positions of each linear arm chain in a star are denoted by $r_i (i = 1, 2, 3, ..., f)$. The mean squared distance from center-to-end R^2_{ce} of a star polymer is:

$$\langle R^2_{ce} \rangle = \frac{1}{f} \sum_{i=1}^{f} \langle (r_c - r_i)^2 \rangle \tag{2.3.25}$$

2.4 Dynamics of star polymer

In the previous section, we have introduced the ideal and real chains as a model to describe the equilibrium (or statics) features of star polymer. We will now apply the Rouse model such that we can use it to explain the dynamics properties as well. The dynamics of polymers require a time scale in which the theoretical derivations of most the parameters of interest from tiny monomeric movements are challenging [77]. A significant problem for the kinetics of polymeric materials with a more complicated conformation like the homogeneous star polymer is that not to be secure an elegant mathematical expression for the collection of dynamical eigenmodes [78]. Using the Rouse dynamic model, it is possible to characterize the time-dependent aspects of a single-star polymer by monitoring the mean-square displacement [79].

Suppose that a spherical monomer of radius a and mass m is moving through a solvent. It will experience a force that is proportional to the magnitude of bead's velocity but in the opposite direction. This fact is due to the monomer will collide more often on the front-side than on the back-side. The monomer also experiences a stochastic or random

force that varies with time $\mathbf{F}(t)$ [79]. This force is because of the continuous bombardment of solvent molecules. These two forces are summarized as depicted in Fig. (2.18).

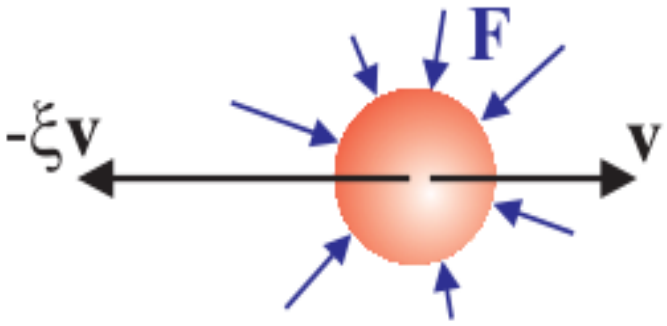

Figure 2.18: Pictorial representation of a spherical bead which experiences a frictional force and random forces **F**.

According to Newton's second law, the equation of motion is stated mathematically as [80]:

$$\frac{d\mathbf{r}}{dt} = \mathbf{v} \tag{2.4.1}$$

$$\frac{d\mathbf{v}}{dt} = -\xi\mathbf{v} + \mathbf{F} \tag{2.4.2}$$

Note that both sides of the Equation (2.4.2) are divided by the mass m of the bead. As a result, the friction constant ξ is a frequency, and **F** is an acceleration. Regarding Stokes' law, the frictional force F_s on a sphere moving with constant velocity v is given by:

$$F_s = -\zeta v = -6\pi\eta a v, \tag{2.4.3}$$

where F_s is the Stokes friction, η is the viscosity coefficient and ζ is a viscous friction constant that retards the monomer moving in the solvent. By applying Equation (2.4.3), the friction constant ξ is expressed as:

$$\xi = \frac{\zeta}{m} = \frac{6\pi\eta a}{m} \tag{2.4.4}$$

By solving Eq. (2.4.2) we have:

$$\mathbf{v}(t) = \mathbf{v}_0 e^{-\xi t} + \int_0^t d\tau e^{-\xi(t-\tau)}\mathbf{F(t)}, \tag{2.4.5}$$

where $\mathbf{v}_0$ is the initial velocity. Also, by applying integration on Eq. (2.4.2) we find:

$$\mathbf{r}(t) = \mathbf{r}_0 + \frac{\mathbf{v}_0}{\xi^2}(1 - e^{-\xi t}) + \int_0^t d\tau^{'} \int_0^{\tau} d\tau e^{-\xi(\tau-\tau^{'})}\mathbf{F}(\tau^{'}), \tag{2.4.6}$$

from which we can measure the average square displacement as:

$$\langle(\mathbf{r}(t) - \mathbf{r}_0)^2\rangle_{\mathbf{v}_0} = \frac{v_0^2}{\xi^2}\left(1 - e^{-\xi t}\right) + \frac{3\kappa_B T}{m\xi^2}\left(2\xi t - 3 + 4e^{-\xi t} - e^{-\xi t}\right) \tag{2.4.7}$$

As the value of t approaches to infinity, Eq. (2.4.7) reduces to:

$$\langle(\mathbf{r}(t) - \mathbf{r}_0)^2\rangle = \frac{6\kappa_B T}{m\xi}t = 6Dt, \tag{2.4.8}$$

where we have applied $\langle(\mathbf{r}(t) - \mathbf{r}_0)^2\rangle = 6Dt$ and from which we obtain the Einstein equation [80]:

$$D = \frac{\kappa_B T}{N\zeta} \sim \frac{1}{N} \tag{2.4.9}$$

provided that ζ is used for a single bead, but in the Rouse model, the total frictional coefficient for N number of monomers is $N\zeta$. Also, D refers to the diffusion coefficient, which is independent of the bead mass.

Besides, the dynamical feature of the star-branched chain can also be specified by the quantity we call it the center-to-end vector correlation function. From Eq. (2.4.2) we have:

$$\mathbf{r}(t) = \mathbf{r}_0 e^{-t/\tau_p} + \int_0^t d\tau e^{-(t-\tau)/\tau_p}\mathbf{F}_p(\tau) \tag{2.4.10}$$

where τ_p is the characteristic relaxation time, and F_p is a weighted mean of the random forces. Multiplying Eq. (2.4.10) by $r_p(0)$ and taking the ensemble average in all possible realizations of the stochastic force, we determine the correlation function of center-to-end vector $C_{ce}(t)$:

$$C_{ce}(t) = \langle\mathbf{r}_p(t).\,\mathbf{r}_p(0)\rangle = \langle r_p^2\rangle exp(-t/\tau_p) \tag{2.4.11}$$

2.5 Translocation of star polymer

The phenomenon of polymeric material translocation into a nanopore has been widely studied over the past couple of decades [81]. Translocation is a process of biomolecule propagating a membrane via a hole of nanometric size from the cis-side to the trans-side. As it was stated previously, translocation of polymers is crucial for diverse biological processes: transport of DNA and RNA via nuclear pores, protein transport across the membrane, swapping of the gene within bacterial pili, injection of virus into the cell, for chromatographic separation and refinement of artificial and natural polymers, and biological molecules on nanoporous substrates [81, 82]. Differently, it also has compressive technological capabilities, such as gene therapy, sequencing of rapid DNA, separation of polymers, and controlled drug delivery [83]. Additionally, the translocation of polymers from (ejection) a confining cavity has an impressive contribution to sequencing and diagnostic technology [83, 84].

A considerable number of scientific work have been devoted to examining the polymer translocation process by evaluating the average translocation time, which may be influenced by several factors: the structure of a nanopore, the polymer-pore interaction, the property of the solvent, the chain conformations, and so on, for linear chains [85]. In contrast, the translocation of polymer for the branched-chain structure, for instance, star polymers, has only started to be investigated recently. Star polymers are a special kind of branched polymers with a single branching point. They have a smaller hydrodynamic radius and viscosity in solution or melt as compared to linear polymers of an equal molecular weight [85]. These characteristics are also appealing for various utilizations such as pharmaceutical, coating, lubrication, and oil industries [86], as was reported earlier. Several scholars have also noticed the possibility of manipulating star polymers in the applications of biomedical like drug and gene deliveries [85–87]. Being structurally contrasting to linear chains, they display rich in dynamics peculiar to their structure under several experimental situations. For instance, star polymers translocation is distinguished

from the reputation mechanism whereby linear chains move in gels and concentrated solutions [17]. Also, star polymers translocation via a pore is examined by an alternative method for separation and characterization of such polymers [88].

2.5.1 Nanopore types

The process of translocation needs to be predictable and manageable as it works as an accurate measuring tool. So using suitable nanopores are significant. In the 1940s, Wallace Coulter has suggested the first applicable microscopic hole to count blood cells [89]. They have measured the size of the holes as $10\mu m$, which is somewhat larger than the cell size. In the last twenty years, the idea of threading across the hole has illustrated using the opening with the size in a few nanometers scale. This typical hole is called 'nanopore' [90]. The ion current is blocked as the polymers like proteins and DNA pass via a nanopore connected between two partitions (*cis* and *trans*), that is, filled with solvents. Thus the polymer conformation can be explained by examining the patterns of the ionic current blockade into the pore [90, 91].

One of the efficient applications of a nanopore device is DNA sequencing. The nanopore sequencing provides low cost and high speed that can allow operating at a level of single-molecule [89]. Because of technological applications and biological significance, different nanopores have been developed [92]. As displayed in Fig. (2.19a), the most general biological nanometric pore is $\alpha-$hemolysin [93]. It is produced by the *Staphylococcus aureus* (bacterium), and also causes the death of a cell by adhering with the outer membrane [93] and subsequent liberation of essential molecules such as cell depolarization, ATP, *etc.* The $\alpha-$hemolysin nanopore has a width of $1.4nm$ in the narrowest section. The amount of current nearly $100pA$ is produced across the membrane by applying $100mV$ source voltage, which depends on the content of nucleotide as a single-stranded DNA retains a nanopore [94]. The passage time of a DNA chain of a hundred (100) Cytosine bases (nucleotides) with a single-stranded is roughly $0.1msec$, which is

nearly $1\mu sec$ per Cytosine base [94]. The cavity made of an $\alpha-$hemolysin molecule is too long to illustrate current variations because of specific nucleotides of a translocation DNA. Additional biological pore (discovered by Biochemists) like the protein MspA (see

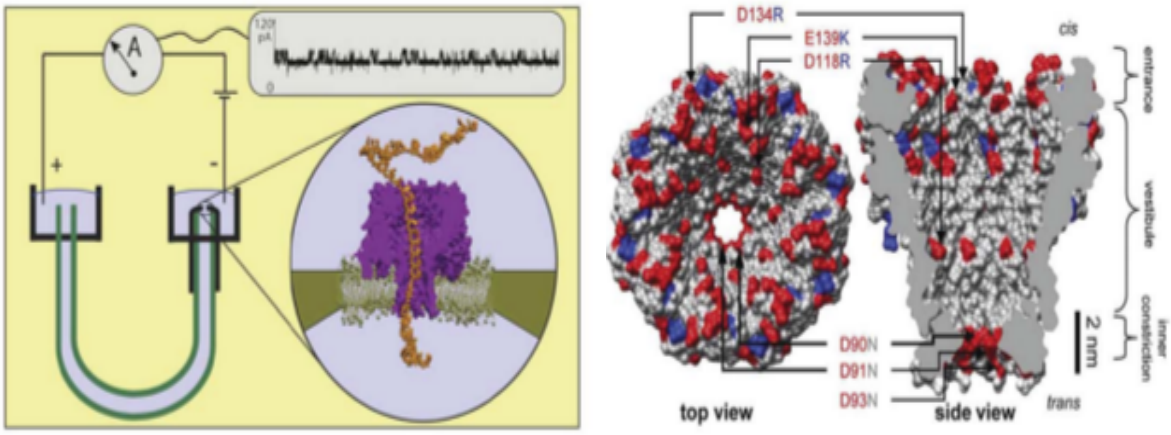

(a) (b)

Figure 2.19: Representation of types of a nanopore applied for polymer translocation. Polymer translocation describes with the aid of an $\alpha-$hemolysin pore of Staphylococcus aureus (a). Also, *Mycobacterium smegmatis* expresses using MspA porin (b).

Figure (2.19b)) was produced by using *Mycobacterium smegmatis* [95]. This biological nanometric pore has numerous benefits as compared to the α-hemolysin pore. One of the most advantages of MspA is the reduced barrel length of the narrow section of the device. For example, the narrowest part of the MspA can hold only three (3) nucleotides, whereas $\alpha-$hemolysin has ten to twelve $(10-12)$ nucleotides long $\beta-$barrel [95]. The narrower depth of a pore allows a more favorable resolution and flow rate. Due to ionic current variation, MspA requires to be adjusted to counteract gating, that is, the change of cavity arrangement [95]. Consequently, it can significantly distinguish sets of trinucleotides such as AAA, CCC, *etc.* Therefore, the advantages of biological pores cover the atomic precision of their assembled arrangement and the possibility to adjust them through genetic alteration. In contrast, biological pores rarely above $2nm$ in diameter, which is wide just solely for single-stranded RNA or DNA and chains of unfolded protein

as well [95]. These bio-pores can lose their stability when temperature, PH, and other quantities are varied. The engineering of synthetic pores was a superior solution to solve those mentioned problems [94].

Over ten years ago, numerous research groups synthesized solid-state nanopores (see Fig. (2.20)) by puncturing a hole into a membrane of thin insulating (for instance, silicon nitride (SiN), aluminum oxide (Al_2O_3)), and silicon oxide (SiO_2) [96]. They are significantly higher resistant and durable, their dimension can be tune-tuned with precision at the sub-nanometre level, and they have enhanced thermal, mechanical, and chemical characteristics. Solid-state pores can also be incorporated with optical and electronic readout mechanisms [94]. Golovchenko *et al.* accomplished the demonstration for the first time on the viability of a solid-state nanometric pore approach [97]. They have used the sculpting technique of ion-beam to fabricate well-defined sizes of nanopores in SiN membranes. The pore diameter can be increased or decreased by changing the temperature and ion rate. Recently, a 2D layered material such as molybdenum disulfide and

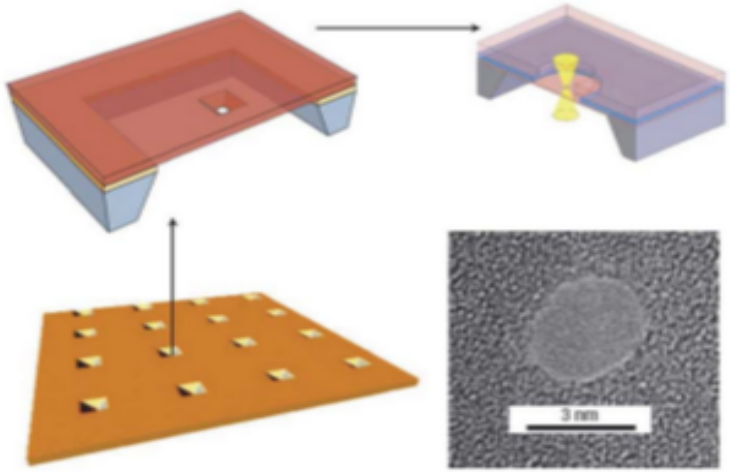

Figure 2.20: The pictorial representation shows a solid-state nanopore and the potential to generate various shapes and arrangements.

graphene also served as a layer for the solid-state pore. In recent times, hybrid pores have been developed. The first hybrid pores were developed by grabbing the $\alpha-$hemolysin proteins within SiN nanopores [98]. Enormous scientific work has been applied for adjusting

a nanopore to form a high flow rate and resolution at a low-priced [99].

2.5.2 Forced and unforced translocations

The polymer translocation into a pore faces a high entropic barrier because of the loss of a large number of possible conformations. The process of translocation includes an artificial limitation, that is, imposed to limit the first bead from leaving the pore (this limitation is unphysical), and the middle monomer is placed initially inside the pore. Also, the transport of polymeric materials across a pore is driven by other means such as electrophoretic field and pulled at one end. Consequently, the translocation process can either be classified into two types: natural (unforced) and forced [100–102].

Unforced translocation of the polymer is a kind of translocation that occurs in the absence of any driving force (or field) (see (a) in Figure (2.21)). Before starting the process of polymer translocation, the common point of the chain is anchored inside the pore. Additionally, sufficient molecular dynamics steps should be performed to ensure the two halves of the entire chain on both sides of the plane wall to get relaxed [102]. Once the equilibrium phase of the chain is secured, the middle bead is then released, and the actual translocation process begins. We signify this moment as initial (or zero) time. The escaping time is defined as the time taken by the polymer starting from either side of the wall at $t = 0$ and finishes, as the entire chain passes a nanopore for the first time.

The chain molecules are exposed to an entropic barrier as the polymeric material is moving across a narrow pore. Hence, a localized force is needed for successful translocation. The translocation kinetics of the system exposed to the current entropic limit constitutes the basic concept of translocation of DNA into pores [103]. Classified among the natural characteristics of a separated flexible chain within the solutions is its capacity to assume a large total number of beads. As a consequence, the entropy of a system (that is, $\kappa_B ln N$) becomes very high [103]. There may have additional premiums of entropic

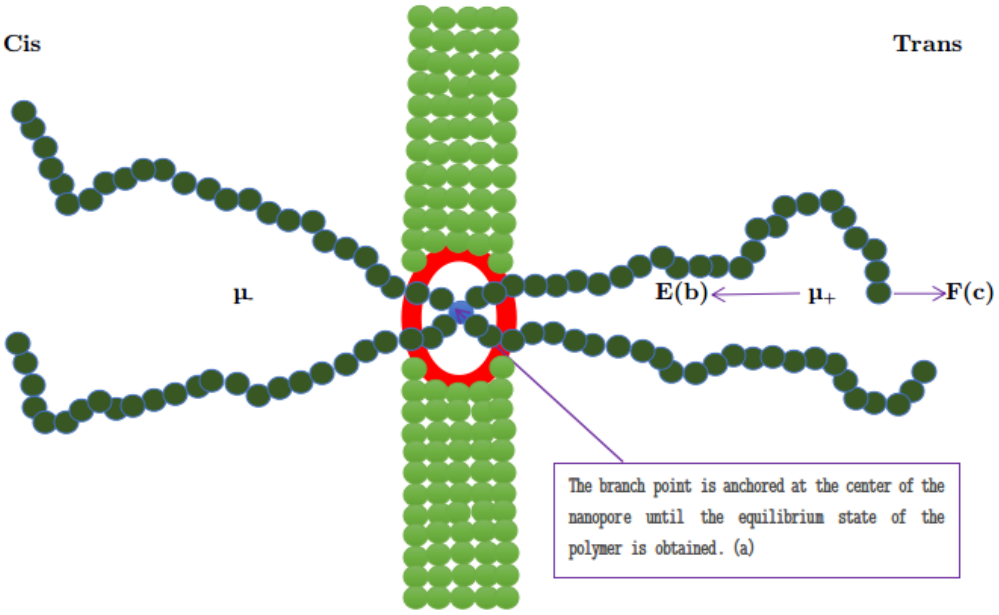

Figure 2.21: The prototype setup displays star-shaped polymer translocation via a narrow pore fastened in a membrane. Progress of the translocation is measured regarding the co-ordinate of the bead directly in the pore.

limits to the free energy because of a restructuring of solvent molecules leading to the conformational changes of the chain. As the chain is subjected to a confined constraint like a nanopore (the total polymer mass that can be any other way assumed by the polymer is reduced), the chain entropy decreases and then increases the chain free energy [103].

The study of forced translocation is the more relevant problem in the advanced level of technology since classified among the fundamental motives in the area of translocation emanates from the potential use of a nanopore translocation as a speedy and a cost-effective sequencing device for polynucleotides. Most of the experimental works considered an electrophoretic field as a means of driving force for the polymers translocation (see (b) in Figure (2.21), which displays the polymer encounters a potential difference or chemical potential between both sides) [104]. That is translocation driven under an electrophoretic field (**E**), applying on the molecules of the chain only at the center of the pore. On the other hand, in recent times, the scientific work have been examined the problem of polymer translocation via a nanometric pore subjected to a pulling force, F,

at one end of the whole chain (see (c) in Figure (2.21)) [104]. Interestingly, the mean exit times have shown a strong dependence on a technique whereby the external force is applied. Additionally, most analytical and numerical works revealed that the mean exit times are much longer when the polymer is subjected to a localized pulling force at one end than the chemical potential is involved inside a nanopore [104].

2.5.3 Translocation out of and into a cavity

Explicitly, if there is confinement, a considerable number of conformational states available in the chain will decrease, leading to the polymer's entropy reduces and thereby increases the free energy [94]. If the polymeric material is allowed to escape from the confined tube, then it will translocate out of a constraint across a pore. Also, the translocation process will proceed because of the variation of free energy among the confined tube and the chain's free state. Thus, the constrained cavity then serves as an external driving force of polymer translocation [94]. The ejection of a biomolecule out of a restricted cavity is very common in most biological systems [105]. For instance, molecules of DNA are packaged in and liberated from viral capsids. Inside a tube, the number of available structures is significantly decreased, and the restricted space enhances the interaction of the many-body system between segments. The ejection of DNA is rather involved since, inside the capsid, there might be five (5) distinct pressure contributions [106]. Those pressure exerted on DNA are the hydrostatic pressure, the osmotic pressure, the pressure by the chemical potential, the direct pressure, and the pressure by the capsid. Additionally, the translocation process also considers the DNA chain out of a confining cavity under a localized pulling force [106].

During the translocation process, Luijten and Cacciuto assumed that the chain drives by its gyration radius. But the scholars didn't reflect the fact that the chain is deformed and effectively signifies a string of blobs. Therefore, it should proceed by the size of the blobs string to propagate [107]. In recent times, Shenga and Luo performed the ejection

of a polymer in the form of a ring from a nanochannel, considering two regimes [108]. For long chains, the escape time observed in ring polymer was smaller than linear chains of equal chain size due to a higher pulling force. While for shorter chains, they were noted oppositely because the chain covers the longer free diffusion before it begins to experiences the pulling force. In reference [109], the remarkable impact of the geometric configuration of the cavity enclosing the polymer on the exit time and packaging of a polymer was reported. For flexible chains, a spherical configuration displayed a quicker packaging but slower translocation than an ellipsoid shape [109]. The scholars recommend this impact as an interpretation for preferably spherical configurations of viruses within translocation under pressure-driven, including phage λ, bacteriophage T7,*etc* [110].

Translocation of polymer from free space into an enclosed cavity is the most general case in nanotechnology and biology. For instance, the propagation of molecules of protein molecules to different cellular chambers via narrow layer tubes [105], the escaping of polymer molecules out of solutions across gel patterns in electrophoresis [111], and the transport of RNA or DNA molecules into protein and nano- or micro-fluidic canals [112]. The polymer translocation process is monitored by several factors. But the main factor is the entropic limit emanating from the contraction of chain structures in the constrained regions. Hence, a localized driving force is needed for successful translocation. While the entropic hindrance imposed by the confined region is the most common, external driving agent can take various forms, such as pulling force, electric field, *etc*. For instance, the molecules of DNA can be propagated across an enclosed cavity subjected to an electric field [112], a pressure-driven flow [113], or an electro-osmotic flow because of the surface charge of the bounded region [114].

The translocation of polymeric materials into a constrained cavity was investigated using 2D LD simulations for forms of circular [115] and ellipsoidal [116] confinements. As a comparison of these two incidents, the exit time increases in anisotropic confinement and also increases with increasing the aspect ratio in an ellipsoid geometry. Regarding

the qualitative aspects of the problem of driving a chain into an enclosed volume has biological and technological importance. The Bustamante group reported the first experiment that showed packages of bacteriophage $f29$ $66cm$ long dsDNA into a capsid of size $42 \times 54nm$ with the aid of a portal complicated molecular motor [117]. Noticeably, this occurs against a quickly increasing bending energy cost and electrostatic as well as a decrease of the chain structural entropy, leading to packaging forces as many as $57pN$ [94].

2.5.4 A brief research works on polymer translocation

Because of the universality and significance of translocation of the polymer, most simulation, experimental, and theoretical scientific works have been given attention to this problem [88]. Here, we remark the scientific works which are studied as advances in the history of translocation of the polymer.

A. Experiment

In 1940, Wallace Coulters was initiated on the notion of a translocation experiment to count the blood cells passing via the hole. In 1994, Bezrukov *et al.* applied the Alamethicin cavity to count the molecules of polyethylene oxide (PEO) [118]. Kasianowicz *et al.* (in 1996) used an $\alpha-$hemolysin channel. He noted that the nucleotide order in RNA was recognized by observing the ionic current over the channel [119]. This experimental analysis covered the mechanism for the use of translocation to describe single objects such as proteins, double- or single-stranded DNA, or, at broader scales, even cells. In 2001, Li *et al.* developed the technique of ion-beam sculpting and established a solid-state pore [120]. The movement of DNA is also recognized using the approach mentioned above. In 2005, Dekker and his collaborators assessed the time of translocation of large DNA (as many as 97000 base pairs). They obtained the scaling relationship among the exit time and the total polymer mass [121]. To examine the rate of biomolecule translocation via the solid-state pore, in 2006 Keyser *et al.* [122], in 2008 Movileanu's group [123] and

Pedone *et al.* (in 2010) [124] applied optical tweezers, electrostatic trapping, and the pore-cavity-pore complex, respectively. Recently, scholars have concentrated on developing the more complex biomimetic nanometric pores. Dekker and his partners (in 2010) showed the practicality of hybrid pore by introducing protein of $\alpha-$hemolysin into a graphene pore [125]. Most recently, Wei Guo *et al.* improved the biomimetic guards of living cells by the self-assembly of the cross-linked DNA oligomers (low molecular weight monomers) inside a solid-state pore [126]. Besides, Ge *et al.*, in recent times, conducted experiments on the ultra-filtration of star-shaped polymers of various functionality, and total polymer mass revealed that the critical rate of flow profoundly depends on the functionality and the forwarding arms within the nanochannel during translocation [127]. To this end, over the last two decades, many other experimentalists performed various experiments to study the arrangements and kinetics of polymers translocation into a pore.

B. Theory and simulation

In the last twenty years, several theoretical and simulation studies have been conducted by many scholars for both biased and unbiased translocations. Translocation of a polymeric material was initially interpreted as a quasi-equilibrium method and theoretically reduced to a problem of drift-diffusion set up using the Fokker-Planck equation. In 1996, Sung and Park started the theoretical study to examine the unbiased polymer translocation [128]. By considering the polymer as a Gaussian chain, they analyzed the natural translocation in the limit of equilibrium. Using the dynamics of Rouse and Zimm, they predicted the scaling translocation time as N^3 and $N^{2.5}$, respectively. In 1999, Muthukumar showed that the escaping time scales as N^2 for the self-avoiding chain [129]. In 2001, Chuang *et al.* confirmed that the exit time can't be smaller than Rouse equilibration time [130]:

$$\tau \sim N^{\beta}, \tag{2.5.1}$$

where $\beta = 1 + 2\nu$ and ν is a Flory exponent ($\nu_{3D} = 0.58$ and $\nu_{2D} = 0.75$). This power-law features deviated from the theoretical prediction by the nucleation theory and the Fokker-Planck equation [131, 132]. On the other hand, using the size of the star polymer in 3D shown in Eq. (2.3.19), the diffusion constant in the Rouse scaling model is displayed in Eq. (2.4.9) and the translocation time estimated in the form of $\tau \sim R^2/D$ [94], the translocation time of star polymer in terms of chain size and functionality scales as:

$$\tau \sim f^{1-\nu} N^{\beta} \tag{2.5.2}$$

In chapters four and five, using MC and LD approaches, we present a far more inclusive view of unforced translocation dynamics by proposing a scaling relationship between the translocation time and several factors such as pulling force, chain size, functionality, *etc.*

Typically, for forced polymer translocation, two main approaches have been proposed. First, the potential bias where the electrophoretic field acts inside a pore is facilitating the polymer translocation [17]. This technique can easily be checked experimentally using electrophoresis. Second, the mechanical forces in which it is acted directly to one end of the polymer is promoting the polymer translocation, that is, experimental such a technique can be confirmed by using optical or magnetic tweezers [133]. The scaling investigation of the exit time for driven translocation includes two main quantities, the total number of monomers N and an external applied force F. As noted previously, pulling a polymer at one end takes much longer times than applied the chemical potential inside a pore. This idea was verified by Kantor and Kardar (in 2004) [104]. In these cases, the power-law grows as $N^{1+\nu}$ and N^2, where ν is the scaling exponent that relates the gyration radius to N. For a linear chain polymer, Huopaniemi *et al.* (in 2007) suggested the scaling law of translocation time subjected to a pulling force [134]. For strong pulling forces, ($F > \kappa_B T/\sigma$), or moderate pulling forces, ($\kappa_B T/N^{\nu}\sigma \leq F \leq \kappa_B T/N^{\nu}\sigma$), they

found that the mean exit time obeys:

$$\tau \sim N^2, \tag{2.5.3}$$

while for weak forces, $(F < \kappa_B T/N^{\nu}\sigma)$,

$$\tau \sim N^{\beta} \sim N^{1+2\nu} \tag{2.5.4}$$

Liu *et al.* (in 2014) examined the relationship between mean exit time and the total polymer mass for field-driven translocation of star-shaped polymers across a nanochannel [16]. Accordingly, they revealed that the power-law of exit time in a strong field regime, $(N_{arm}|\triangle\mu|/\kappa_B T \gg 1)$,

$$\tau \sim N_{arms}, \tag{2.5.5}$$

and for weak-field regime, $(N_{arm}|\triangle\mu|/\kappa_B T \longrightarrow 0)$,

$$\tau \sim N_{arm}^2, \tag{2.5.6}$$

where $\triangle\mu$ takes the translocation potential of flow-driven. Moreover, the mean exit time as a function of the magnitude of a pulling force, F, is scaled as [134]:

$$\tau \sim F^{-1} \tag{2.5.7}$$

In chapters six and seven of this dissertation, we have presented a comprehensive description of the translocation of homogeneous star polymers by examining the scaling relation between the translocation time and the total polymer mass and the magnitude of a pulling force.

In recent times, despite its technological significance, comparably few studies investigating the impact of the functionality of star-shaped polymers translocation into a nanopore. In this respect, the flow-induced translocation was conducted by Liu *et al.* [16], in 2014, who manipulated dissipative particle dynamics simulations to investigate the influence of the functionality and the number of monomers per arm upon the mean escape

time. They noted that the mean escape time varied weakly with the number of leading arms. While the exit time remarkably increased with the number of trailing arms due to the limitations of the chain's functionalities that could enter a pore at the same time. In 2018, H. H. Katkar and M. Muthukumar [17] studied a field-driven translocation of star-shaped polymers into a nanopore. They used LD simulations to examine the effect of star polymer functionality, a pore length, and radius of a pore as well upon mean escape time. For star-branched chains of identical molecular masses, they noted that there exists a critical f at which τ attains a local minimum. Changing a nanopore diameter didn't significantly alter the dynamics of linear chains. For higher values of f, the average exit time became larger for narrower pores because of steric constraints, resulting in large numbers of backward arms to enter into a nanopore simultaneously can be prevented. Shing Bor Chen and Karthik Nagarajan [135], in 2019, studied on the flow-induced translocation of star-branched chains across a cylindrical pore using dissipative particle dynamics simulations. The functionality was varied with the total polymer mass is kept constant. Mean exit time exhibits non-monotonic variation with functionality. Its value is higher and shows a more variation with f when the quality of the solvent is preferred. In chapters five, six, and seven of this dissertation, the impact of translocation dynamics on the homopolymer star's functionality has been presented.

Chapter 3

Computational methods and models

In doing any simulation work, there are many approaches to be used based on the problem at hand. The most widely used simulation models are molecular dynamics (MD) and Monte Carlo (MC). In this dissertation, the translocation of multiple arms star polymers in the presence of various constraints, we have employed both MD, typically the Langevin dynamics and MC computer simulation methods. Apart from these simulation techniques, we have also implemented the coarse-grained models where the chemical details are neglected. In this chapter, the details of methods and models used for the polymer system are provided. Included are the details of the coarse-grained models and two distinct simulation techniques. Also, the overview of the simulation algorithms is described.

3.1 Coarse-grained models

By using a detailed atomistic simulation with a continuum approach, it is possible to apply the coarse-grained models for interfacial systems. The original coarse-grained modeling procedures drew from several methods. These are both molecular dynamics integration and Monte Carlo systems, lattice and off-lattice models, Lennard-Jones potentials, and hard-sphere [136]. A coarse-grained numerical simulation model that incorporates

a set of chemical monomers with a bead has been neglected all microscopic degrees-of-freedom (vibrations, bond length, *etc.*) and represents a polymer by a simplified structure (see Figure (3.1)).

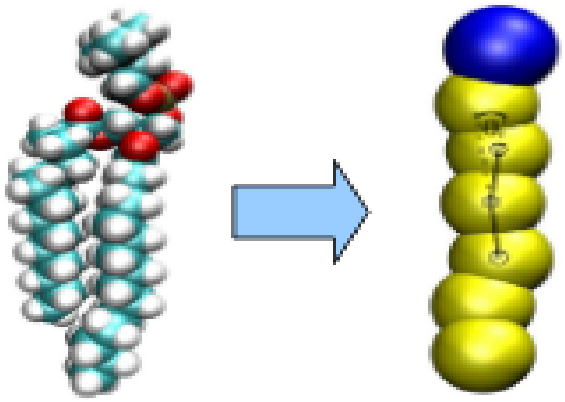

Figure 3.1: Diagrammatical representation of an atomistic model (left) and coarse-grained model (right).

A prior, we may be notified two classes of coarse-grained models: coarse-grained model is derived from a specific polymer and has no direct attachment to any explicit polymer. The first model, in practice, usually suggests that the characteristics of the model (density, potential parameters, *etc.*) needs to be managed to ensues the atomistic approach of the polymeric system in hand [136]. The purpose of devise such models rests upon the fact that they may be simulated much more effectively than their atomistic analogs. Hence, it is fascinating to split the simulation levels into two: First, one uses the coarse-grained model for determination and equilibration of large-scale features. Then, atomistic looks may be reinserted to permit a detailed comparison with experiments [136]. The second model is a universal model containing only features common to every polymer of identical chain topology [137]. For linear polymers, these features are excluded-volume interactions, bead-bead attractions, and chain connectivity as well if one needs to simulate bad- or θ-solvent situations [137]. Many of these universal models can be classified as continuum or lattice models.

3.1.1 Lattice models

Nearly half a century ago, Montroll and Orr suggested the self-avoiding walk (SAW) as a model for a linear chain in a suitable solvent [138]. Mainly, a discrete lattice like a simplistic cubic or a square lattice described the SAW, as displayed in Fig. (3.2). Every monomer takes up a single lattice site, and the bond length is the same as the dimension of a lattice constant. Also, the angles of the bond are governed by the lattice system of geometry and by the repulsive hard-core bead-bead interaction (for example, 90^0 and 180^0 for a cubic lattice, as immediate rear folding is forbidden) [138]. This model can be accompanied by attractive interactions if, for instance, a gain of energy $-\epsilon$ is linked with each occupied pair of the nearest neighbor [139]. In addition to excluded volume interactions, the numerical simulation then also has to take into account the Boltzmann factor $exp(n_{nn}\epsilon/\kappa_B T)$, where n_{nn} is the total number of nearest neighbors [139].

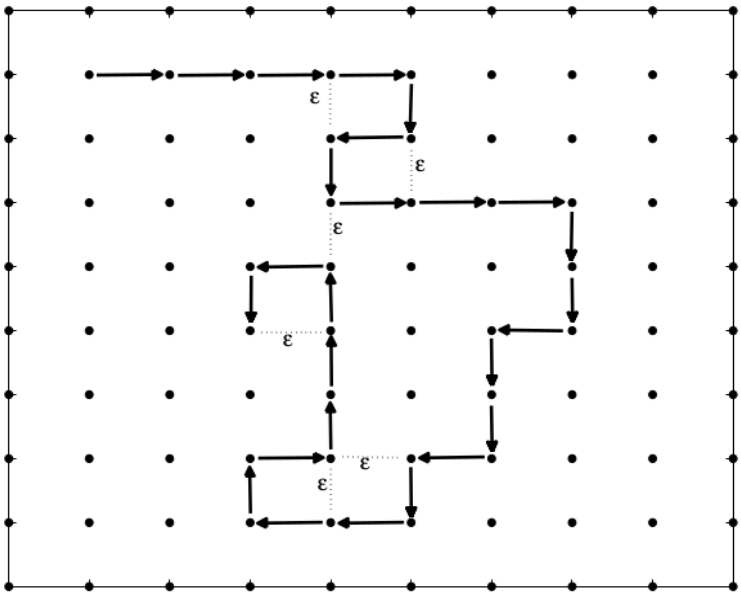

Figure 3.2: A lattice chain with twenty-seven beads is modeled by an interacting SAW. Two beads on neighborhood lattice positions but not joined by a bond constitute an unbonded neighborhood contact. The dotted lines represent the contacts.

Verdier and Stockmayer (in 1962) conducted a single SAW with a unit bond length between beads on the cubic and square lattices [140]. Under the relaxation features of

initially stretched chains and equilibrium distributions, they investigated the end-to-end distance of the chain. A SAW is a random walk (RW) that doesn't visit a lattice position it has already visited (see Figure (3.3)). In a SAW model, interactions between segments are negligible for the chain at too high temperatures [140]. Thus, the interactions among segments get into action at the smaller temperature. A SAW is an athermal walk, which considers an ensemble of RW. The following energy values are allocated for a particular walk. If parts of the walks overlay or if the walk intersects itself, it may be said that the energy is infinity ($E = \infty$), leading to the Boltzmann measurement vanishes ($exp(-E/\kappa_B T) = 0$) [140]. If the walk is SAW, then the energy value will be zero, resulting in the corresponding Boltzmann measurement becomes one ($exp(-E/\kappa_B T) = 1$). In conclusion, the Boltzmann measurement can be zero if it not SAW and one if it is SAW. If the Boltzmann measurement is not dependent on temperature, the energy is said to be athermal energy [140]. Indeed, if there is no scale of energy, the self-avoiding walks in statistical mechanics are determined exclusively using entropy [31].

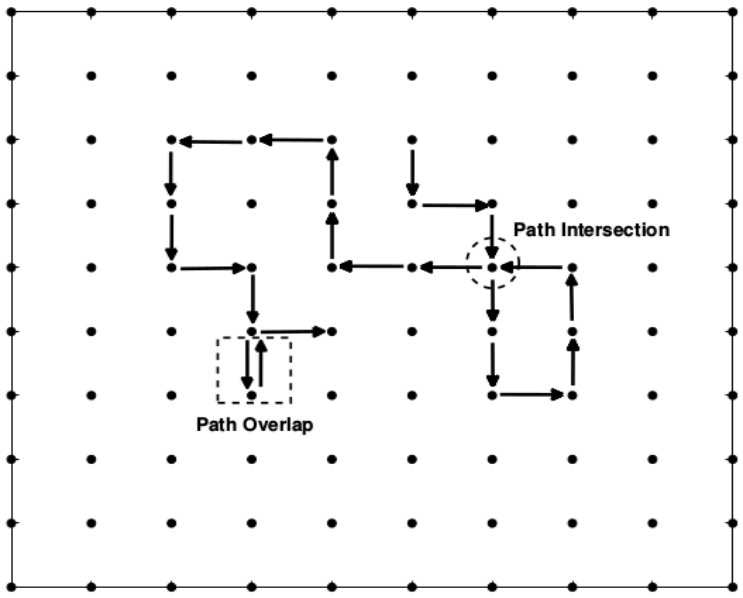

Figure 3.3: A simple RW with path overlap and path intersection for twenty-two steps.

On the other side, the bond fluctuation model (BFM) was reported by Carmesin and Kremer [141, 142], where the initial version is represented by using a two-dimensional

space. Every bead holds a considerable lattice position, while the bond length can only be allowed at $2, \sqrt{5}, \sqrt{8}, 3, \sqrt{10}$, or $\sqrt{13}$ [142]. The dynamics of the entire system are restricted to a single bead moves over the spacing of unit lattice. In later manifestations, the model is extended to 3D space, which helps to study the dense systems in keeping with its applications [143]. BFM was proposed as an option to a SAW model (single-site), which maintains the computational capability of the lattice without being interrupted by crucial challenges of ergodicity [144]. The fundamental role of BFM is to raise the dimension of a bead which now owns, rather than a single position, an entire single cell of the lattice (for instance, a square for 2D or a cube for 3D hyper-cubic lattice, see Figure (3.4)) [144].

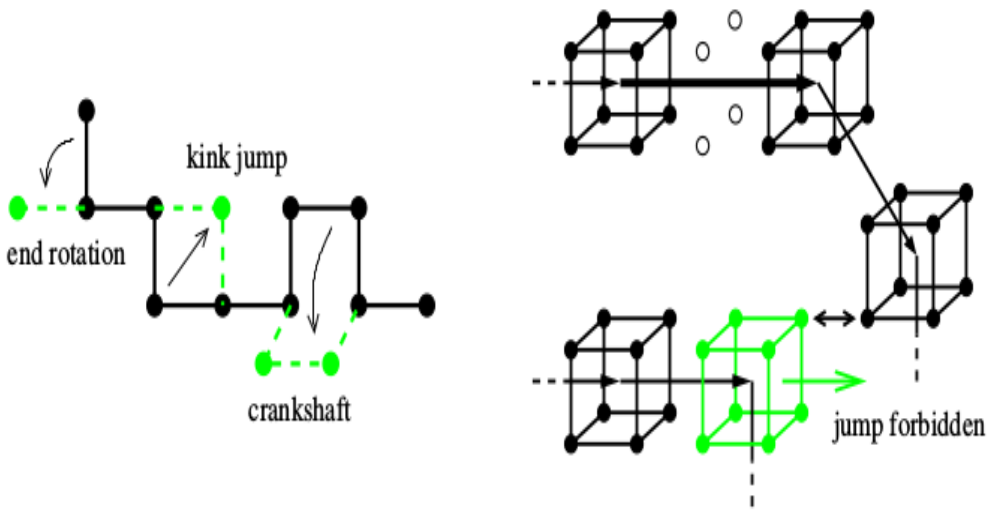

Figure 3.4: Pictorial representation of a possible configuration of beads in a 3D BFM (right-side) and SAW (single-site) of chain length $N = 10$ on a simple cubic lattice (left-side).

BFM is a lattice model that helps us to perform simulations for systems of polymers. It is useful for achieving statics and dynamics characteristics of polymers. Concerning BFM, a trial arrangement is executed by shifting a randomly picked bead from its existing location to a cite of unit lattice spacing away, in addition to classified among the

possible directions, and arranged arbitrarily with an equal probability [144]. While the entire system is set into motion, we must confirm that bond crossing doesn't happen, and the self-avoidance situation is satisfied. Thus, BFM maintains the interest of both Sokals and growth algorithms [144]. Like in a growth algorithm, the bead move is local, that is, a trial arrangement is performed by shifting a randomly picked bead. Related to the Sokals algorithm, we start with a chain of suitable dimensions. A trial arrangement, created by local rule, is granted or rejected by the Metropolis algorithm [144]. In **section 3.4**, this idea will be explained in more detail. Also, we will generate a Markov chain of lattice polymer structures; the asymptotic part of the polymer comprises a canonical ensemble from which the required macroscopic characteristics can be fixed [31].

3.1.2 Continuum model

The bead-spring model (a kind of continuum model) was introduced primarily by Kremer and Grest [145]. This approach is also called the Kremer-Grest model. Here, the closest neighbor beads along the backbone of the chain are joined together by a kind of potential that we call finitely extensible non-linear elastic (FENE). But, all the beads, both bonded and unbonded, interact via a shifted and truncated potential, the so-called Lennard-Jones (LJ) repulsion [145]. In this dissertation, we have used these two bead-spring models (FENE and LJ potentials), as depicted in Figure (3.5). These models will be described further in detail in the next section. Most importantly, to perform simulations tasks using the polymeric materials with N monomers connected by springs, explicit analytical forms for the spring potential U_{spring} and excluded volume need to be selected. A chain comprised of beads joined by springs will be employed in the numerical simulations. The excluded volume effect can also be modeled by using the repulsive potential is called the Weeks-Chandler-Andersen (WCA) [83]. This potential is the sort of LJ potential where the cutoff distance equals to $r_c = 2^{1/6}\sigma = 1.1224\sigma$, which represents the minimum value in such a way that this specified potential is to serve as purely repulsive

[145]. Even though this potential is encountered frequently in theoretical physics, there

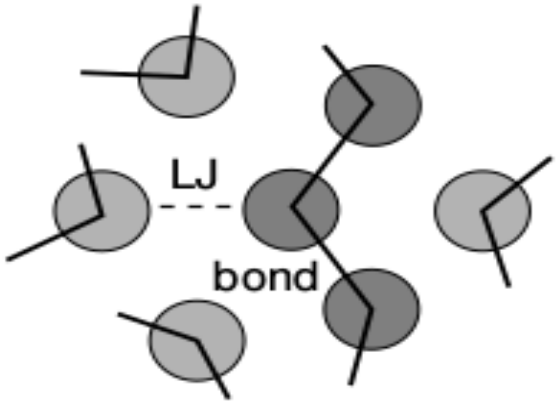

Figure 3.5: Representation of LJ (unbonded) and FENE (bonded) interactions of coarse-grained model.

is no concrete interpretation for this specific functional report here. It works just as an appropriate repulsive potential, which possesses a continuous slope so that its related force can be found after discrete displacements. Such a potential gives the point-like bead with a diameter of σ, and it is applicable for several constraints (for instance, cylinders, spheres, walls, *etc.*) in which the parameter r represents the distance normal to the geometrical surface to the center of a bead [145]. We should give attention to define the equivalent objects' dimension since this potential constitutes an exclusion length of $\sigma/2$ to the distance where the geometrical surface is nominally assigned. For example, a double-faced thin wall will have a corresponding thickness of σ, which leads to an exclusion layer of $\sigma/2$ per individual side. Then, like the WCA potential (U_{WCA}), the finitely extensible non-linear elastic springs potential (U_{FENE}) can also be observed in the theory of physics [145]. Taking the related force $F_{FENE} = -\nabla U_{FENE}$ will result in an approximation to the more general force, which pulls the two ends of the chain.

Moreover, bead-spring approaches play a crucial role in the modeling and theory of polymer kinetics. Mainly, the use of polymer kinetics and bead-spring approaches are for single-chain polymers in which the chain comprises a linear sequence of monomers

attached by harmonic springs [146]. The Rouse dynamic model presents comprehensive analytical calculations for any dynamical quantity, which provides the reason why the Rouse dynamic model deserves a special notice lies in this reality. Thus, we can consider the Rouse modes instead of using the equation of motion in favor of the specific beads [146]. Further on the profoundly studied of the non-branched chains, there are several types of polymers whose dynamics justify a closer examination. In most cases, a vital difficulty of chain dynamics with a more complex conformation like star polymers is that an elegant analytical formulation for the set of dynamical eigenmodes can't be found [146].

Currently, for homogeneous star polymer with a branching point, the dynamical eigenmodes can also be addressed. Subsequently, the dynamical features of various quantities

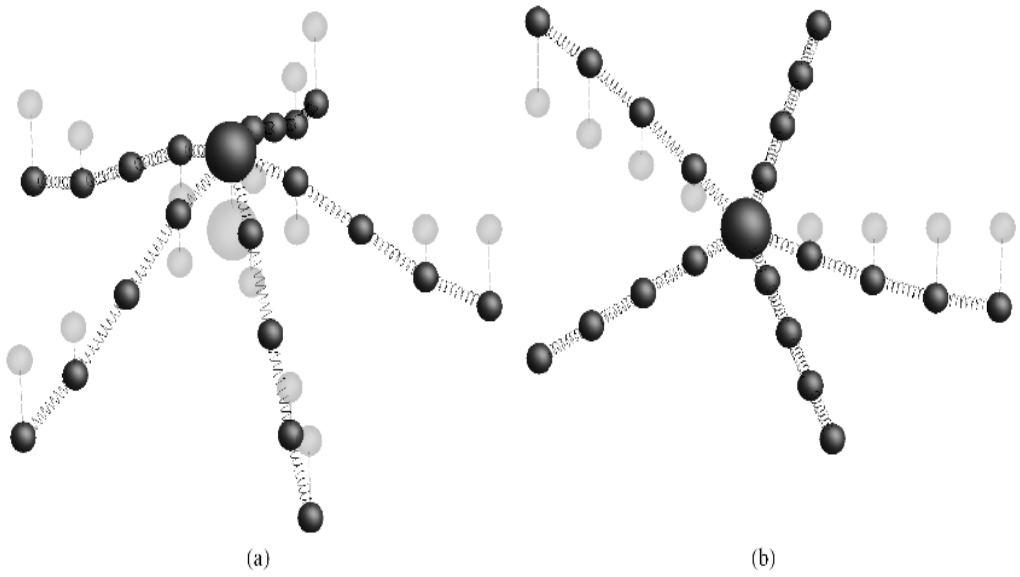

Figure 3.6: Diagrammatical representations of homogeneous star-shaped polymer to imagine the Rouse modes. Represented is a star polymer with 5-arms and consists of four beads per arm with a unit bead at the center, which has a friction coefficient five times that of the arms monomers. The transparent versions are represented the branched chains in the origin that stretched in the xy-plane for visual preference with no Rouse mode displayed in the z-direction. The dark versions are like the transparent ones just with a pure $\mathbf{X}_1$ mode (a) and $\mathbf{Y}_1^{(i,j)}$ modes (b) in the z-direction.

can be found accurately [146]. Hence, in commensuration with the Rouse dynamic model, these dynamical eigenmodes are also known as Rouse modes. A schematic representation

of star polymers with f = 5 and N = 4 can be illustrated in Fig. (3.6). Note that a superior approach to synthesize a star polymer is to connect the linear arms to a common point with attaching the ends [146].

3.2 Langevin dynamics simulation

Coarse-grained three-dimensional Langevin dynamics simulations are used to study the dynamics and statics properties of uncharged star polymers of varying functionalities through an uncharged solid-state nanopore and from a cylindrical cavity under the influence of a pulling force. Additionally, we have also performed the simulation without using any localized force, where the central monomer is fixed inside the nanopore.

3.2.1 Coarse-grained models for the polymer and the constraints

In this work, we have been used coarse-grained bead-spring models that combine several atoms into a single bead, as depicted in Fig. (3.7), and allows for a much longer length and time scales. Coarse-grained models are often manipulated in polymer studies.

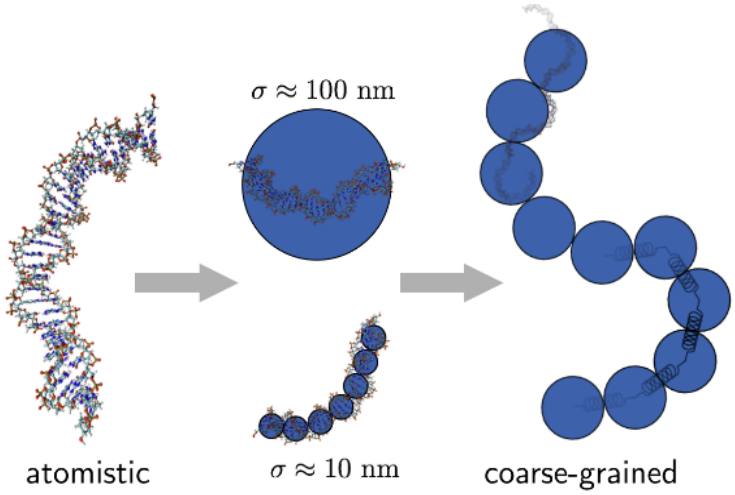

Figure 3.7: Schematic representation of the dsDNA structure that displays the atomistic model (left) and coarse-grained model (right).

A coarse-grained model treats a set of chemical monomers as a bead (active monomer)

by neglecting the microscopic degrees of freedom. It retains only the most crucial traits common to all chains of the same conformation. Such a model includes characteristics such as chain connectivity, excluded volume effect, interactions between monomers, and interactions between polymer and constraints (that is, polymer-nanopore, polymer-wall, and polymer-cavity).

A star-shaped polymer is composed of flexible arms, each with N_{arm} monomers of mass, m, joined to a branching point by the ends monomers. For the representation of star polymer, a simulation snapshot is illustrated in Fig. (3.8). Star-shaped polymers are modeled using a coarse-grained model, that is, a bead-spring model in which polymers are treated at the bead level rather than considering the atomic detail, as noted previously. Valuable atomistic features are coarse-grained out by using coarse simulation beads, which promotes numerical computation. The choice of such a model is supported by the capacity to be applied to a large group of chains since it doesn't take into account detail chemical compositions [147].

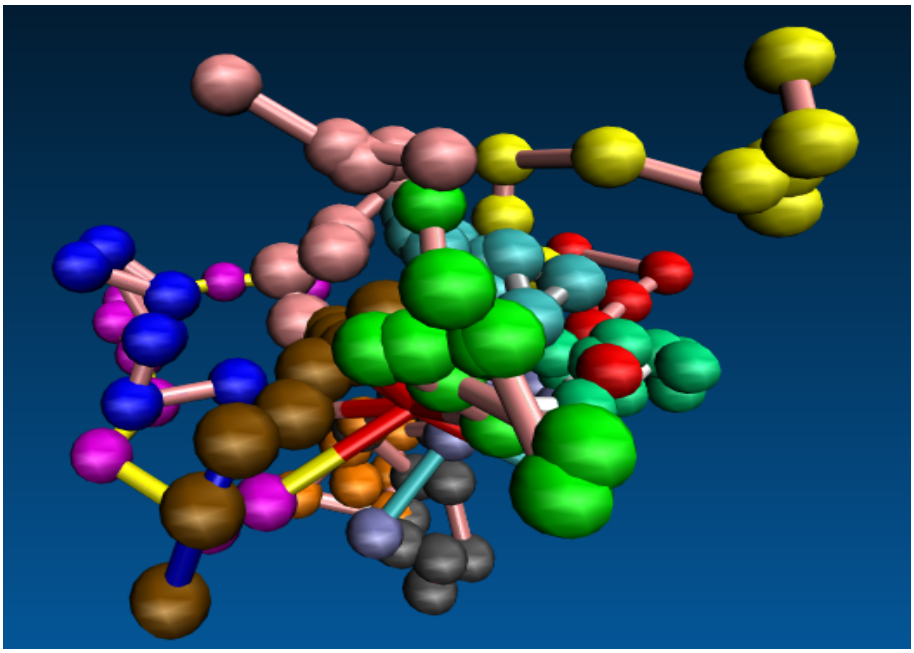

Figure 3.8: Simulation snapshot of a 12-arms star polymer with the number of monomers $N_{arm} = 10$ in each arm at the state of change of conformation (equilibrium). For better visibility, various arms are colored differently.

In this model, star polymers are described as a set of monomers sequentially connected between them to form the arms. Then, the arms are attached to a central monomer (the core unit of the entire chain), where the consecutive beads are connected by using U_{FENE}. As shown in Fig. (3.9), bonded interactions (the connectivity between neighborhood beads) are treated through a spring potential function. This function can be written as [148]:

$$U_{FENE}(r) = -\frac{1}{2}kR_0^2 ln(1 - r^2/R_0^2), \tag{3.2.1}$$

where R_0 is the maximally allowed distance between consecutive monomers, k represents a spring constant, and r is the distance among bonded monomers.

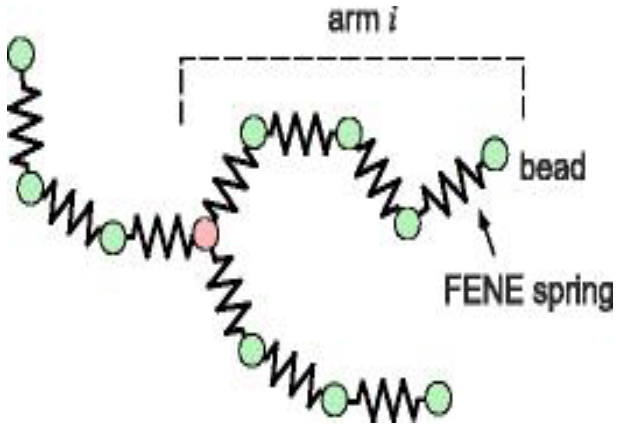

Figure 3.9: Pictorial representation of a coarse-grained model of three-arms star polymer in which the beads connected each other using springs (FENE).

The effect of excluded-volume interactions among unbonded beads are modeled by the truncated, shifted, and short-range repulsive Lennard-Jones potential (U_{LJ}). LJ potential is accounted for the interaction between non-bonded monomers. This potential is truncated and shifted at $r_c = 2^{1/6}\sigma$, which only emphasizes its repulsive part. Mathematically, this potential can be defined as:

$$U_{LJ}(r) = \begin{cases} 4\varepsilon\left[\left(\frac{\sigma}{r}\right)^{12} - \left(\frac{\sigma}{r}\right)^{6}\right] + 4\varepsilon, & r \leq 2^{1/6}\sigma \\ 0, & r > 2^{1/6}\sigma, \end{cases} \tag{3.2.2}$$

where U_{LJ} is the standard 12 – 6 LJ potential, r is the distance between consecutive beads, σ is the bead diameter, ε is the potential depth, and 4ε is the constant energy

term added to obtain the continuous potential at $r = r_c$. Using Equations (3.2.1) and (3.2.2), these two potentials are depicted in Fig. (3.10) in terms of the distance among two successive monomers. Combing purely attractive U_{FENE} and purely repulsive U_{LJ} gives a non-symmetric potential with the value of energy minimum at $r_{min} \approx 0.9609\sigma$. The average bond length, $\langle r \rangle$, shows a temperature-dependence since the potential is asymmetrical. For $\kappa_B T = 1.0\epsilon$, $\langle r \rangle$ nearly equals to 0.9679σ, while for $\kappa_B T = 0.02\epsilon$, it shows $\langle r \rangle \approx 0.9610\sigma$, which approaches to the minimum potential.

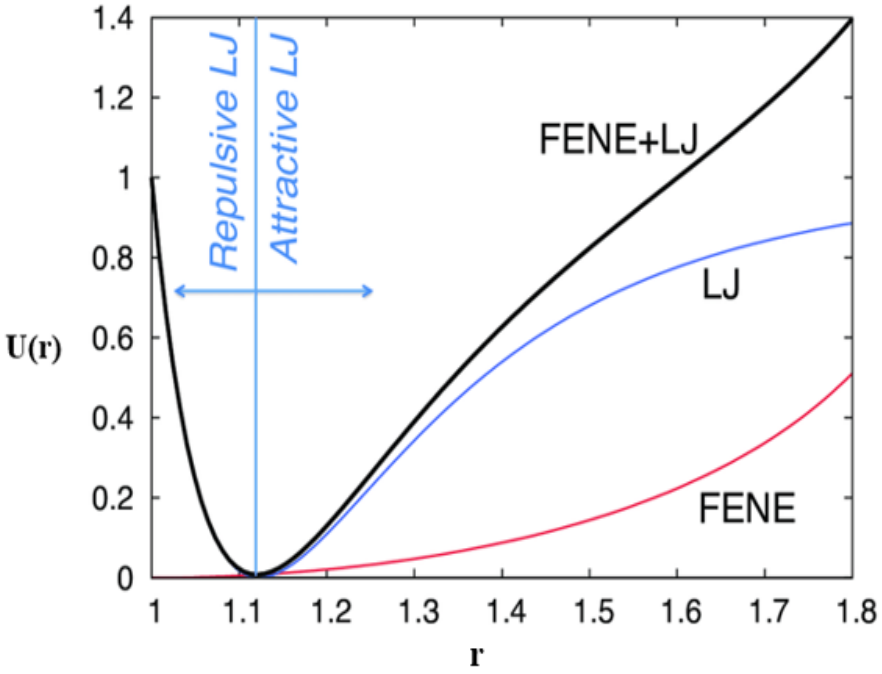

Figure 3.10: Pictorial illustration of a FENE potential (red line), a modified LJ potential (blue line), and the sum of both contributions (black line) using the Kremer-Grest quantities leading to slightly asymmetric energy encompassed by steep walls that inhibit rigorous overstretching and overlap. The blue vertical line denotes the cutoff-distance r_c, where the WCA potential as purely repulsive interaction vanishes for $r \geq r_c$.

Additionally, a three-dimensional simulation box is partitioned into two compartments, cis and trans, by a w unit thick rigid membrane modeled using a single vertical wall. A small hole of radius r is built at the center of the wall. Also, we have considered the case where the wall is connected to a cylindrical cavity of length L. The wall of the cavity and nanopore are made of immobile and uncharged spherical monomers of sizes 1.0σ.

3.2.2 Pulling force

In a typical translocation experiment, a localized pulling force is subjected to the first monomer of the leading arm, which resides at the center of the nanopore. The pulling force remains constant throughout the translocation process. To simulate this in an approximate sense, we set a constant pulling force, which is acting along the axial direction of the cavity. The pulling force is set to a non-zero value after the system has been completed the equilibration phase. A pulling force is a constant force of magnitude F, which acts only on a single monomer located inside the pore (or the end monomer of the leading arm), and it is given by:

$$\mathbf{F}_{pulling} = F\hat{\mathbf{e}}, \tag{3.2.3}$$

where $\hat{\mathbf{e}}$ is a unit vector perpendicular to the plane of a nanopore.

3.2.3 Equation of motion

In this simulation task, the Kremer-Grest bead-spring model is used to mimic a DNA strand, only involving sterical repulsion and binding of the monomers [147–149]. Every monomer trajectory is computed by integrating a 3D Langevin equation. The Langevin equation is a stochastic differential equation in which two force terms have been included in Newton's second law to approximate the influences of neglected degrees offreedom. The first term is a frictional force, and the second one is a stochastic (random) force. For instance, the impacts of solvent molecules not explicitly exist in the system being simulated would be estimated in terms of frictional pull on the solute as well as casual kicks associated with the thermal movements of the solvent molecules. Since friction resists the motion, the former additional force is proportional to the particles velocity but in the opposite direction. In the LD simulation, the two models of potentials (mentioned in Eq. (3.2.1) and (3.2.2)) and the driving (pulling) force (described in Eq. (3.2.3)) along with the random and frictional forces, are used to solve the equations of motion for every

monomer. Langevin's equation for the motion of each monomer i is:

$$m\ddot{\mathbf{r}}_i = \mathbf{F}_i^C + \mathbf{F}_i^R + \mathbf{F}_i^F, \tag{3.2.4}$$

where each bead i with mass m and position vector $\mathbf{r}_i$ is subjected to conservative, random, and frictional forces, $\mathbf{F}_i^C$, $\mathbf{F}_i^R$, $\mathbf{F}_i^F$, respectively. The conservative force, $\mathbf{F}_i^C$, is a combination of the repulsive excluded volume potential (LJ), the bonded bead-spring potential (FENE) and single pulling force, $\mathbf{F}_{pulling}$, which only applied on the end monomer of the leading arms; it is expressed as:

$$\mathbf{F}_i^C = -\nabla(U_{LJ} + U_{FENE}) + \mathbf{F}_{pulling}. \tag{3.2.5}$$

The random force, the second term in Eq. (3.2.4) represents frequent collisions with implicit solvent molecules, and its magnitude can be derived from the fluctuation-dissipation theorem [150]. If you want to get useful information out of this, we have to average over all possible realizations of $\mathbf{F}^R(t)$ with the initial velocity as a condition (refer Eq. (2.4.5)). Thus, a useful quantity, for example, is:

$$\begin{aligned}\langle \mathbf{v}(t)\cdot\mathbf{v}(t)\rangle_{\mathbf{v}_0} = v_0^2 e^{-2\xi t} &+ 2\int_0^t d\tau e^{-\xi(2t-\tau)}\mathbf{v}_0\cdot\langle\mathbf{F}^R(t)\rangle_{\mathbf{v}_0} \\ &+ \int_0^t d\tau' \int_0^t d\tau e^{-\xi(2t-\tau-\tau')}\langle\mathbf{F}^R(\tau)\cdot\mathbf{F}^R(\tau')\rangle_{\mathbf{v}_0}\end{aligned} \tag{3.2.6}$$

Then, we have to make some assumptions about the conditional means of the stochastic forces. In the sense of the chaotic nature of the stochastic forces of the following assumptions seems to appropriate:

$$\langle \mathbf{F}_i^R(t)\rangle = 0, \tag{3.2.7}$$

$$\langle \mathbf{F}_i^R(t)\cdot\mathbf{F}_i^R(t')\rangle_{\mathbf{v}_0} = C_{\mathbf{v}_0}\delta_{ij}(t-t'), \tag{3.2.8}$$

where δ_{ij} is the Dirac delta function. Inserting Equations (3.2.7) and (3.2.8) into Eq. (3.2.6), we get:

$$\langle \mathbf{v}(t)\cdot\mathbf{v}(t)\rangle_{\mathbf{v}_0} = v_0^2 e^{-2\xi t} + \frac{C_{\mathbf{v}_0}}{2\gamma} \tag{3.2.9}$$

where γ is the friction coefficient. For large t, this should be equal to $3\kappa_B T/m$, from which it follows that:

$$\langle \mathbf{F}_i^R(t) \cdot \mathbf{F}_i^R(t') \rangle = \frac{6\kappa_B T\gamma}{m} \delta_{ij}(t - t'). \tag{3.2.10}$$

This result is called the fluctuation-dissipation theorem.

Finally, the frictional drag force applied to each bead mimics the viscous damping due to solvent molecules. This force is expressed as:

$$\mathbf{F}_i^F = -\gamma \mathbf{v}_i, \tag{3.2.11}$$

where $\mathbf{v}_i$ is the velocity of the bead.

The three-dimensional equations are integrated using the velocity-Verlet algorithm implemented in the molecular dynamics package ESPResSo [30] using a time step $dt = 0.001$. The above algorithm is employed based on a Taylor expansion of the coordinate of a monomer at time $t + \triangle t$ and $t - \triangle t$ about time t:

$$r(t + \triangle t) = r(t) + v(t) \triangle t + \frac{f(t)}{2m} \triangle t^2 + \frac{\partial^3 r}{\partial^3 t} \frac{\triangle t^3}{3!} + O(\triangle t^4), \tag{3.2.12}$$

and

$$r(t - \triangle t) = r(t) - v(t) \triangle t + \frac{f(t)}{2m} \triangle t^2 - \frac{\partial^3 r}{\partial^3 t} \frac{\triangle t^3}{3!} + O(\triangle t^4), \tag{3.2.13}$$

Adding these two equations and subtracting $r(t - \triangle t)$ on both sides gives:

$$r(t + \triangle t) = 2r(t) - r(t - \triangle t) + \frac{f(t)}{2m} \triangle t^2 + O(\triangle t^4). \tag{3.2.14}$$

This new position is accurate to order $\triangle t^4$. The velocity is calculated from the trajectory and accurate to order $\triangle t^2$:

$$v(t) = \frac{r(t + \triangle t) - r(t - \triangle t)}{2 \triangle t} + O(\triangle t^2). \tag{3.2.15}$$

For instance, the velocity will be used for finding the kinetic energy or temperature. Typically, this algorithm is useful as it conserves the total linear momentum and the net energy of the system.

3.2.4 Simulation parameters

In our simulations, physical quantities are described by using the reduced units to manipulate numerical values of the order of unity. Thus, LJ parameters ε and σ are used as units of energy and length, respectively. Additional reduced units are LJ time which is found by combining LJ parameters $t_{LJ} = (m\sigma^2/\varepsilon)^{1/2}$, time step $dt = 0.001t_{LJ}$, temperature $T = \varepsilon/\kappa_B$, and friction coefficient $\gamma = m/t_{LJ}$. As displayed in Table (3.1), the reduced units used in the simulation are related to their corresponding system of international (SI) units.

Table 3.1: Summary of variables with the respective dimensions in both SI and LJ units: $\kappa_B = 1$ in LJ units.

Variables	**LJ units**	**SI units**
$Length$	σ	$1.0 \times 10^{-9} m$
$Mass$	m	$5.2 \times 10^{-25} kg$
$Energy$	ε	$4.1 \times 10^{-21} J$
$Temperature$	ε/κ_B	$295K$
$Force$	ε/σ	$4.1pN$
$Time$	$\sqrt{m\sigma^2/\varepsilon}$	$11.26ps$
$Friction$	γ	$4.6 \times 10^{-14} kg/s$

As noted previously, in a coarse-grained LD simulation, every atom is represented by a model force-field, which accounts for the interactions between the atom and the system. ESPResSo uses contributions to the potential energy function from the following interactions: $U_{total} = U_{bonded} + U_{non-bonded}$. U_{bonded} defines the bonded interaction between monomers, which is the FENE potential. The bond strength is monitored by the force constant of the spring k (see Eq. (3.2.1)). The minimum value is chosen so that it inhibits the chain crossing. If the value of k is too large, due to the large FENE energy, the long time simulation is unfavorable. Therefore, the choice of k should be within a certain range, which blocks the chain crossing and also give the convergence of the simulation for reasonably long LD simulation time. Besides, the limit of the chain extensibility is

represented by R_0. As in reference [12], the values $R_0 = 2\sigma$ and $k = 7\varepsilon/\sigma^2$ are used for the FENE potential parameters. However, $U_{non-bonded}$ describes the non-bonded potential, which is the Lennard-Jones 6-12 potential (see Eq. (3.2.2)). To save computational time, the long-range interaction is calculated only for the pair, which are within a fixed distance, namely a cut-off distance r_c. The strength of the attractive LJ potential ε also depends on the solvent condition. The solvents which are responsible for the negligible attractive LJ interaction are considered as the good solvents. In such a condition, the non-bonded pairwise interaction is given by the repulsive part with cut-off distance $r_c = 2^{1/6}\sigma = 1.12246\sigma$. The bead diameter σ and the potential depth ε have the same value, which is equal to 1.00. On the other hand, the magnitude of an external pulling force F is varied between 3 and 10.

3.3 Monte Carlo simulation

Monte Carlo approaches are a part of simulation techniques that deal with the statistical mechanics of a system, generating configurations based on probability, and measuring the mean of desired parameters. This approach allows processes that signify a long physical time to be replicated in simulations as it doesn't follow time evolution in a deterministic way. Trajectory data acquired from Monte Carlo simulations are approximate due to the dependence on statistical mechanics [151].

Monte Carlo simulations of branched polymer chains using a lattice model were conducted. The object of this simulation is a homogeneous star-branched polymer of equal arms length, which consists of two different arms $f = 3$ and 4 and put into a simple square lattice. In this simulation, we have used the maximum number of monomers 301 and 401 for $f = 3$ and 4, respectively. Initially, the chain configuration resides in the middle of the Monte Carlo box, where the simulation is conducted with and without using constraints. That is, free diffusion and unforced polymer translocation approaches are considered. The

chain model of the system undergoes a series of local conformational changes to mimic the kinetics of a polymer [151]. Among the most crucial attributes when simulating this system is characterizing the equilibration phase. Thus, before trying to perform any computation, the system should be allowed to attain equilibrium. Characterization of the equilibrium state is a highly sensitive duty, particularly for our system, whose characteristics varying considerably in time. Thus, equilibration can be done via a simple monomer moves in a reasonable amount of computing time (not significantly longer than the final run to determine characteristics). Therefore, we have used an efficient Monte Carlo algorithm to study the equilibrium and kinetics features of a single-star branched polymer. The Monte Carlo simulations have been conducted along with the excluded volume effect. The excluded volume is recognized by prohibiting the double possession of lattice sites. To this end, the detailed static and dynamic features of the star-branched polymer have been investigated through the examination of widely used physical quantities.

3.3.1 Bond fluctuation model

As noted previously, Kremer and Carmesin introduced the original bond fluctuation model (BFM). In our simulations, we have used a modified version suggested by Shaffer. A detailed investigation of Shaffer's version reveals that it reproduces the significance of qualitative properties of the dynamics of entangled polymer chains [151]. In Shaffer's approach, the beads are placed on a simple square lattice and satisfied the excluded volume effect in which only a single monomer may occupy a given position at any given time. The bonds connecting the monomers are limited to a set of three possible bond lengths: $1, \sqrt{2}$, and $\sqrt{3}$, where their units are represented in the lattice spacing [151]. The bond crossing is prevented by imposing restrictions upon bond mid-points (unspecified bond crossing must proceed through an arrangement in which bond mid-points intersect). The chain movement is performed by attempting to relocate a randomly chosen monomer to a randomly chosen nearest-neighbor lattice site. The movement is accepted if it obeys

the excluded volume effect, bond-crossing limitations, or approved bond lengths, and discarded if it does. $N \times n_{star}$ attempted moves set to a unit Monte Carlo time step

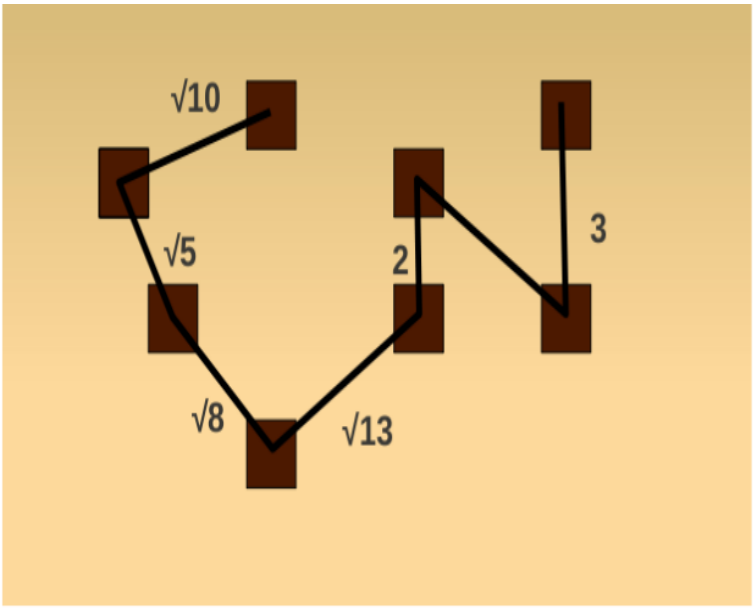

Figure 3.11: This diagram displays a two-dimensional system based on the bond fluctuation approach with the corresponding bond length restriction: $2 \leq l \leq \sqrt{13}$ and with all possible moves in between these bond length restriction boundaries.

(MCS), where MCS is eventually used as the dimension of time (N is the total number of monomers per chain and n_{star} is the number of star polymers in the simulation box) [152].

The name bond fluctuation approach obtains from the fact that the bond length (or vector **v**) joining between consecutive monomers along a chain varies over a notable degree. The basic idea is to enhance the size of a monomer, which now occupies rather than of a single site, an entire unit cell of the lattice (for instance, a 2D square lattice). This increased monomer size has two significant outcomes:

i) A priori, several distinct bond vectors can occur. This multitude is limited by two situations. First, neighboring beads may not overlap. This restricts the bond length $l \geq l_{min} = 2$ (in units of the lattice spacing). Second, the hard-core bead- bead interaction should serve to avoid two bonds from crossing each other in the course of the simulation.

In the case of 2D, this only enforces an upper bound on the bond length $l \leq l_{max} = \sqrt{13}$, and some other smaller bond vectors also have to be excluded (see Figure (3.11)). The

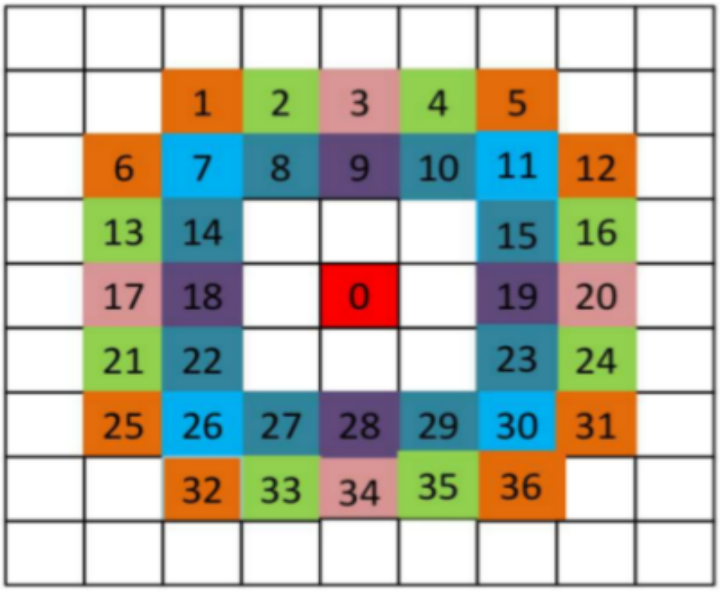

Figure 3.12: Description of a monomer 0 on the plaquette in the center, the bead connecting bead 0 can occupy one of the thirty-six allowed plaquettes, which are labeled by numbers 1 to 36.

resulting collections of possible bond vectors are $\mathbf{v} = [2,0], [2,1], [2,2], [3,0], [3,1], [3,2]$, where $[\cdot]$ represents a class of bond vectors sharing equal bond length, but varying in direction [152]. For example, the class $[2,0]$ includes all vectors with a length of 2 and direction along the lattice axis (4-directions).

ii) Ergodicity challenges are much less strict than for the single-site SAW. For the BFM, a local N-conserving move includes choosing a bead at random and of trying a displacement by a unit lattice spacing in a randomly selected lattice direction. If the tried displacement serves both the bond vectors restraints of the above requirements and the effect of excluded volume interaction, the trail move is confirmed [152]. In conclusion, the lower limit $l_{min} = 2$ assures the effect of excluded volume interaction, while the upper limits $l_{max} = \sqrt{13}$ avoids bonds from crossing each other. This idea is favored by considering that various local conformations produce segments of the backbone of varying lengths (see Fig. (3.12)).

3.3.2 Metropolis algorithm

The MC methods can also be used based on the Metropolis algorithm, which is a weighted sampling technique that checks out the configurational part of the phase-space. The method relies on the application of a Markov chain to produce a set of states for the system that indicates a state only depends on its immediately preceding state and the presence of a finite number of before-mentioned states. Moreover, at equilibrium, the detailed balance condition must be noticed. Accordingly, the number of transformations from the state of equilibrium to some other different state exactly cancel each other [31]. The non-deterministic algorithm of the MC approaches suggests that there is no fixed time associating with relaxation toward the equilibrium state, causing this method a poor selection for the sampling of dynamic features. But such approaches do exist and are commonly practiced. If this requirement is not satisfied, then the system may be brought in a state of non-equilibrium. For each change of a given system, the energy of the current (new) state is measured. Then, the difference in energy from the earlier state is determined. To this end, the new state is allowed when the energy difference between them is less than zero. If the new state energy is higher, still, the state may only be granted based on a partially random ground. The following algorithm displays in six steps how a trial moves from one state to another is performed for a system of N-particles identified by their position coordinates $r_p = [x_p, y_p, z_p]$ and a maximum displacement quantity σ [31]:

(1) Pick a particle p at random and pick three random numbers n_1, n_2, n_3 in the given interval $[0, 1]$.

(2) Calculate the new positions of the particle:

$$x_p^{new} = x_{old} + (2n_1 - 1)\sigma$$
$$y_p^{new} = y_{old} + (2n_2 - 1)\sigma$$
$$z_p^{new} = z_{old} + (2n_3 - 1)\sigma$$

(3) Calculate the change in energy between the new and old positions of the particle: $\triangle U = U_{new} - U_{old}$.

(4) If the energy difference is less than zero ($\triangle U < 0$), then accept the move and replace the old coordinates: $r_p^{new} = r_p^{old}$. Then update the energy: $U_{new} = U_{old} + \triangle U$.

(5) If the energy difference is greater than zero ($\triangle U > 0$), pick another random number n_4 on the given interval $[0, 1]$, and calculate the following:

$n_4 < e^{-\beta \triangle U}$: accept the move, update positions and energy.

$n_4 > e^{-\beta \triangle U}$: reject the move, leave position and energy unchanged.

(6) Pick another particle at random and proceed again regarding steps 1 through 6.

3.3.3 Simulation parameters

As noted earlier, our simulation work on free diffusion of star polymers is based on coarse-grained lattice Monte Carlo simulations via the Bond Fluctuation method. In this lattice model, the simulation box is prepared by using a square lattice of dimensions 5000 by 5000 (in lattice units). Star polymers of two functionalities ($f = 3$ and $f = 4$) are considered. For both arms, the arm length N_{arm} = 10, 20, 30, 60, 80, and 100 what corresponded to total number of beads N = 31, 61, 91, 181, 241, and 301 for $f = 3$ and N = 41, 81, 121, 241, 321, and 401 for $f = 4$, respectively. To obtain a fully equilibrated configuration, 10^6 Monte Carlo Steps (MCS) per monomers is allocated. After equilibration, 3000 sets of data are recorded for every $N \times 10^6$ MCS. Unlike the Langevin dynamics simulation, any local interaction potentials such as LJ and FENE are not be considered. However, in a two-dimensional simulation box, the neighbors along the chain must be within a certain bond distance, which is to vary in the range $2 \leq b_l \leq \sqrt{13}$, where b_l is the bond length between two consecutive beads in units of lattice spacing. The minimum distance that guarantees the excluded volume effect is set to 2 while the bond crossing is restricted by using the value of the upper limits, which is equal to $\sqrt{13}$.

Regarding the unforced translocation of star polymers through a nanopore, the entire chain is propagated into the pore without applying any driving force of the external field, the pulling force, or the chemical potential gradient. Thus, the driving force in the simulation is zero. For 2D simulation, the membrane is in the x-y plane and perpendicular to the x-axis, and the nanopore is a rectangular void with length $l = 3$ and width $w = 4$. Like the case of free diffusion, the same values are assigned in the following simulation parameters: the functionalities of star polymer, the dimension of the simulation box, Monte Carlo time steps for the phase of equilibration, and also for the actual process of the simulation, and the extreme values in the bond fluctuation method. However, in this particular case, different values of chain sizes are used, which are ranging from $N = 31$ to 151 and $N = 41$ to 201 for $f = 3$ and 4, respectively. In addition, the final results of the simulation are averaged over 100, 000 independent simulations run. To this end, all the above simulation parameters, including both the free diffusion and the unforced translocations, will be described in detail in the next chapter.

Chapter 4

A 2D Monte Carlo simulation of three and four arms star polymers

4.1 Introduction

In this chapter, we present a detailed study regarding the statics and dynamics features of single stars. The main reason for working on single-star simulations is to ensure that our lattice stars are adequately free. It should be indicated that our single star is not a good model for a star polymer in dilute solution, as we do not recognize any hydrodynamic interactions. In our simulation work, we analyze the movement of such branched polymers using a 2D Monte Carlo approach, which involves the bond fluctuation algorithm and writing the Fortran code. We have categorized the simulation tasks into two forms: one is the free diffusion in which the polymer is diffused without any constraints, and the other is the undriven translocation where the polymer is propagated in the presence of a nanopore. Here we have studied various equilibrium and kinetics features of star polymers with three and four homogeneous arms. We investigated the mean radius of gyration and the distance from the common center to the end monomer of star polymers to specify its statics properties. We also examined the average center-of-mass-displacement of star polymers to describe its dynamical features. From this time-dependent parameter, we found the self-diffusion coefficient. Finally, the dependence of mean exit time on the total number of monomer displays a standard scaling behavior.

4.2 Description of the model

For computational convenience, we have employed $f = 3$ and $f = 4$ arms star polymers with similar arms of length N_{arm} emanating from and connected to a common origin called a branching point. For star polymers, the total number of monomers is set to $N = f \times N_{arm} + 1$, where it includes the common origin. Star polymers were developed just on a square lattice, with and without constraints, under the condition of volume excluded effect, that is, bond crossing or bond lengths restriction. The polymers movement is obtained by trying to relocate a randomly chosen monomer to a randomly chosen nearest-neighbor lattice site, which indicates one of the four lattice directions. The trail move is accepted if it does not violate excluded volume and rejected if it does. Hence, in our system no long-range attractive and local potentials were present.

In the absence of obstacles, the polymer beads are randomly distributed throughout the available space of the simulation box with dimensions 5000×5000 (in lattice units).

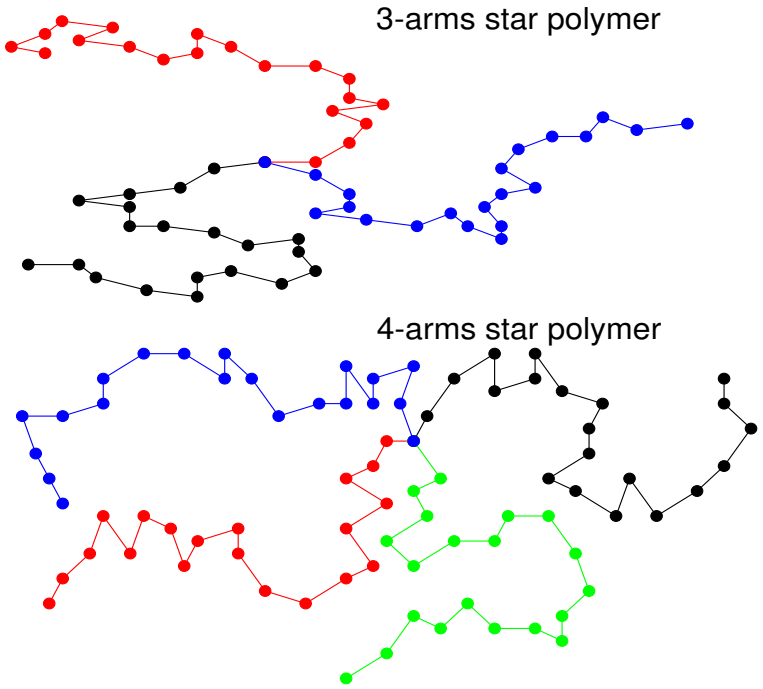

Figure 4.1: The scheme showing the conformational change of star polymers with three arms (top) and four arms (bottom) in an unconfined simulation box.

The schematic representation of the polymers free diffusion in the present study is displayed in Figure (4.1). The corresponding maximum polymer's total number of monomers are $N = 301$ and 401, for $f = 3$ and 4, respectively. The polymer is then allowed the equilibrium state by executing a Monte Carlo simulation of 10^6 time steps per monomers, which is sufficiently long for the dimension of the polymer to attain its equilibrium value. To get reliable numerical results, we conducted a long run during which the trajectory was registered. Typically, the averaging is done over 3000 independent simulation runs. Each experimental step continued with the equilibration phase.

Next, we have considered an undriven translocation of three and four arms star polymers into a nanopore. Undriven translocation is also termed as a free translocation that occurs without driving force (for instance, the external field, the pulling force, etc.). Figures (4.2a) and (4.2b)) are depicted the simulation setup. In the first stage, we built a 2D plane wall with a rectangular nanopore in the center of the simulation box. The constraint wall is composed of immobile and neutral monomers. However, all other monomers of the polymeric materials are in motion. The nanometric pore is formed by clear away the monomers around the middle of the square wall. Its dimensions (length l and width w) are kept fixed at $l = 3$ and width $w = 7$ in lattice units. The position of the common point of the polymer is in the center of the nanopore. But the chain arms are shared on either of the two sides (cis and trans) of the wall. Due to the symmetrical features of branched polymers with functionality $f = 4$, the arms are distributed equally on each side of the wall. While the arms arrangement is more complex for $f = 3$. Here two possible arrangements are observed, including two arms in the cis-side or one arm in the trans-side and vice versa. Before starting the simulation of polymer translocation, the central bead is anchored in the center of the nanopore, and the arms are held in long MC steps on either side of the wall to achieve equilibrium position, as shown in Figure (4.2a). Once the equilibrium state is achieved: First, the monomer is liberated at the branch point, and then the polymer translocation process begins. The simulation is allowed to run for

$N \times 10^6$ MC time steps. The translocation time is the time that the last monomer of star polymer leaves the nanopore on either side of the wall (see Fig. (4.2b)). Since the dynamics of polymer propagation is a highly fluctuating process, each exit time interval can vary greatly. For all translocations of various chain sizes, which is ranging from $N = 31$ to 151, and $N = 41$ to 201, for $f = 3$ and 4 respectively, we obtained the final results by averaging the recorded data over $100,000$ independent simulations.

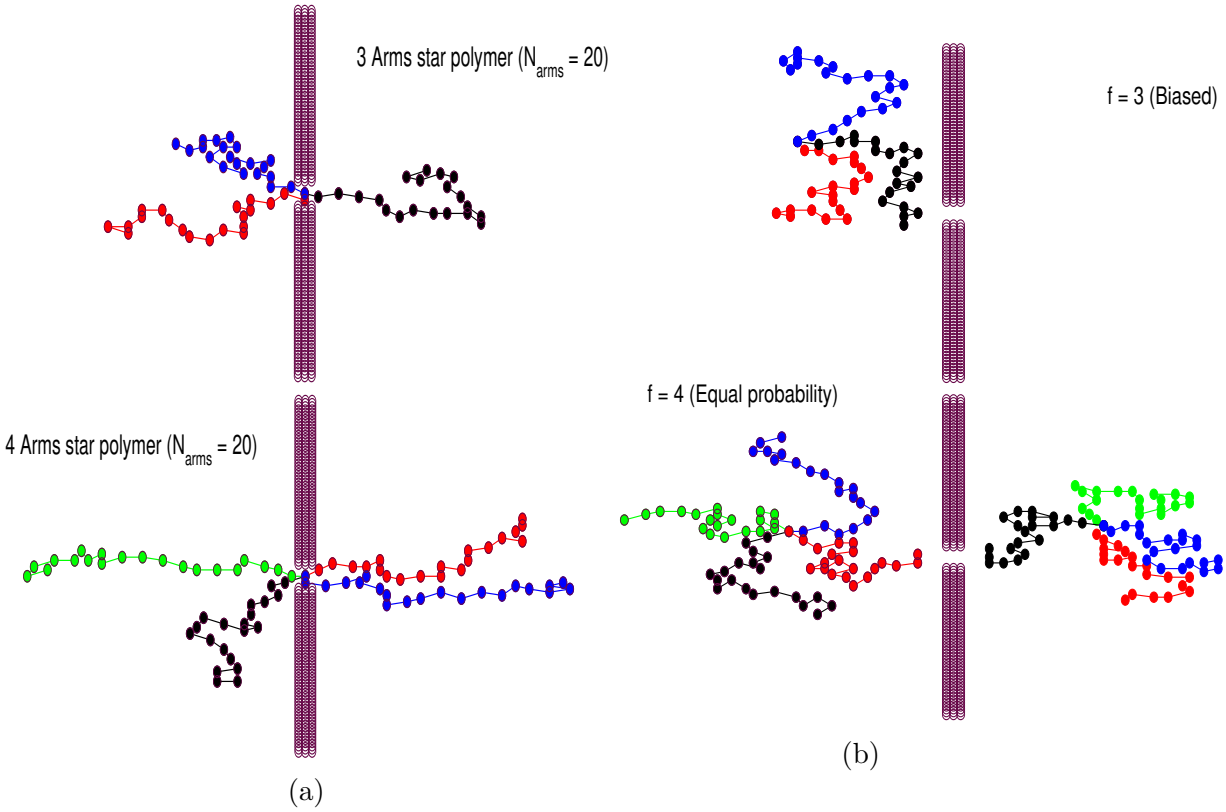

Figure 4.2: Snapshots of unforced translocation of star polymers through a nanopore: (a) before translocation and (b) after translocation. Top) three arms, bottom) four arms. The total number of the beads is $N = 61$ for $f = 3$, while $N = 81$ for $f = 4$.

4.3 Results and discussion

A. Statics properties

Simulations were performed for the given model of homogeneous star polymers on two different numbers of arms and then the increase in molecular mass. Each branched macromolecule consisted of the arm length $N_{arm} = 10, 20, 30, 60, 80,$ and 100 what corresponded to the total number of beads $N = 31, 61, 91, 181, 241$ and 301, and $N = 41, 811, 121, 241, 321$ and 401, for $f = 3$ and 4 respectively. Quantities specifying the size of the macromolecular chains were calculated for the systems under consideration. Thus, the dimension of the star-shaped polymer was characterized by the mean radius of gyration, $\langle R_g \rangle$, and the mean center to end distance, $\langle R_{ce} \rangle$. In our Monte Carlo approaches, the simulation results of both $\langle R_g \rangle$ and $\langle R_{ce} \rangle$ were listed in Table (4.1). As a detailed analysis of scaling behavior has been described recently, we have limited our study to the impact of the molecular mass of a polymer on the equilibrium shape of a chain [76]. Based on the Flory theoretical method, we have examined the scaling predictions of the mean radius of gyration and mean center to end distance.

Table 4.1: The data of $\langle R_g \rangle$ and $\langle R_{ce} \rangle$ for the statics properties of star-branched polymers with two distinct number of arms ($f = 3$ and 4) and various polymer masses. The size of a bead is equal to $b = 1$ lattice unit.

	$\langle R_g \rangle$	$\langle R_{ce} \rangle$		$\langle R_g \rangle$	$\langle R_{ce} \rangle$
N	$f = 3$		**N**	$f = 4$	
31	10.13	15.46	41	10.85	13.93
61	16.75	26.06	81	18.00	23.47
91	22.64	35.19	121	24.27	31.74
181	38.00	59.19	241	40.95	54.03
241	48.17	75.64	321	51.21	68.85
301	56.45	88.32	401	59.59	79.91

4.3.1 Dependence of $\langle R_g \rangle$ on the total mass of the chain

One of the most important demonstration of statics features of star polymer is evaluating the radius of gyration through Eq. (2.3.23). It can be noticed that $\langle R_g \rangle$ increases

with increasing the size of the polymer, as the simulation data shown in Table (4.1). Consequently, the longer radius of gyration is also seen for star polymer with higher functionality. For the two well-defined functionality that we considered, the values of the mean radius of gyration are sketched versus the total number of monomers with varying N in Figure (4.3). These results under a linear curve fitting display the scaling exponents 0.758 and 0.751 for three and four arms, respectively. As for the two functionalities over a wide range of chain size, our results have been shown that $R_g \sim N^{\nu}$, where $\nu = 0.75$ in 2D. Accordingly, the simulation results of the mean radius of gyration in the log-log plotting agreed with the theoretical predictions of power-law function for the linear chain polymer in two-dimension [76]. That is, the influence of the polymer mass on the radius of gyration, where the impact of the star's functionality is considered, is consistent with the analytical expression in Equation (2.3.20).

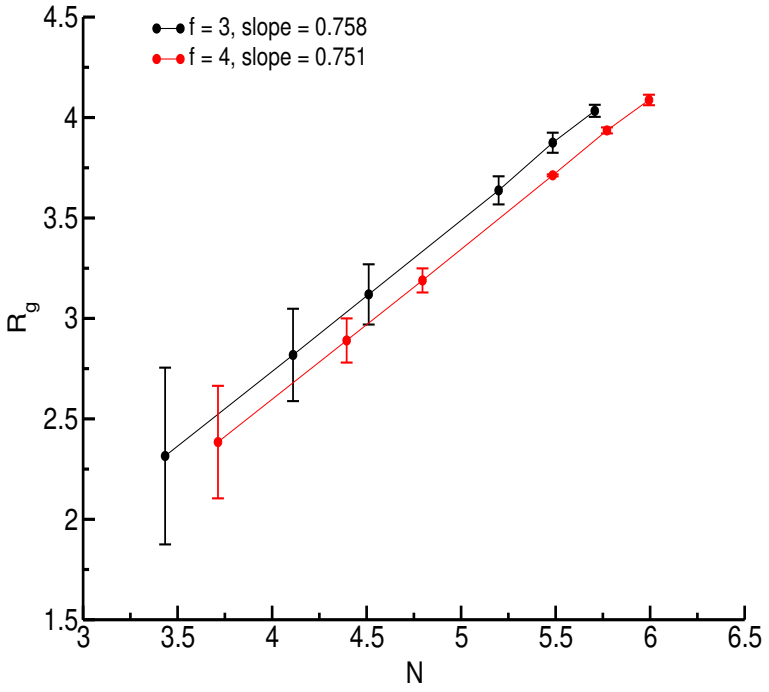

Figure 4.3: A log-log plot of the radius of gyration as a function total mass of the polymer where the number of arms of the star polymer is under consideration. Note that the number of monomers on each arm length of star-shaped polymers (with functionalities f = 3 and 4) is ranging between $N_{arm} = 10$ and 100.

4.3.2 Dependence of $\langle R_{ce} \rangle$ on the total mass of the chain

The other quantity that characterizes the equilibrium size of the star polymers is the average distance from the central monomer to the end monomer of each arm. Like R_g, the center to end distance depends on the total number of segments and the number of arms of the homogeneous star polymers. In order to record the simulation data of R_{ce}, we have used Eq. (2.3.25) for single-stars with two functionalities $f = 3$ and 4. The influence of the total mass of star polymers on R_{ce} is also depicted in Table (4.1). We observed that R_{ce} increases with increasing the total mass of the star polymers. This is due to the increase in the total mass of the polymer leads to the system to occupy a larger space with longer arm lengths. Figure (4.4) presents the results of the log-log plot of the mean center to end distance as a function of chain sizes for two different functionalities with finite intervals of N. The numerical exponent of R_{ce} with N increases from 0.768 for $f = 3$ to 0.770 for $f = 4$. Consequently, we found the scaling behavior of the dimension of star

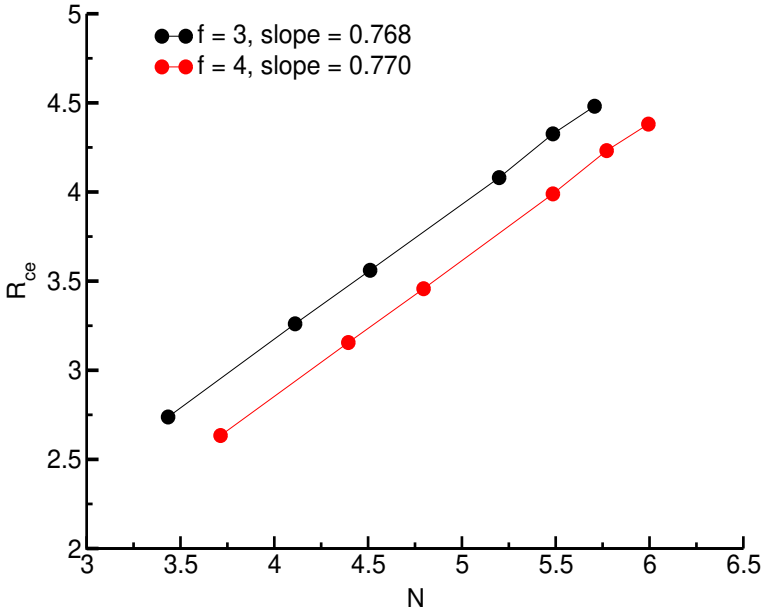

Figure 4.4: log-log plot of center to end distance as a function of the size of the branched polymer where the number of arms of star polymer is under consideration. Here the number of monomers on each star's functionality (f = 3 and 4) is varied between $N_{arm} = 10, 20, 30, 60, 80,$ and 100.

polymers with N close to $R_{ce} \sim N^{0.77}$, as indicated by the solid red ($f = 3$) and green

($f = 4$) lines in Fig. (4.4). This scaling behavior nearly agrees with the self-avoiding random walk exponent in a two-dimensional simulation for a single chain polymer [76].

To this end, the distance from the central monomer to the end monomer is larger as compared with the result of the radius of gyration for both three and four arms of star polymers, as shown in Fig. (4.3) . This is due to the computation of R_{ce} only considers the distance between the common origin and the head monomers (that is, arms in the entire chain are included). However, R_g includes the position of all the beads as they are mostly measured from the chain's center-of-mass.

B. Dynamics properties

In this section, we present our simulation results and discuss them in the view of scaling arguments provided that the dynamics properties are characterized. The change in position of the non-linear polymers at a particular time is usually expressed in two forms. The first is based on the notion that the polymers moved under constraint-free diffusion, provided that the mean square center-of-mass displacement is examined. Then, from this time-dependent quantity, we obtained the self-diffusion coefficient, D. The second means of expressing the change of position of polymeric materials is the translocation of polymers through a nanometric pore in the absence of a local driving force. For the two well-defined functionalities ($f = 3$ and 4), the mean square center-of-mass displacement as a function of MC time steps has been studied by varying the total number of monomers. Additionally, we have investigated the relationship between the total number of monomers and the self-diffusion coefficient and the translocation time as well. These results show the standard power function as predicted theoretically by Rouse dynamics.

4.3.3 Dependence of self-diffusion coefficient on N

To study the impact of the total mass of star polymers on the rate of free diffusion, we first examine the mean square center-of-mass displacement (MSD) in a two-dimensional

lattice (in xy direction). The MSD as a function of Monte Carlo time steps (t) is represented as [36]:

$$\langle (\mathbf{x}_{cm}(t) - \mathbf{x}_{cm}(0))^2 + (\mathbf{y}_{cm}(t) - \mathbf{y}_{cm}(0))^2 \rangle = 4Dt, \tag{4.3.1}$$

where ($\mathbf{x}_{cm}(t)$, $\mathbf{y}_{cm}(t)$) is the position center of mass at a time t and ($\mathbf{x}_{cm}(0)$, $\mathbf{y}_{cm}(0)$) is the position center of mass at a time $t = 0$. Hence, the molecular mass of $f = 3$ star polymer is varied between $N = 31$ and 301. For comparison, we also study star polymer with functionality $f = 4$ where the chain sizes are in the range $N = 41$ - 401.

Figure (4.5) illustrates the simulation results of MSD versus MC time steps for star polymers of functionalities $f = 3$ and 4 with various polymer sizes. As expected, we

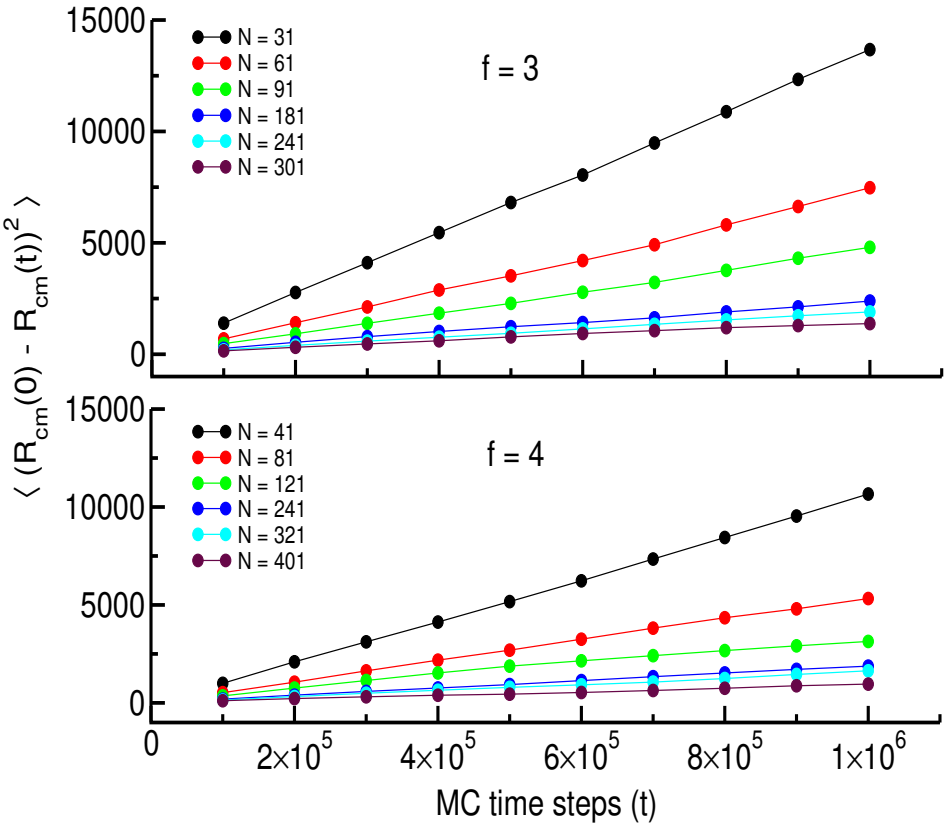

Figure 4.5: The mean square center of mass displacement versus MC time steps for single-star systems with three-arms (top) and four-arms (bottom). Note that the number of monomers in each arm of a star polymer is 10.

find a pronounced system-size dependence with a slower dynamics in a larger polymer functionality (or molecular weight). For the given number of arms, MSD increases linearly

with time (that is, the MSD reaches the linear diffusive regime).

By exploiting the MSD, we can determine the infinite system size of the center-of-mass diffusion coefficient for a single-star polymer with two distinct functionalities. Thus, the self-diffusion coefficient can be calculated from MSD according to Eq. (4.3.1) as:

$$D = \frac{\langle (\mathbf{x}_{cm}(t) - \mathbf{x}_{cm}(0))^2 + (\mathbf{y}_{cm}(t) - \mathbf{y}_{cm}(0))^2 \rangle}{4t} = \frac{s}{4}, \tag{4.3.2}$$

where s is the slope of the graph of MSD versus MC time steps (see Fig. (4.5)), and it can also be expressed mathematically as $s = \text{MSD}/t$. The values for these quantities are listed in Table (4.2).

Table 4.2: The data of s and D for two different star's functionalities ($f = 3$ and 4) with various polymer masses.

	s	**D**		**s**	**D**
N	$f = 3$		**N**	$f = 4$	
31	0.013615	0.00340375	41	0.010691	0.00267275
61	0.0074424	0.0018606	81	0.0053611	0.001340275
91	0.0047975	0.001199375	121	0.0030716	0.0007679
181	0.0022933	0.000573325	241	0.0018796	0.0004699
241	0.0018982	0.00047455	321	0.0016156	0.0004039
301	0.0013955	0.000348875	401	0.00091118	0.000227795

Figure (4.6) displays the diffusion coefficient versus the total mass of the polymers with functionalities $f = 3$ and 4, where D is extracted from the mean-square displacement. The self-diffusion coefficient can be evaluated by considering the log-log linear curve fitting with the help of Eq. (4.3.2), as described in Fig. (4.6). Consequently, the numerical values of D decrease as the total number of monomers increase for both three and four arms of star polymers. However, for smaller N, the difference in diffusion coefficient between the arms is insignificant, while for larger N, we explore a pronounced variation on D. Thus, the effect of N on D can easily be described as the total number of monomers is increasing.

As a consequence, the active polymer movement is retarded as the total polymer mass increases (due to the formation of a denser structure). Therefore, the simulation outcomes of D reveals a power-law behavior $D \sim 1/N$. This result agrees with the standard Rouse scaling law, which is observed in a single-chain system [80].

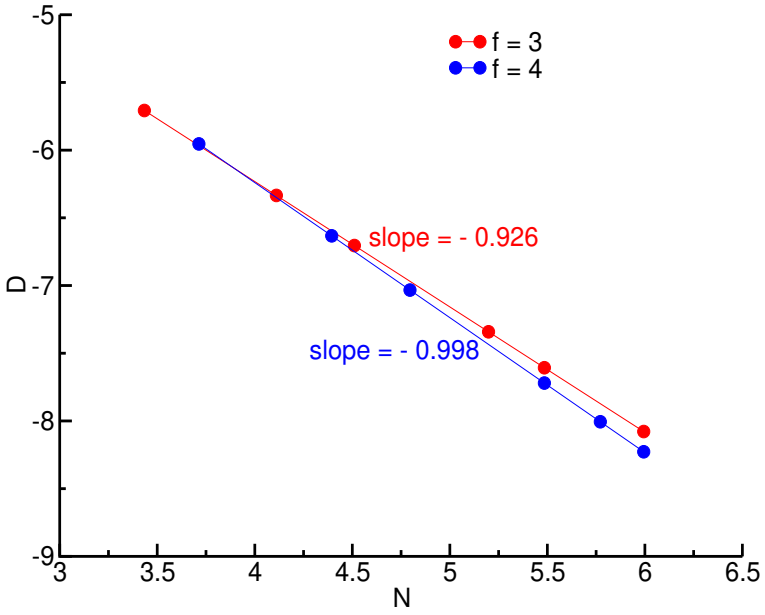

Figure 4.6: A log-log plot of the self-diffusion coefficient as a function of the total polymer mass. Here, the number of monomers in each arm is varied between $N_{arm} = 10, 20, 30, 60, 80,$ and 100.

4.3.4 Mean translocation time as a function of N

To study further on the dynamics features of star polymers with $f = 3$ and 4, we have considered the translocation process of polymers through a nanopore in the absence of driving force. To study the system translocation dynamics, we examined the effect of the total mass of the chain upon the average exit time. In this case, the number of monomers in each arm is allocated between $N_{arm} = 10$ and 50. Since the translocation is remarkably slow in the absence of a local driving force, we considered polymers with the total number of monomers only up to $N = 151$ and 161, for $f = 3$ and 4, respectively. In addition, we used the constant parameters such as length, $l = 3$ and width, $w = 7$, of nanopore in

lattice units.

We first described the translocation time distribution profile of star polymers with two distinct functionalities, $f = 3$ and 4. Figure (4.7) is depicted as the probability distribution curve of mean escape times of star polymers with four different chain sizes. The probability distribution profile of these two functionalities, denoted as $f = 3$ and $f = 4$, indicates the successful translocation ratio of the two arms left and two arms right, and two arms left and one arm right or vice versa translocation events to all successful translocation attempts, respectively. A successful translocation event can be defined as the system propagation through the nanometric pore either to the left or the right side for 4-arms and nearly to one side for 3-arms. For the two conformations in the overall

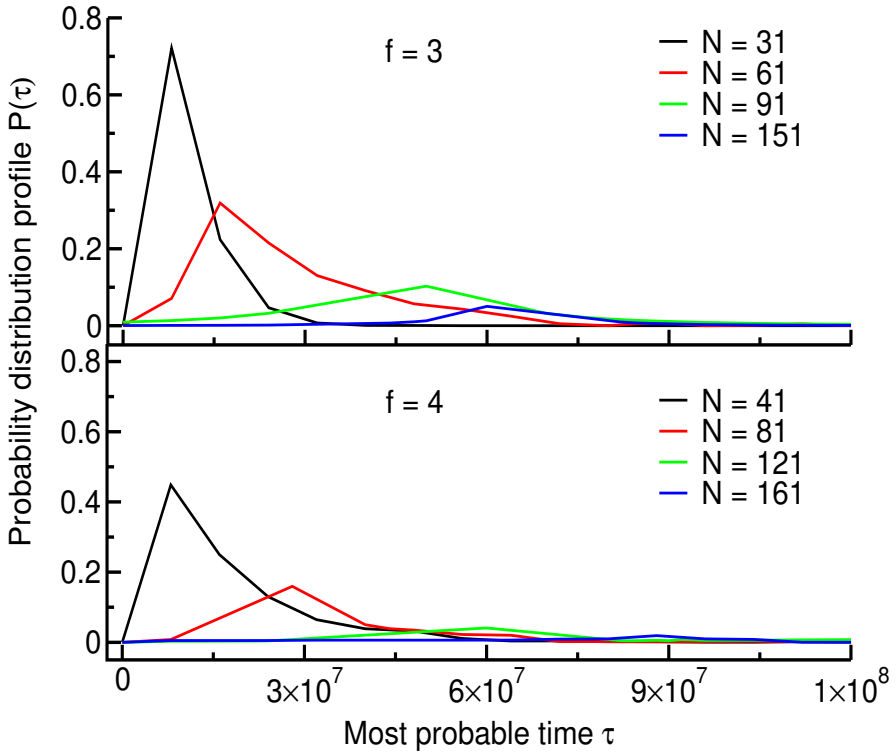

Figure 4.7: Probability distribution function $P(\tau)$ as a function of most probable time for the translocation under two different functionalities and molecular mass within a two-dimensional simulation.

successful polymer propagation, the peak value of $P(\tau)$ decreases with the increase of the total number of monomers or functionality. This is because of decreasing the possibility

of identifying the given number of arms entering the nanometric pore at the same time in the equilibrium state. We describe the most common probable exit time τ_p as the time corresponding to the tip in the distribution profile. Additionally, the number of arms or the total number of monomers increases with the most probable time. We also find that the escape times are distributed on a wide range with a long tail and wider distribution width for larger polymers size. While at a smaller total mass of polymers, the long-tail character becomes weak but still exists, and the distribution of translocation time gradually becomes narrow and symmetric.

Now let us discuss how the translocation time depends on the chain sizes for both arms of star polymers and compare their respective mean escape times with each other. In such a case, examining the power-law relation between the translocation time, τ, and chain size is our main interest. In our simulations, to obtain the scaling relation between the mean exit time and the total number of monomers, the motion of star polymers propagation via a nanometric pore can be considered as the Rouse motion. For this reason, the hydrodynamic interaction is ignored. The mean exit time may be thought as the time cost by the polymer chain to propagate a distance of the order of its radius and scales as:

$$\tau \sim R_g^2/D \sim N^{1+2\nu}, \tag{4.3.3}$$

where R_g is the radius of gyration with $R_g \sim N^{\nu}$ and D is the diffusion coefficient with $D \sim 1/N$ for the Rouse model, as it was stated earlier for linear chain polymer [94, 104].

Figure (4.8) shows the simulation results of the mean translocation time, $\langle\tau\rangle$, as a function of the chain size N. We find that the scaling exponents $1+2\nu = 2.55 \pm 0.04$ and 2.57 ± 0.04, for the two functionalities $f = 3$ and 4, respectively. Therefore the log-log plot of $\langle\tau\rangle$ vs total mass of the polymers at $f = 3$ and 4 gives a good scaling law of $\langle\tau\rangle \sim N^{1+2\nu}$, with the Flory exponent $\nu = 0.75$, which corresponds to the scaling law of the polymer translocation in the $2D$ good solvent. Using Fig. (4.8), the simulation result is nearly agreed with the analytical expression of Rouse dynamical model predictions for

linear chains of applied to single-stars (see Eq. (4.3.3)) [94, 104]; however, four arms star polymer has better escaping time relative to three arms. Besides, we have been suggested that the scaling exponent does not change if we substitute the most probable time τ_p for $\langle\tau\rangle$ to interpret the scaling law between the translocation time and the total mass of the polymers. It is also fitted with a log-log plot of τ_p against the total number of monomers. The maximum level of significance from the distribution of escape times is considered as the average exit time. It is known that the average escape time is quite different from τ_p. But we have verified that their scaling slopes are nearly the same.

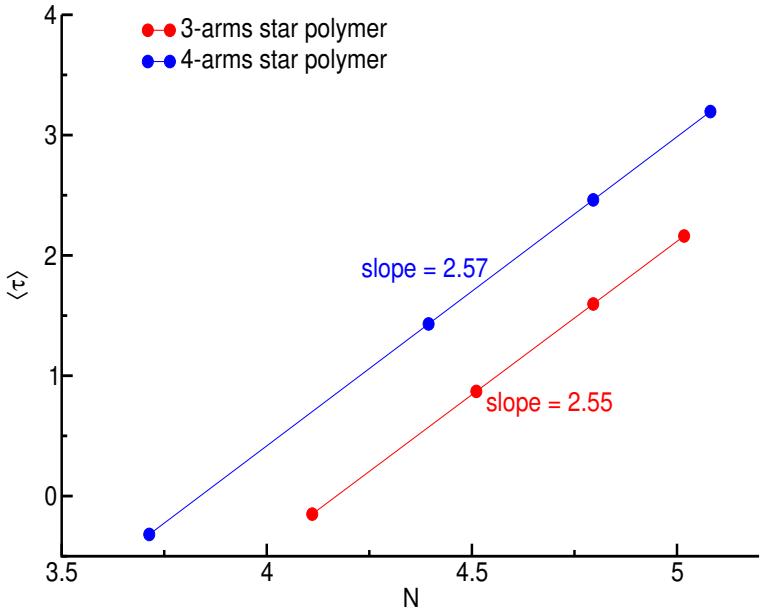

Figure 4.8: log-log plot of the mean translocation time $\langle\tau\rangle$ as a function of polymer chain size N in a 2D simulation with $N = 31, 61, 91, 151$ for $f = 3$ and $N = 41, 81, 121, 161$ for $f = 4$. Note that the dimensions of the nanopore length and width are 7 and 3, respectively, in lattice units.

Chapter 5

Unforced translocation of star polymers through a nanopore

5.1 Introduction

In this part of the dissertation we consider a three-dimensional Langevin dynamics computer simulations to study the dynamics of undriven translocation of star polymers through a nanopore. This allows us to locate the branching point of star polymer at the center of the nano-scaled pore, as it was discussed in the previous chapter. The process during which the polymers move into a very small pore depends on various physical parameters and fundamental mechanisms. Most importantly, we have studied the effect of the number of arms of single-stars and the total number of monomers as well on the translocation kinetics. Besides, the influence of both the coefficient of friction and temperature on the mean exit time is also considered. In the absence of a pore, to measure the dimension of star polymers, we monitored the mean-square radius of gyration as a function of star's functionality where the total number of monomers is kept constant. Further, our simulation outcomes confirm the power-law relationship between the radius of gyration and the chain size, based on the number of arms.

5.2 Computational procedures

As shown in Figure (5.1), the initial configuration of a polymer was created by putting the chain's branching point at the center of the nanopore. The arms of single-stars are arranged symmetrically on the left and right sides of the wall. Before starting the actual transporting process, the central bead of the system is fixed in the middle of the pore; this ensures the two halves of the branched-chain on each side of the wall to get relaxed, which reduces the system's initial free energy. Consequently, the polymer was released and then translocated. We describe this instance as zero time. All the simulations were conducted with different initial arrangements and without using any driving force. The polymer exit time is defined as the spending time for the branched-chain escaping the pore from either side of the wall (that is, *cis* or *trans*). The translocation time was estimated as the average durations over 1000 different runs of only successful translocations.

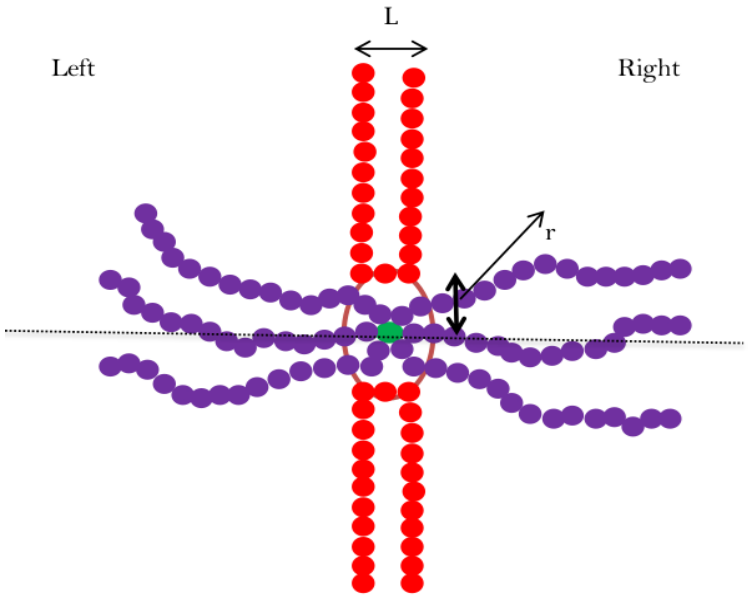

Figure 5.1: Schematic representation of 6-arms star polymer translocation through a nano-scaled pore with radius r. The width of the pore is L.

5.3 Results and discussion

In the absence of a nanopore, the relationship between the mean-squared radius of gyration, $\langle R_g^2 \rangle$, and multiple arms of star polymers with the same total number of beads is examined. The number of arms is varied between 2 and 30. In Fig. (5.2) we show $\langle R_g^2 \rangle$ as a function of f with different chain sizes $N = 121, 241, 361, 481, 601$. For each curve, we observe that the radius of gyration systematically decreases with increasing star's functionality. Hence, for relatively smaller functionality, noting that the radius of gyration increases with increasing N. In contrast, the size of star polymers is independent of N for larger functionality ($f > 12$).

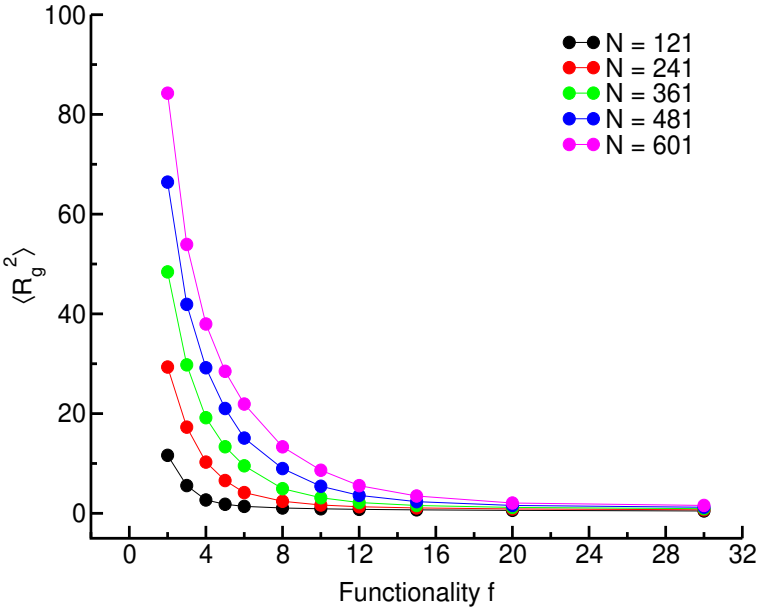

Figure 5.2: $\langle R_g^2 \rangle$ versus f for various polymer chain sizes.

To study further on the statics features of branched-chain polymers, we examine the dependence of $\langle R_g^2 \rangle$ on the total polymer mass for the three different number of arms. The simulation results are listed in Table (5.1). For the given N, the polymer with the lowest number of arms is found to have a higher $\langle R_g^2 \rangle$. Besides, $\langle R_g^2 \rangle$ increases with the total mass of the chain, as expected. Figure (5.3) illustrates the log-log plot of $\langle R_g^2 \rangle f^{-1}$ as a function of $Nf^{-1/2}$ for different functionalities $f = 2, 3, 4$. As the number of arms increases the dimension of the chain gets smaller. In addition, for each curve, the equilibrium size of star polymer increases with N. For $f = 2$, and 3, we found the two scaling slopes

$\nu = 0.58$, and 0.62, respectively. But the Flory exponent in the curve fitting slightly increases to $\nu = 0.68$ for $f = 4$. Anyway, these scaling exponents for such given values of f are still quite close to $\nu \sim 0.6$. As described in Equation (2.3.19), for f-arms star polymers in a free diffusion, our simulation results are in a good agreement with the slope scaling argument predictions of J. Paturej *et al.* [76].

Table 5.1: The data of $\langle R_g^2 \rangle$ for three different f with the same polymer mass.

	$\langle R_g^2 \rangle$		
N	$f = 2$	$f = 3$	$f = 4$
121	11.63	5.576	2.682
241	29.34	17.29	10.28
361	48.43	29.78	19.19
481	66.43	41.91	29.19
606	84.26	53.92	37.97

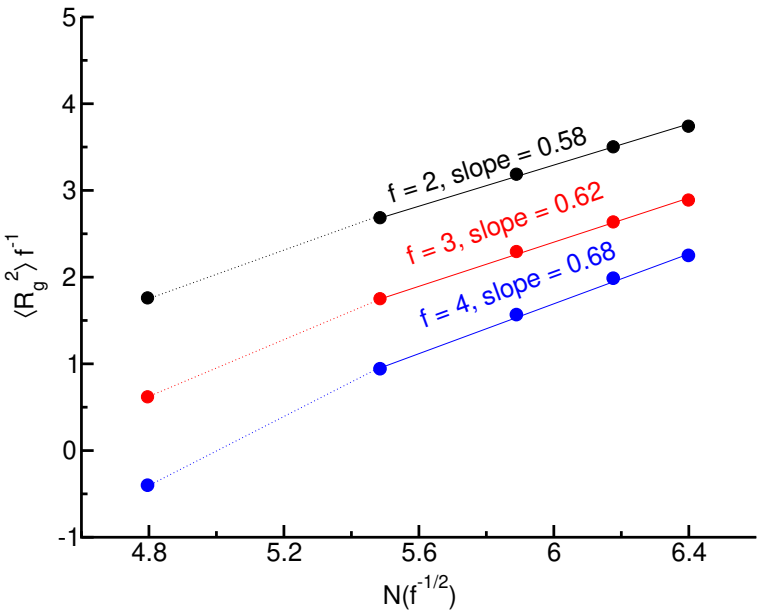

Figure 5.3: A log-log plot of $\langle R_g^2 \rangle f^{-1}$ vs. $Nf^{-1/2}$ for three different arms of star polymers with the same molecular mass.

5.3.1 Effect of f on the mean exit time

To examine the effect of the number of arms of branched chains on the mean exit time, the values of the total number of monomer, wall thickness, and pore diameter are set at $N = 121, L = 2.0$, and $D = 4.6$, sequentially. But we have considered star polymers with six different symmetric (even number) functionalities $f = 2, 4, 6, 8, 10$, and 12. Each arm length of single-stars decreases as the number of arms increases and the total polymer mass decreases since the expressions are related by $N_{arm} = (N - 1)/f$. In all cases, our simulation results are obtained without the involvement of any driving force, that is, $F = 0$. For the temperature T and coefficient of friction ξ, we set $T = 1.0$ and $\xi = 1.0$ unless otherwise stated.

As depicted in Figure (5.4), we first present the translocation time distribution function, $P(\tau)$, of star polymers as a function of most probable time with constant molecular weights and various functionalities. For natural translocation, we have seen the non-

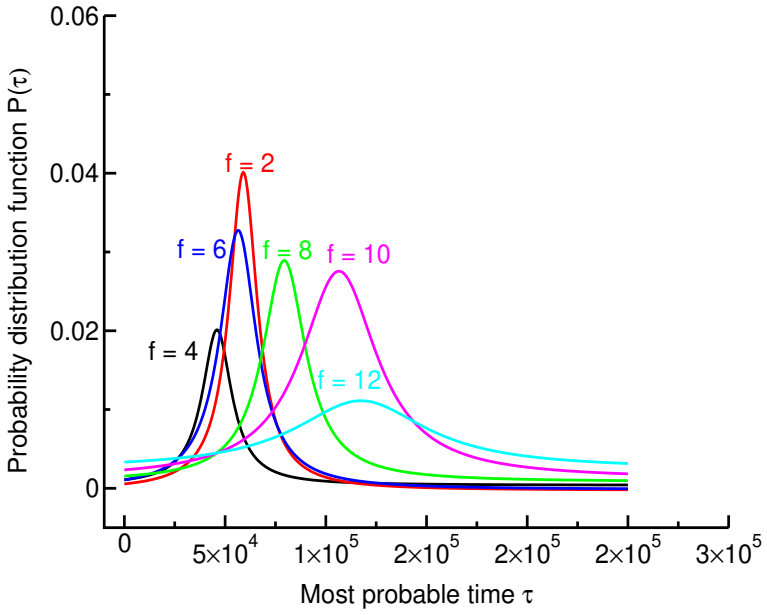

Figure 5.4: The distribution function of mean exit time for the translocation of star polymers under different functionalities with $N = 121, L = 2.0$, and $D = 4.6$.

monotonic trend in the distribution of average escape times. As the number of arms increases, the most probable time first decreases until the minimum functionality at $f = 4$

and then increases with the number of arms. Also, at $f \leq 6$, the forms of distribution mean escape times are narrower and symmetric. While at $f > 6$, the distribution of average translocation time becomes wider with the character of the long tail.

Figure (5.5) describes the variation of mean translocation time $\langle \tau \rangle$ as a function of star functionality for the same set of values, as mentioned in the above case. As the number of arms increases, the mean exit time first decreases until the minimum value $f = 4$, and then beyond this point, it increases with the star's functionality. Branched-chain with

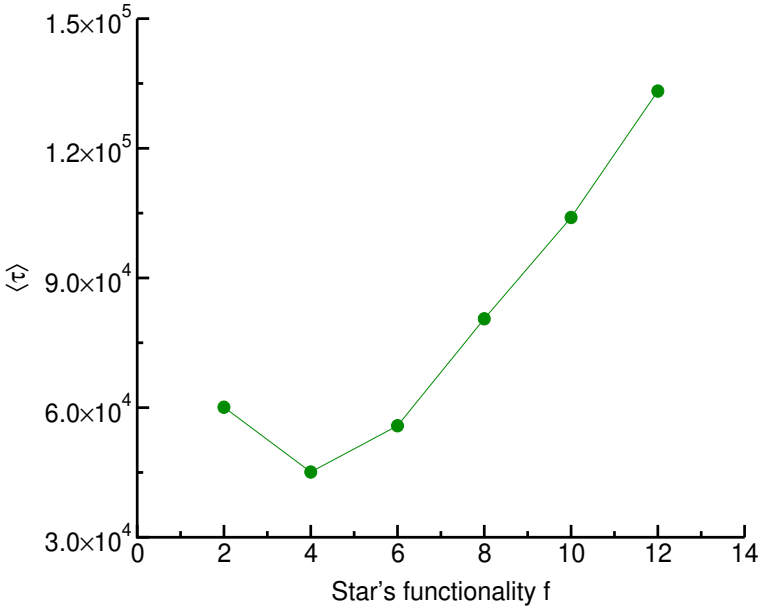

Figure 5.5: Mean translocation time versus f of single-star polymers with the same N. Note that the wall thickness and a nanopore diameter are fixed, while f is varied.

the lower f, results in the smaller chain density and reduces the mean escaping time that the polymer leaving out of the nanopore. However, for the higher functionality due to the greater inter-arms repulsion, the chain density inside the nanopore is increased, resulting in increased resistance of the arms to leave the pore. This idea corresponds to the regime where the mean escape time increases with the functionality of single-star polymers. A minimum average escape time is also observed, in which case, the entropic barrier balances the opposite force due to the crowding effect inside the pore, as presented in Figure (5.5). Additionally, the mean exit time and the most probable time (see Figure (5.4)) are

nearly similar. So, the average escape time $\langle\tau\rangle$ is well defined.

5.3.2 Effect of coefficient of friction on $\langle\tau\rangle$

As described within a $3D$ Langevin equation in Eq. (3.2.4), the coefficient of friction, ξ, explores the strength of coupling to the solvent. Without the solvent molecules, the value

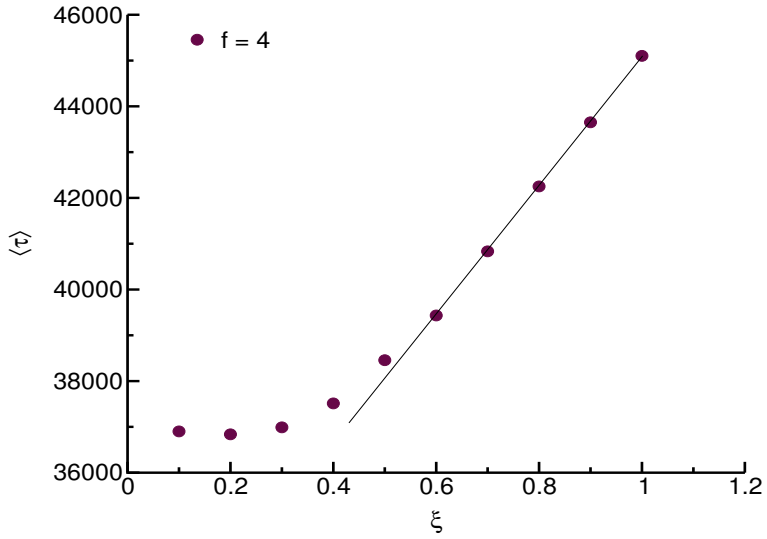

(a)

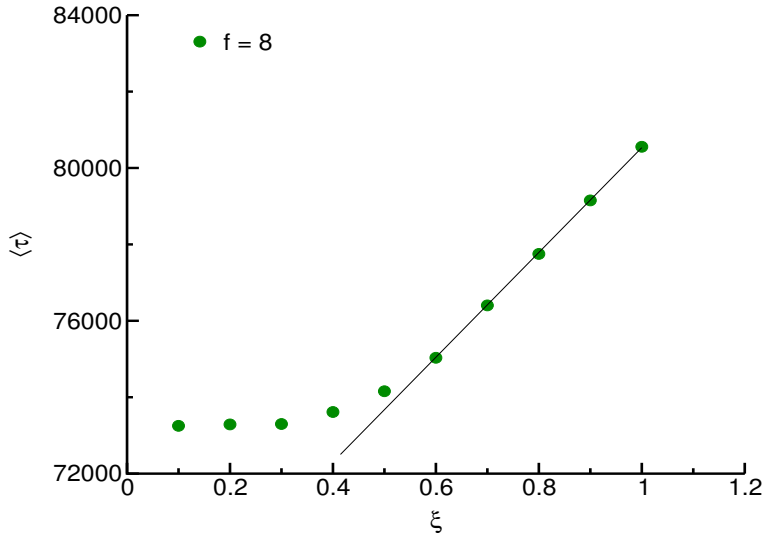

(b)

Figure 5.6: $\langle\tau\rangle$ as a function of ξ for $f = 3$ (a) and $f = 8$ (b). Note that ξ is varied from $\xi = 0.1$ to 1.0 and $L/N < 1$.

of the friction constant is set at $\xi = 0$, which reasonably results in an extremely rapid

flow of particles. In the opposite limit, ξ approaches to infinity, that is, the overdamped limit, inertia holds no part in the dynamics. The translocation time as a function of ξ for $N = 121$, $L = 2$, and $r = 2.3$ is depicted in Figures (5.6a) and (5.6b). The mean exit time increases with the coefficient of friction due to the increases of the frictional force. Also, mean translocation time increases with f. Most importantly, two distinct regimes are observed. For $\xi < 0.5$, the translocation time increases very slowly with increasing ξ. However, for $\xi > 0.5$, it increases more rapidly with ξ. These outcomes can be explained from the inter-relationship among the influence of thermal noise and the frictional force. For small ξ, the thermal variation and inertia take part in a dominant role as compared with the force of friction. Consequently, the translocation time increases slightly with an increasing ξ. However, when ξ is large enough, the influence of inertia can be ignored due to the state of balance between the thermal variation and the frictional force. This finding is in good agreement with the results of Huopaniemi *et al.* [10], who simulated linear chain translocation through a nanopore under an electric field.

5.3.3 Temperature as a function of $\langle\tau\rangle$

In order to further understand the translocation dynamics, we have also examined the dependence of mean translocation time on the temperature for two different functionalities of star polymers with molecular mass $N = 121$, nanopore length $L = 2.0$ and diameter $D = 4.6$, as shown in Figure (5.7). The collection of assigned values of the system temperature T is varying between 0.2 and 2.0. As expected, the average escaping time decreases with the functionality of star polymers. In the given interval of temperatures, the mean escaping time first rapidly decreases as the temperature increasing and then reaches the saturation level of exit time at higher temperatures. The presence of saturation level results from the fact that the thermal noise is balanced simply by the opposing force during the propagation process. However, for the lower temperature, the influence of thermal noise is undermined over the frictional force. At higher temperatures, the

translocation times difference between the two functionalities, 4-arms and 8-arms, are very small. Our results nearly agreed with the simulation outcomes of forced translocation of a linear polymer under the LD approaches, which is conducted by M.-B. Luo, D. A. Tsehay, and L.-Z. Sun [153].

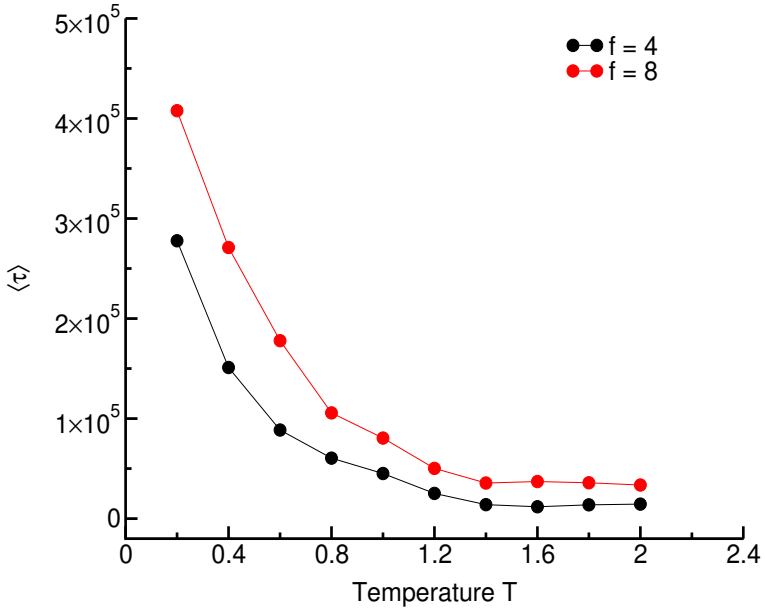

Figure 5.7: Mean translocation time as a function of temperature for unforced translocation with two distinct star's functionalities $f = 4$ and 8.

5.3.4 Dependence of $\langle\tau\rangle$ on N

For understanding the relationship between $\langle\tau\rangle$ and N, we have described the translocation dynamics for star polymers with the same molecular mass and using two different nanopore radii. In Fig. (5.8a), we show the non-monotonic dependence of the mean translocation time on functionality for four different polymer chain sizes $N = 49, 73, 79$ and 121 with the naopore radius $r = 2.3$ and length $L = 2.0$. A mean exit time first decreases with the increase of f until it reaches to the minimum point and then increases with f is clearly illustrated. Besides, the minimum points are noticed whereby the entropic barrier is balanced by the opposing force. These points are affected by the total polymer mass. The minimum point is observed at $f = 4$ for $N = 121$, while $f = 6$ for

the polymer masses between $N = 49$ and 97. This result has qualitatively explained as the star polymers with higher functionality result in strong arm-arm and arm-pore interactions. However, the influence of f on the translocation dynamics is insignificance for star-shaped polymers with a smaller functionality.

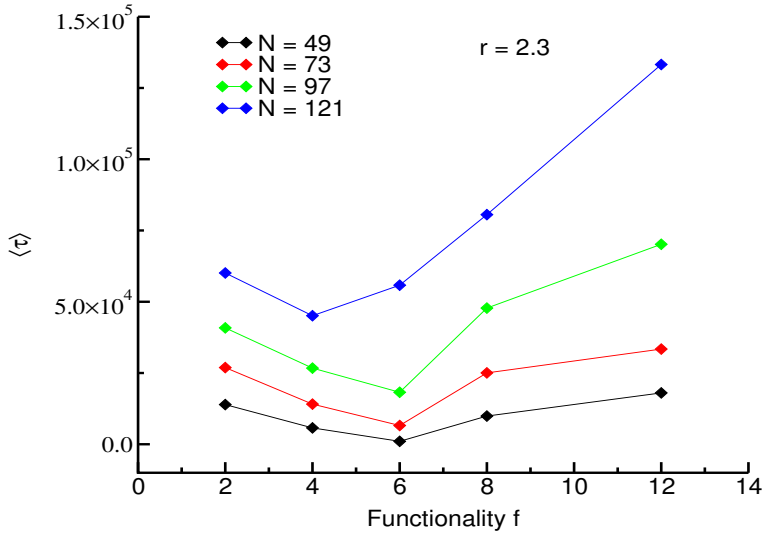

(a)

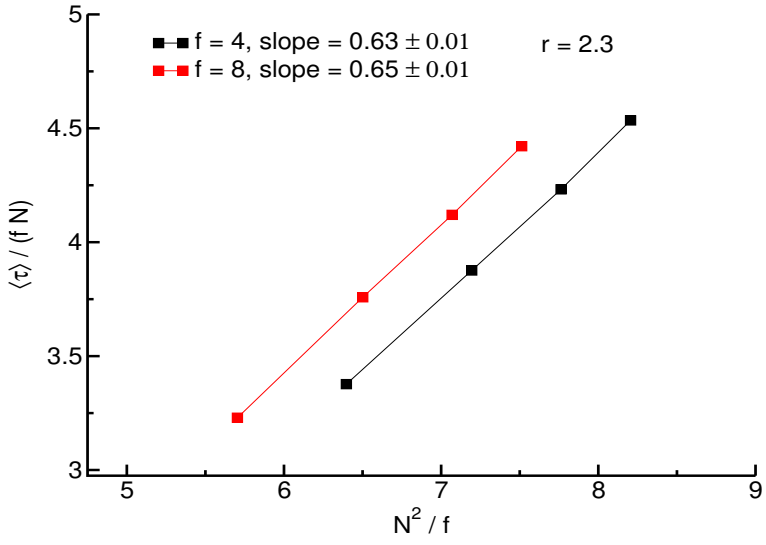

(b)

Figure 5.8: $\langle\tau\rangle$ as a function of $f(= 2, 4, 6, 8, 12)$ with different values of N (a). A log-log plot of the $\langle\tau\rangle/fN$ versus N^2/f for $f = 4$ and 8 (b), i.e., remarkably the nanopore radius and length are kept constant.

Figure (5.8b) shows the simulation result of the ratio of mean translocation time to

the functionality of star polymers and molecular mass, $\langle\tau\rangle/(fN)$, as a function of the ratio of the total polymer mass squared to functionality, N^2/f. As expected, the rate of polymer translocation is faster in star's polymer with $4-$arms than $8-$arms. Here the scaling slope begins to increases with functionality. At $f = 4$ the Flory exponent shows $\nu = 0.63$, while the scaling exponent at $f = 8$ equals to $\nu = 0.65$, which is almost the same as $f = 4$. But the log-log plot of $\langle\tau\rangle/(fN)$ versus N^2/f at $r = 2.3$ gives a good power-law

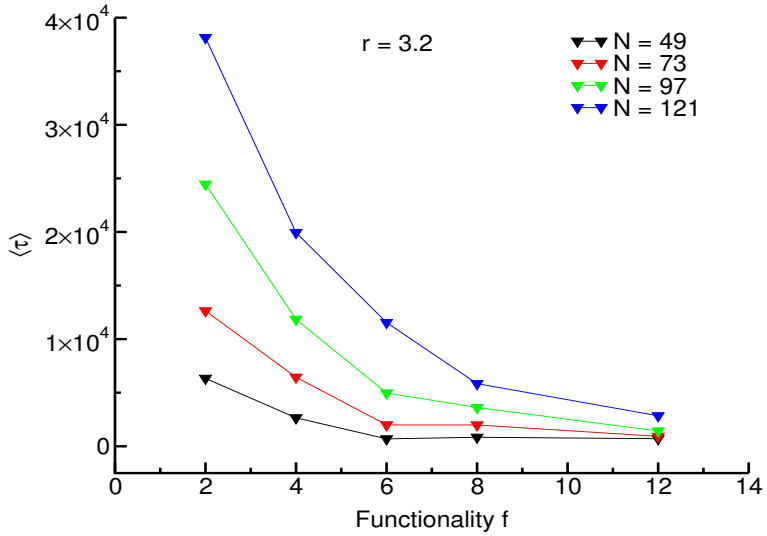

(a)

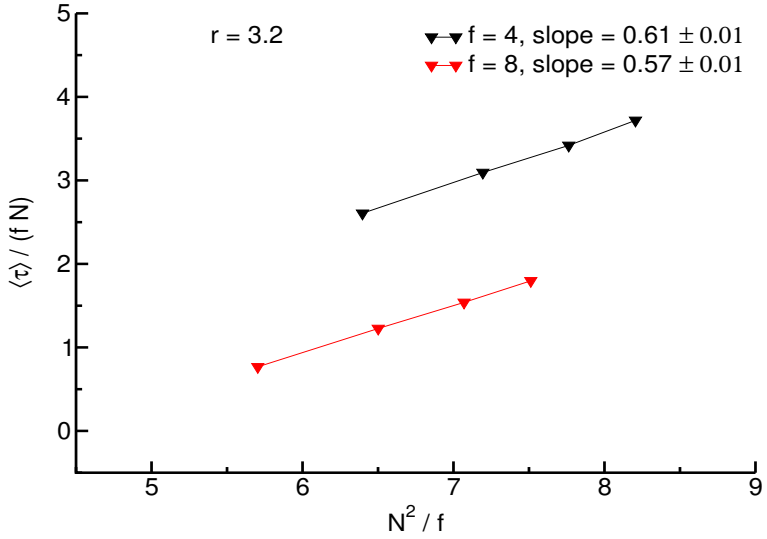

(b)

Figure 5.9: $\langle\tau\rangle$ as a function of $f(= 2, 4, 6, 8, 12)$ (a). A log-log plot of the $\langle\tau\rangle/fN$ versus N^2/f for $f = 4$ and 8 (b), and the total polymer mass that is considered $N = 49, 73, 97, 121$ for undriven translocation of polymers with $r = 3.2$ and $L = 2.0$.

of $\tau/fN \sim (N^2/f)^{\nu}$ with an approximate scaling exponent $\nu \approx 0.6$, which corresponds to the scaling law of unforced translocation of star-shaped polymers in a three-dimensional simulation box. As a result, the scaling law relation explores a good agreement with the theoretical expression, as mentioned previously in Equation (2.5.2).

On the other hand, the above results are repeated for different nanopore radius $r = 3.2$, which is relatively wider. The rest of the simulation quantities are the same, as noted previously. Results of $\langle\tau\rangle$ plotted as a function of functionality are shown in Fig. (5.9a) for various number of arms of star polymers $f = 2, 4, 6, 8, 12$ with chain sizes $N = 49, 73, 97$ and 121. For the given N, we notice that the mean exit time decreases with the functionality. Besides, τ is higher for $N = 121$ than $N = 49$, because of the larger radius of gyration of the star arms results in the longer exit time through a nanopore, as expected. It is also found that τ decreases as f increases from 2 to 6, for chain sizes between $N = 49$ and 97. For $f < 6$, the frictional force that is exerted on the star polymers easily overcome the loss of configurational entropy during the movement of the chains. However, for $f > 6$, τ remains nearly constant. This result may be explained by the fact that the thermal fluctuation due to free diffusion and the entropic barrier that both the arms need to overcome are balanced. Note that τ decreases monotonically with the increase of f is observed for the total polymer mass $N = 121$.

As depicted in Figure (5.9b), τ is higher for $f = 4$ than $f = 8$, due to the larger nanopore radius and smaller radius of gyration for star's with arms of $f = 8$ to exit easily through a nanopore, as expected. As compared with the results found in Figures (5.8a) and (5.8b), the faster translocation is observed as the nanopore radius increases, which displays in Figs. (5.9a) and (5.9b). It is also observed that the average exit time decreases as the functionality increases. The difference in τ between $r = 2.3$ and $r = 3.2$ is due to the assumption that all the functionalities on each side eject and inject the nanometric pore collectively, which disregards the severe structure variation of the arms as they move via a pore. For large mismatches among the mean escape time and the functionality, star

polymer arms on each side must meet with a conformational elongation in the course of a pathway to exit the pore. A power-law fit finds the exponent is nearly 0.6 for the two values of functionalities examined, although the fitting regime is limited. Here, we find that the theoretical method presented in Equation (2.5.2) is better for our data.

Chapter 6

Langevin dynamics simulation of star polymer translocation into a circular nanochannel

6.1 Introduction

The aim of this chapter is to study the translocation kinetics of homogeneous star polymers into a circular nanochannel under a constant pulling force using 3D Langevin dynamics simulations. Such an approach leads to promote the problem of exploring various dynamical modes of the polymers. The influence of simulating the total polymer mass and the magnitude of a pulling force upon the mean translocation time has been investigated by varying the channel length. We have also examined the dependence of mean exit time on the cavity channel length of single-stars of the same polymer mass but different functionalities. Interestingly, the impact of the functionality of star polymers on the mean exit time with polymers of equal molecular masses is analyzed by changing the nanopore diameter. This effect helps us to arrive at specific conclusions about the role of polymer functionality. Moreover, the influence of the total number of monomers on the translocation velocity is also investigated.

6.2 Description of the simulation

In the present work, the translocation of a self-avoiding branched-chain in a 3D box is considered, as depicted in Fig. (6.1), wherein the polymer moves into a nanochannel through a nanopore. The source of our coordinate system is the same as the nanopore core, which corresponds to the simulation box center. The nanopore has channel length, L, and diameter, D, where both are measured in σ units. The tube wall is symmetrical about the central line of the nanometric hole. The interaction between bead-pore and non-bonded bead-bead, there is the short-range repulsive LJ interaction with cut-off distance $r_c = 2^{1/6}\sigma = 1.12246\sigma$, the bead diameter σ equals to 1.00, and also the potential depth ε is set to 1.00. While FENE spring potential is used for the bonded bead-bead interaction with the values $R_0 = 2\sigma$ and $k = 7\varepsilon/\sigma$

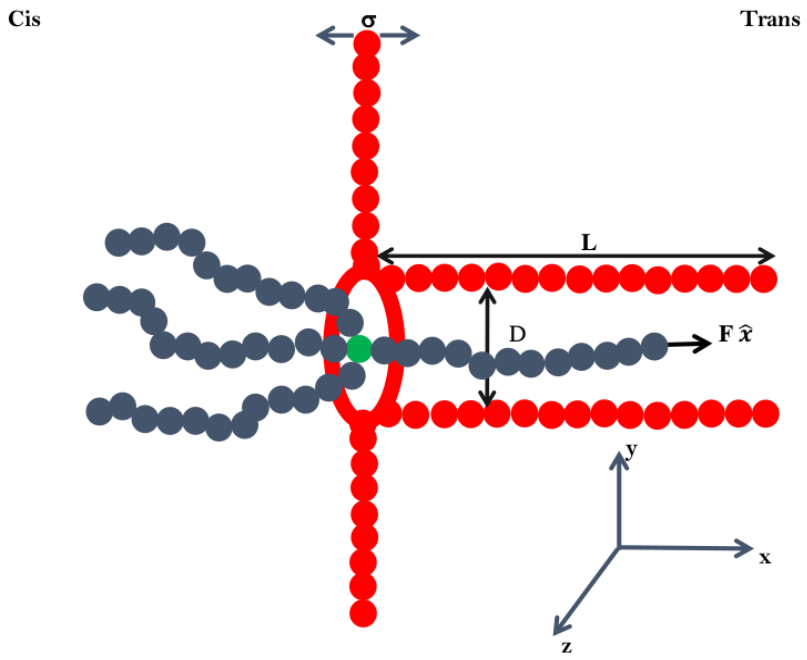

Figure 6.1: A view of homogeneous 4-arms star polymer translocation into a nanochannel subject to a constant pulling force. The monomers are identical and uncharged. The cylindrical channel and the wall are composed of immobile beads (red circles). The chain arms are produced by dynamic beads (black circles), attached to a branch point displayed as a green circle.

Before the actual translocation in progress, the first bead of the leading arm is kept fixed inside the channel, while the other beads are under thermal collisions characterized

by the Langevin thermostat to achieve an equilibrium configuration. Then at time $t = 0$, the first monomer is released, and the local external force is exerted along the hole axis that ensures the polymer propagation towards the trans-side (see Fig. (6.1)). The escaping (exiting) time is specified as the definite time length between the starting of the translocation and the end monomers of all the trailing arms pass the starting point. All of the successful results presented in this paper are averaged over 1000 independent runs.

6.3 Results and discussion

6.3.1 Effect of channel length on $\langle\tau\rangle$

This subsection is concerned with the effect of channel length upon the average translocation times. In the following simulations, the nanopore diameter is kept fixed at $D = 4.6$, while the cavity length L is varied between 2 and 16 in LJ units. Since the driving force is exerted only on the first monomer, the magnitude of F across the nanochannel is kept fixed. The limit of a driving force for the leading arm of the first monomer is set to $F = 10.0$. In addition, star polymers with equal molecular weight, $N = 121$, but different functionalities, $f = 2, 3, 4, 5$ and 6, are considered.

Figure (6.2) presents the variation of mean exit time with the channel length. In each functionality, the average passage time is independent of the cavity length for relatively shorter pores. Also, we noted that the sensitivity of translocation dynamics toward the multiple arms of star polymers declines while the channel length is decreased. But, the average exit time increases with the cavity length for a given constraint with the longer nanopores. Hence, the increment in the tube length enables a much longer interactive instance that occurs between the monomers from different arms and the constraint. This concept gives the reason for the average exit time increases in the longer nanopores. We can also note that the channel length does not significantly affect the translocation time for linear polymer ($f = 2$). Since there is just one backward arm, the translocation

dynamics for $f = 2$ within the range of cavity lengths are not case sensitive.

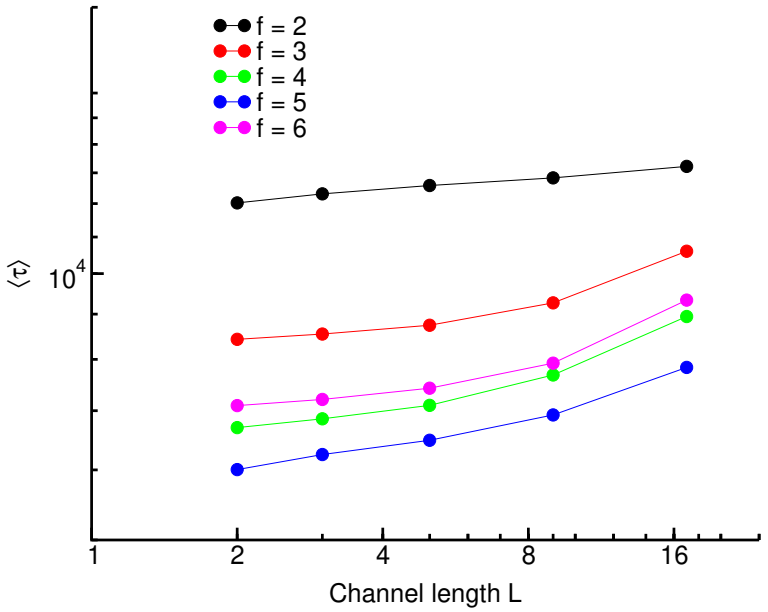

Figure 6.2: Plot of $\langle\tau\rangle$ against L for $N = 121$, $F = 10.0$, $D = 4.6$, and different channel lengths ranging from $L = 2$ to 16. Here $L/N < 1$. Note that the functionality is held constant for each curve (with $f = 2, 3, 4, 5$ or 6).

Moreover, we have also analyzed the behaviors of $\langle\tau\rangle$ at different functionalities with the given L, as demonstrated in Fig. (6.2). $\langle\tau\rangle$ exhibits a non-monotonic dependence upon f. This result shows a good agreement with the translocation of star polymers through uncharged nanopores [17]. Thus, the mean exit time decreases as the functionality increases until it attains a local minimum and then increases. We find the minimum translocation time of the system that appears at the functionality $f_{min} = 5$, which is under the fact that the impact of the end-pulled driving force counter-balances the constraint. For star polymers with smaller values of f, the longer trailing and forwarding arms are observed. This eventually causes to increase the mean exit time as f decreases. For higher functionality polymer, the opposition of the backward arms is harder due to the inter-arms interaction, leading to increments in the mean translocation time.

6.3.2 Influence of polymer mass N on $\langle\tau\rangle$

Figure (6.3a) shows the data for the mean translocation time as a function of polymer mass with functionality $f = 3$ under a pulling force $F = 10$ for different channel lengths, that is, varying from $L = 3.0$ to $L = 17.0$. In our simulations, for a fixed nanopore

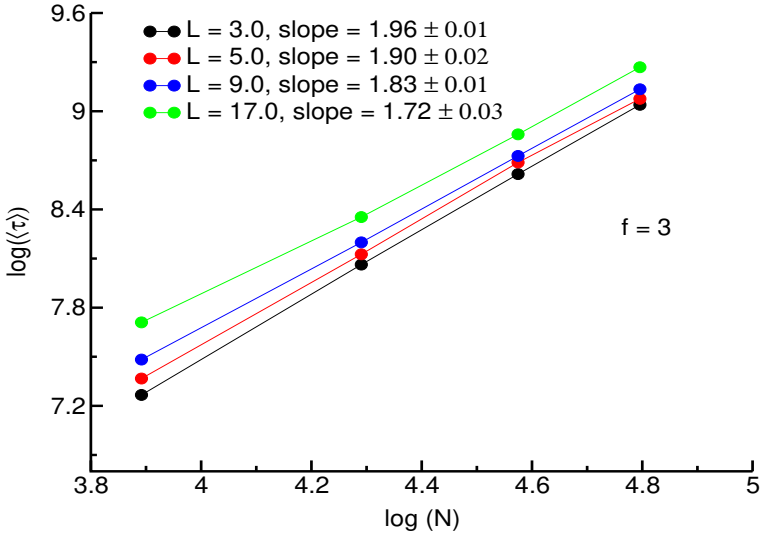

(a) Plot displays results for functionality $f = 3$.

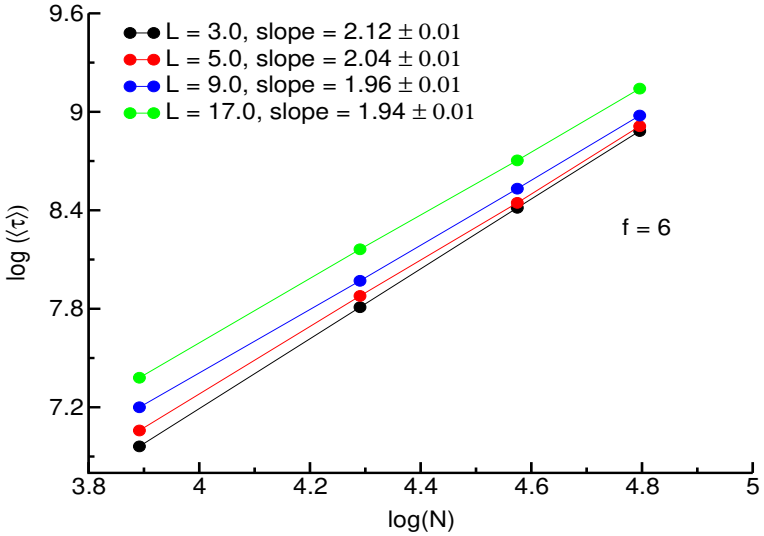

(b) Graph shows results for functionality $f = 6$.

Figure 6.3: log-log plot of $\langle\tau\rangle$ as a function of N with two distinct functionalities for various channel lengths. The nanopore diameter D is kept constant. Here $L/N < 1$.

diameter $D = 4.6$, we varied the channel length for different chain sizes $N = 43, 73, 97,$ and 121. Since the channel length is held constant for each curve, increasing the channel length increases the translocation time. Our result reveals $\tau \sim N^{\alpha}$ with α being the scaling

exponent. We observe that α slightly decreases first from 1.96 to 1.72 with increasing L from 3.0 to 17.0. With increasing L, the motion of such a branched-chain is highly restricted under the cavity, leading to increasing the rate of translocation. This is the reason for the decrease of α. Anyway, these scaling exponents for smaller channel lengths are still quite close to the power-law relation as $\tau \sim N^2$. In the side of theoretical considerations, the dimension of star polymers with f-linear arms, which restricts inside the tube, can be described as $R \sim f^{1/3}N$ [76]. The diffusion constant D in the Rouse scaling model is $D \sim N^{-1}$ and the translocation time estimated in the form of $\tau \sim R^2/D$ [15]. As a result, the exit time of star polymer yields:

$$\tau \sim f^{2/3}N^2, \tag{6.3.1}$$

which is nearly fitting with the numerical results as presented in Fig. (6.3a) for a given f and the shorter channel length ($L/N < 1$). Moreover, the numerical results agreed with the theoretical prediction of Huopaniemi *et al.* for single-chain ($f = 2$) polymer translocation via a nanometric pore subject to a strong driving force regime [10].

As a comparison, Fig. (6.3b) shows $\langle\tau\rangle$ as a function of N with star polymer functionality $f = 6$ under the driving force $F = 10.0$ for a fixed pore diameter $D = 4.6$. Thus, we observed the same features as previously described in Fig. (6.3a). However, the rate of translocation is faster for $f = 3$ than $f = 6$ in the given intervals of L, as predicted. These outcomes agreed with the results that are mentioned in Fig. (6.2). Here, the scaling slope α decreases from 2.12 to 1.94 with increasing the cavity length ranging between $L = 3.0$ and 17.0. Finally, these numerical results also display the scaling power-law behavior $\tau \sim N^2$.

6.3.3 Influence of pulling force F on $\langle\tau\rangle$

Figures (6.4a) and (6.4b) show the translocation time as a function of pulling force for $f = 3$ and $f = 6$, respectively. The magnitude of the pulling force acting on the front

monomer is varied from $F = 3.0$ to 10.0. Mainly, the effect of F on star polymers translocation is examined by varying the cavity length ($L = 3.0, 5.0, 9.0$ and 17.0) but with fixed nanopore diameter $D = 4.6$ and polymer mass $N = 121$. As found previously, the mean

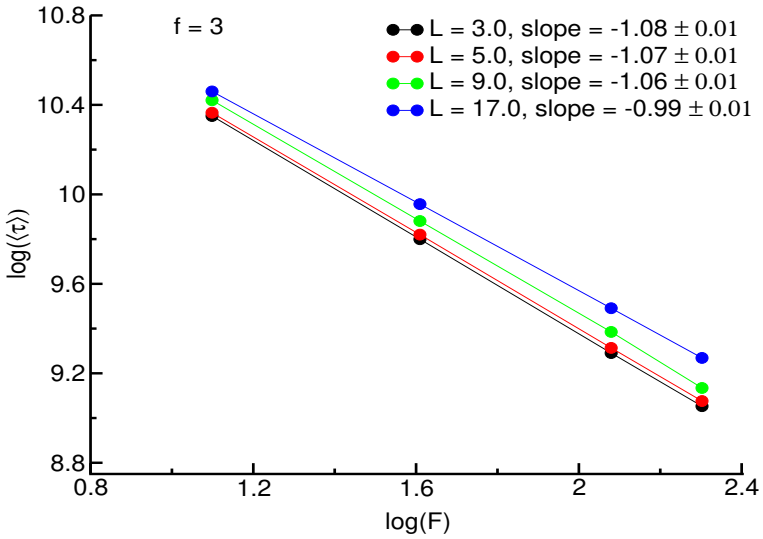

(a) Plot displays results for functionality $f = 3$.

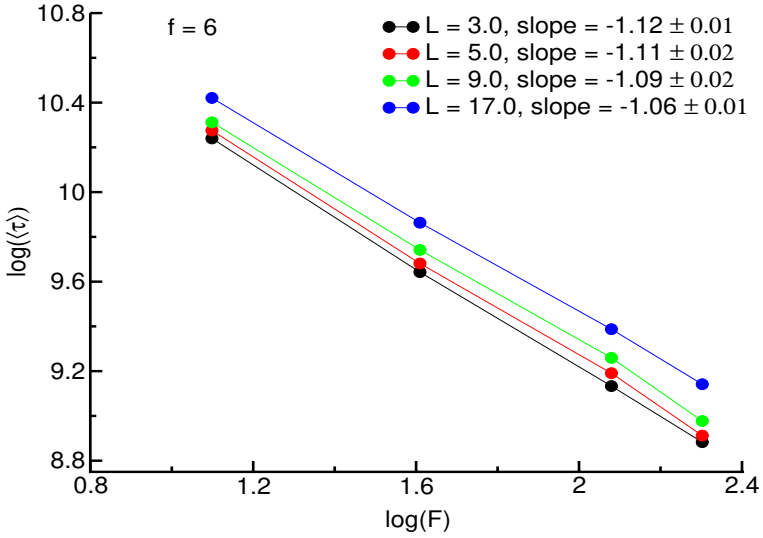

(b) Graph shows results for functionality $f = 6$.

Figure 6.4: Log-log plot of $\langle\tau\rangle$ as a function of F for $f = 3$ (a) and $f = 6$ (b). The polymer mass equals to $N = 121$, and $L/N < 1$.

translocation time is smaller for $f = 6$ than that for $f = 3$. For the given range of F, we also observe that τ increases with the tube length for the above two cases. Despite the different values of pipe length under consideration, the log-log plot of $\langle\tau\rangle$ and F provides

a good scaling law of $\tau \sim F^{\alpha}$, with the scaling slope $\alpha = -1$. This is in agreement with the theoretical predictions of inverse proportional scaling, $\tau \sim F^{-1}$ [134].

Additionally, the rate of translocation across the nanochannel increases with the driving force, which means the strong the pulling force, the faster the translocation rate is, as expected. In a strong pulling force regime, the application of the local driving agent on the star polymer has caused severe deformation, which implies that all arms enter and exit the channel simultaneously. Also, the dimension of the scaling slope decreases with the increment of cavity length, as demonstrated in Figs. (6.4a) and (6.4b). This is due to a decrease in the degrees of freedom of the trailing arms inside the cavity, enabling the polymers to move faster in the axial direction.

6.3.4 Influence of star polymer functionality on $\langle\tau\rangle$

So far, we have been considered the dependence of translocation times on the cavity length, the mass of the polymer, and the magnitude of the pulling force. In the present study, we are mainly inspired by how the functionality of star polymers would affect translocation dynamics. To this end, simulating the influence of functionality upon the mean translocation time has been investigated by varying various parameters, including the nanopore diameter, the mass of the polymer, and the strength of the driving force. In all cases, the tube length is fixed at $L = 2.0$, while the values of f investigated are $2, 3, 4, 5, 6, 8, 10$, and 12.

To understand the impact of the number of arms, we have plotted $\langle\tau\rangle$ in terms of f for the specific values of nanometric pore diameter $D = 4.6$ and pulling force $F = 10.0$. The functionality is fluctuated with the total polymer mass, $N = 121$, kept constant. Fig. (6.5) indicates that the mean exit time exhibits non-monotonic variation with f. Hence, the mean translocation time first decreases as the functionality increases, and then $\langle\tau\rangle$ increases with f for $f \leq 5$ and $f > 5$, respectively. The minimum average exit time is observed at $f_{min} = 5$. This idea can be interpreted as the pulling force acted on the leading

arm and the entropic barrier that both the leading and trailing arms need to overcome to enter the pore are balanced. As studied previously in unit five, the non-monotonic trend in $\langle\tau\rangle$ with f for star polymers of constant molecular weights has also been observed for unforced translocation. The difference of the translocation kinetics in the two distinct intervals of functionality can be understood from observing the polymer configurations during the process of translocation. For $f \leq 5$, the driving force on the forward arm can resolve issues of configurational entropy to drag the star polymer easily into the nanopore. In contrast, for $f > 5$, the energetic cost of the chain under the arm-arm and arms-pore interactions is increased. Finally, our results reveal that the conformational dynamics of star polymers are highly dependent on their functionality. This result is in agreement with recently reported simulation outcomes for electric field-driven translocation of star polymers [17].

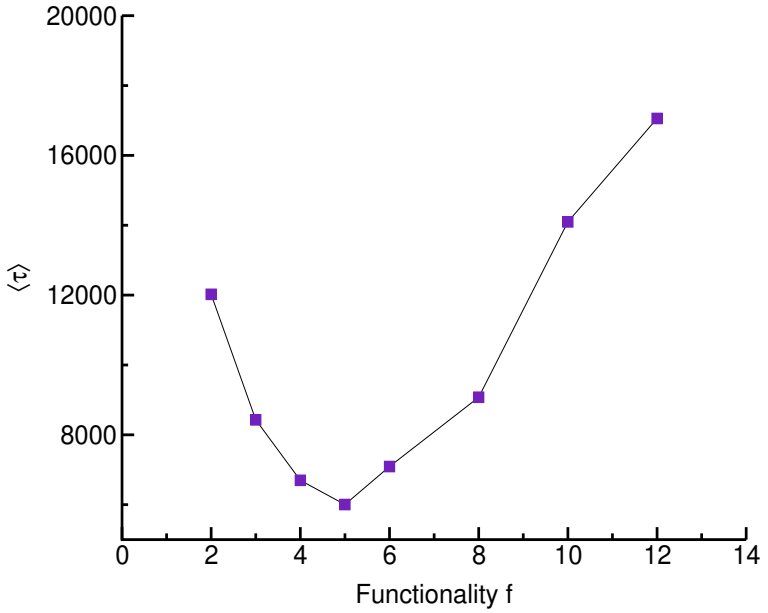

Figure 6.5: $\langle\tau\rangle$ as a function of f for different functionalities $f = 2, 3, 4, 5, 6, 8, 10$, and 12. The values of N, F, L, and D are fixed at 121, 10.0, 2.0, and 4.6, sequentially.

The conformational role of various arms of star polymers can also be characterized by the probability distribution profile of exit time $P(\tau)$. In Figure (6.6), we show the curves of the probability distribution of translocation time of f-arms star polymers translocation

with the total number of monomers is kept constant at $N = 121$, and other similar parameters as mentioned previously in Fig. (6.5). Our simulation results revealed that $P(\tau)$ shifts from narrower (small-tail) to broader width (long-tail) as the functionality increases. Following the distribution profile of escape time, we describe the most likely time τ_p as the time representing for the peak value in the curve (as noted earlier), and we figure out $\tau_p \approx \langle\tau\rangle$ for the specific intervals of f. This result is in agreement with the simulation outcomes of star polymer translocation subject to an electric field [17].

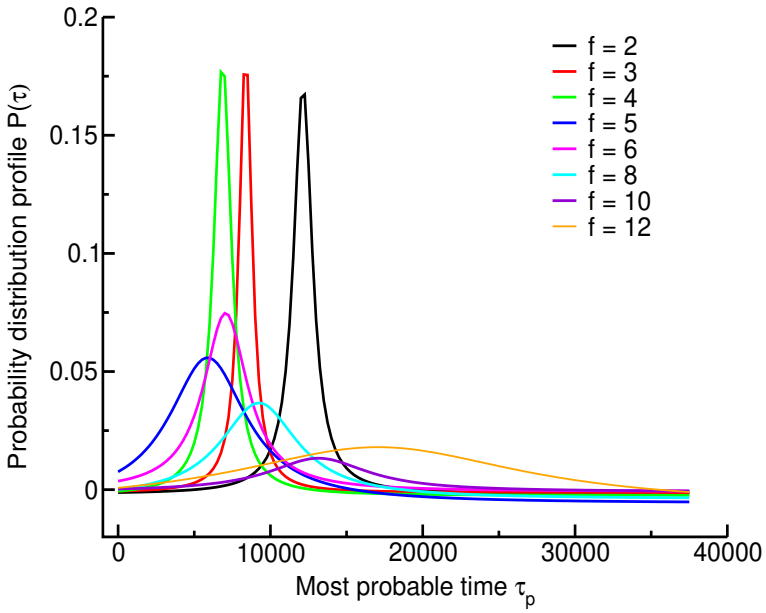

Figure 6.6: A plot of the probability distribution for multiple arms of star polymers translocation through a nanopore within the given range of functionality $2 \leq f \leq 12$. The values, $L = 2.0$, $D = 4.6$, $N = 121$, and $F = 10.0$, are kept constant.

Next, the impact of the functionality of a branched-chain polymer during the ejection process is further studied by considering the contribution of nanopore diameter. In the present simulations, the length of a tube, the chain size, and the strength of a pulling force are held constant at $L = 2.0$, $N = 121$, and $F = 10.0$, respectively, while the nanopore diameter D is varied between 2.8 and 6.4. The number of arms are also extended up to $f = 12$. Note that the length of each arm of the star polymer decreases as its functionality increases. Figure (6.7) shows the mean translocation time as a function of f for different

nanopore diameters under a fixed channel length. $\langle\tau\rangle$ exhibits non-monotonic variation with star polymer functionality. This is in agreement with the result of star polymer translocation into the cylindrical cavity [17]. Its value displays a higher distinction with f when the nanopore diameter is set to 4.0 and 4.6. Altering the pore diameter does not significantly affect $\langle\tau\rangle$ for $f \leq 4$. Particularly, this effect is irrelevant for linear polymer ($f = 2$) since there is only one trailing arm. For star polymers ($f > 4$), the mean exit time increases with decreasing the nanopore diameter. This phenomenon can be explained by the fact that an increase in the number of trailing arms (or the chain density) results with higher inter-arms repulsion between the backward arms, which in turn enhances the resistance among themselves to enter the narrower pore. Moreover, there is a critical

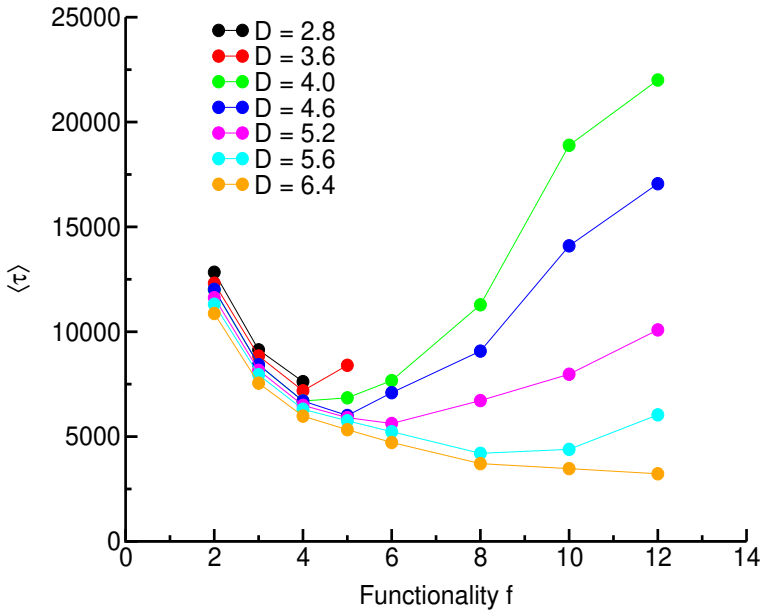

Figure 6.7: Mean exit time as a function of functionality for different nanopore diameters, ranging between $D = 2.8$ and 6.4. The functionality is varying from $f = 2$ to $f = 12$. Note that the following parameters, $L = 2.0$, $N = 121$ and $F = 10.0$, are kept constant.

figure (value) of f at which $\langle\tau\rangle$ attains a local minimum. The minimum translocation time also increases with the nanopore diameter. In addition, the cutoff functionality f_{cut} (beyond which the polymer translocation is prohibited) is attained at $f_{cut} = 4$ for $D = 2.8$ and $f_{cut} = 6$ for $D = 3.6$. On the other hand, the mean exit time decreases as

the functionality increases for $D = 6.4$. As a result, $\langle\tau\rangle$ has decreased for the larger pores due to the weak effect of constraints in which all the trailing arms of the chain can easily enter the nanopore at the same time.

Further, we investigate the dependence of mean translocation on star's number of arms f for different chain sizes, $N = 49, 73, 97$, and 121, in the regime of a strong pulling force $F = 10.0$. The pore dimensions are held constant at $D = 4.6$, which shows a diameter value in between the unsuccessful translocation for higher f and result that display weak arm effect for higher f (see Fig. (6.7)), and $L = 2.0$ to study the translocation of homogeneous star polymers with different functionalities, $f = 2, 3, 4, 6, 8$, and 12. Figure (6.8) illustrates the mean translocation time as a function of star polymer functionality for four distinct total polymer masses. For these N, the mean translocation time increases

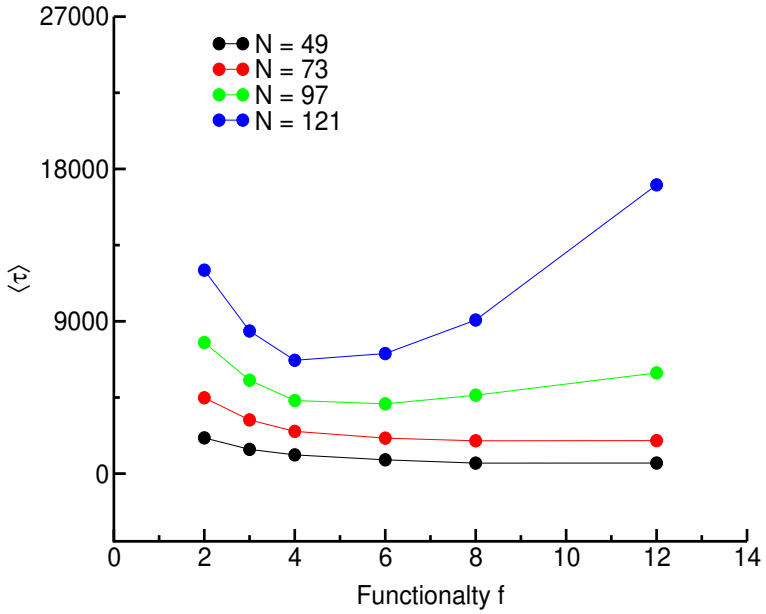

Figure 6.8: $\langle\tau\rangle$ as a function of functionality. The number of arms is varied for four different total number of beads $N = 49, 73, 97$, and 121. The functionality is ranging between $f = 2$ and 12. As noted previously, all the values L, D, and F are kept constant.

with N as expected. Explicitly, for the total number of monomers between $N = 49$ and 97, the exit time decreases with functionality for $f \leq 4$. The rate of translocation decreases with increasing the polymer functionality, as shown in Fig. (6.8). This explanation can be

verified using the fact that the decrease in radius of gyration as the functionality increases for the given intervals of N. However, for $f > 4$, the branched-chain polymer with the given total number of beads only requires to alter its conformation slightly to pass via the nanometric pore, and the exit time doesn't strongly depend on f. For $N = 121$, the mean exit time exhibits non-monotonic dependence on the number of arms of a single-star polymer. As mentioned previously, for $f < 4$, the pulling force on the leading arm can overcome the loss of chain configurational entropy to drive the system in the nanopore. Interestingly, for $f > 4$, the mean escape time increases with f. These aspects can be explained the translocation process corresponding to a highly inter-arm interaction among the backward arms dominates the translocation kinetics in the regime of a strong driving force.

Finally, the influence of functionality upon the translocation kinetics is determined by varying the pulling force. In Fig. (6.9), a plot of mean translocation time versus functionality is given for four different pulling forces, which is varying from $F = 3$ to $F = 10.0$. In the present case, the total number of monomers, pore diameter, and the channel length is set to $121, 4.6$, and 2.0, sequentially. The mean escape time decreases with the local driving force, as expected. Additionally, our numerical results verify the non-monotonic variation of the average translocation time with functionality for the given range of a pulling force. This means that the average exit time first decreases with increasing the functionality until it reaches the lowest points, and then τ increases with f. For polymers with the limit of lower functionality, we notified a faster rate of translocation. When f increases, the number of beads in each arm lengths of the chain decreases. This permits the common point to enter the pore faster once the translocation begins as it needs to be propagated through a shorter distance. Differently, the branched-chain density inside the nanopore is higher for polymers with a larger functionality. This effect causes a delay as the common origin gets closer to the nano-sized pore and also results in the backward arms encountering greater opposition to enter the pore due to stronger repulsion among

arms. Besides, the minimum point where the influence of driving force counterbalances the entropic barrier increases with F. It is observed that the turning point occurred at $f = 4$ for the driving force $F \leq 5$, while it is shifted to $f = 5$ in the regime of a strong pulling force ($F > 5$). This result is mainly due to the influence of decaying the entropic force and the compression of the polymer under a strong driving force.

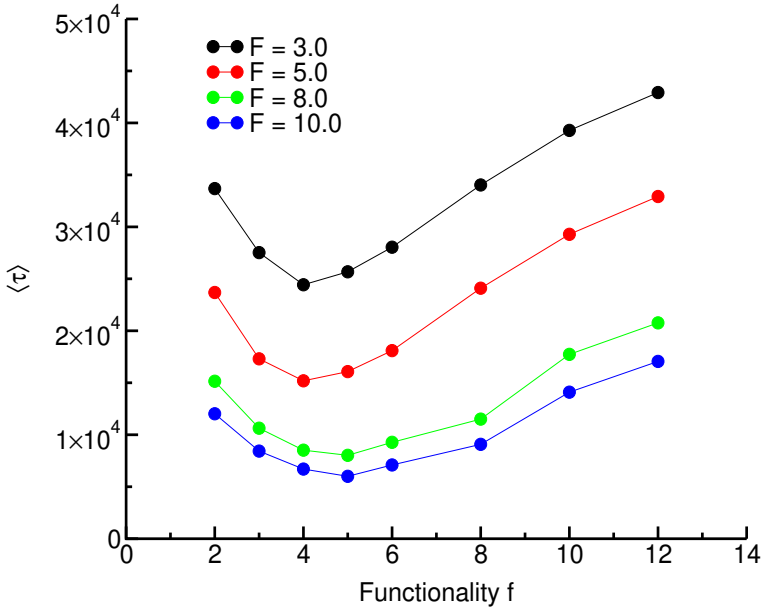

Figure 6.9: Mean exit time as a function of functionality for different driving forces. The functionality of star polymers is varied between $f = 2, 3, 4, 5, 6, 8, 10$ and 12. The simulation parameters, including $L = 2.0$, $D = 4.6$, and $N = 121$, are kept constant. Here, the ratio of cavity length to total polymer mass is $L/N = 0.0165$.

6.3.5 Dependence of translocation velocity on N

To study further on the translocation kinetics, we have considered the dependence of translocation velocity v on the total polymer mass under a constant and a strong driving force, that is, $F = 10.0$. Note that the number of beads on each functionality decreases as the molecular mass of the chain is increasing. In the present simulations, the total polymer mass is ranging from $N = 49$ to $N = 121$. As was described previously, the nanopore dimensions are fixed at $D = 4.6$ and $L = 2.0$. Our simulation results, translocation velocity versus the total number of beads for star polymers with three different functionalities

($f = 2, 3$, and 4), are presented in Figure (6.10) within the logarithmic coordinates. The scaling law relationship between v and N seems applicable to the systems.

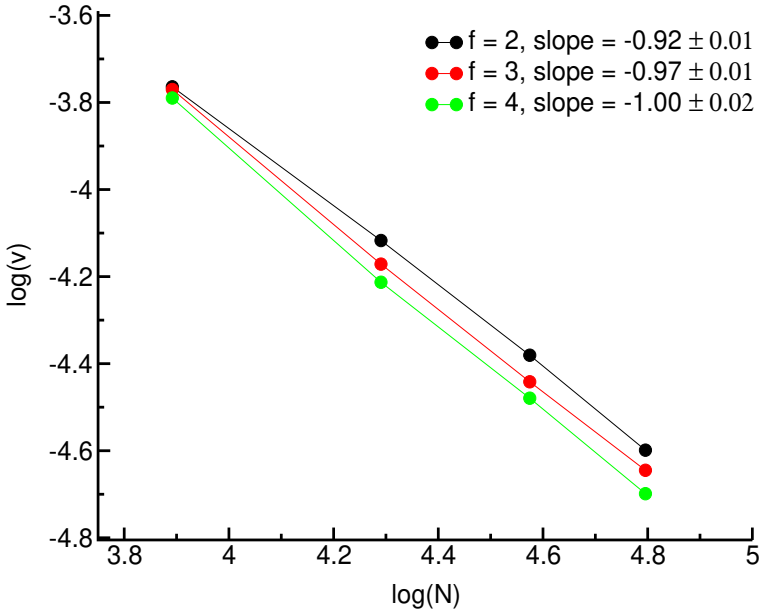

Figure 6.10: Scaling of translocation velocity (logarithmic scale) as a function of total polymer mass (logarithmic scale) for $f = 2, 3$, and 4 with the following constant parameters: $F = 10.0$, $D = 4.6$, and $L = 2.0$. Here, N is varied from $N = 49$ to $N = 121$.

Theoretically, the translocation velocity can be expressed in different ways. Most simply, we can define the translocation velocity as:

$$v = \frac{\langle x_l \rangle}{\langle \tau_e \rangle} \tag{6.3.2}$$

where x_l is the horizontal coordinate of the last monomer in the initial state of the conformational change of the polymer before the translocation and τ_e is the translocation time for every successful run. Average is taken over 1000 independent runs, in which $\langle x_l \rangle$ corresponds to the horizontal coordinates and $\langle \tau_e \rangle$ to exit times defined as in Eq. (6.3.2). This idea suggests that the translocation velocity decreases as the mean exit time (or the total number of beads) increases. According to the theoretical results of Ilkka H. *et al.* for single chain polymer, the scaling behavior that the translocation velocity dependence on N shows $v \sim N^{-\nu}$ and $v \sim N^{-1,}$, for small N and long N respectively [14].

The above theoretical consideration leads to a possible conclusion on our numerical

results for homogeneous star polymers with $2 \leq f \leq 4$. As expected, v decreases with increasing the total polymer mass. For the given N, the translocation velocity increases with f. This permits the common origin of the polymer to enter the pore faster due to N_{arm} decreases as f increases. Additionally, we also note that the sensitivity of v toward f reduces with decreasing N. As illustrated in Fig. (6.10), we find the scaling relation between the translocation velocity and total polymer mass nearly as $v \sim N^{-1}$, which is in a good agreement with the theoretical prediction for linear polymer with long N [14].

Chapter 7

End-pulled translocation of a star polymer out of a confining cylindrical cavity

7.1 Introduction

Using three-dimensional Langevin dynamics simulations, we examine the kinetics of star polymers translocation out of a cylindrical cavity, which is connected to a plane wall having a circular nanopore along the tube axis. In this chapter, we have explored single-star polymers of different masses and numbers of arms or functionalities. The translocation aspects are performed using a localized driving force, which exerts only on the leading arm of the front bead. Here we concentrate on the effect of the functionality of star polymers on the mean exit time with the same N. The impact of nanometric pore radius on the translocation kinetics is also studied in this case. Additionally, we have examined the scaling law relationship between the mean exit time and the total number of monomers and the magnitude of a pulling force as well. Also, the average translocation time has been investigated in terms of tube dimensions and the cavity aspect ratio.

7.2 Simulation methods

The illustration in Fig. (7.1) depicts the simulation set up of the system, where the cylindrical cavity with diameter D and length L is located at the *cis* side of a wall, to which it is connected, and the polymer is initially distributed inside the cavity. The movement of f-arms single-star polymer has been started from the enclosed cavity and then propagating to the *trans* side of the wall via a nanopore of radius r and thickness w formed in the wall. Wall and tube bead positions do not change during the simulations, avoiding thereby time-consuming additional integrations. But, the interaction among beads belonging to the cavity and wall surfaces and chain monomers is governed by the repulsive part of the LJ potential, while the bonded interactions among the beads are treated by a FENE potential. Note that the pore diameter is chosen sufficiently large to accommodate a fully stretched arm of star polymers.

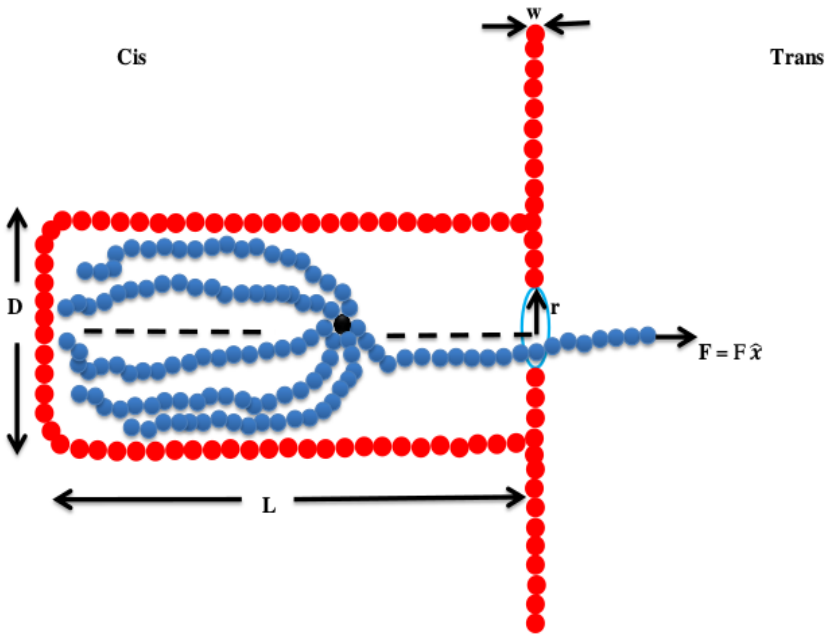

Figure 7.1: A schematic representation of the 6-arms homogeneous star polymer translocation out of a confined cylindrical cavity subject to a pulling force of magnitude F.

As previously said, the polymer is initially located inside the cavity with the end monomer of the leading arm anchored inside the nanopore. The branched-chain is then permitted to alter its initial arrangement in which the leading arm of the front bead

still immobilized. Once the warm-up process is over, the translocation process starts by freeing the constrained monomer and applying a pulling force of constant magnitude on it along a direction perpendicular to the pore plane, as described earlier. The translocation proceeds until all the backward arms get off the nanopore. A translocation run is said to be successful if the star polymer propagates completely across the nanometric pore onto the *trans* side. The translocation time τ is calculated as the time frame among the beginning of the front bead (i.e, at $t = 0$) and the time required by all the end monomers of the backward arms to exit the nanopore. It is significant to note that not all simulation runs result in a successful translocation, and even when they do, translocation times vary over a wide range of values. The magnitude of the driving force strength is the most crucial factor to increase the success probability. On the other hand, increasing the chain size and the force of friction decreases the success probability. Translocation times are only recorded for successful translocations. Thus, 1000 independent runs with different initial conditions are conducted to calculate the average translocation time $\langle\tau\rangle$

7.3 Results and discussion

7.3.1 Dependence of translocation time on f

Our first investigation is on the effect of star polymer functionality on the translocation time when the total mass of the polymer N is kept constant. Note that the size of each arm N_{arm} decreases as the polymer functionality f increases since these two quantities are inversely related $N_{arm} = (N-1)/f$. We first considered the translocation time distribution profile of star polymers of mass N but different functionalities while all other parameters of the system are kept constant. Fig. (7.2) shows exit times distributions for $N = 121$ but with f varying from 2 to 12. The cavity and nanopore diameters were equal to 16 and 4.6, respectively, while a rather strong pulling force regime was considered with $F = 10$. An inspection of the curves reveals that the exit time distributions are narrow,

highly peaked, and relatively symmetric for star polymers with low functionality, that is, $f \leq 5$. For star polymer functionalities larger than 5, the distributions become wider and are characterized by a long tail. Clearly, our results show that exit time distribution profiles strongly depend on polymer functionality. Moreover, our simulation results are similar to those obtained for field-driven translocation of star polymer via the pore [17].

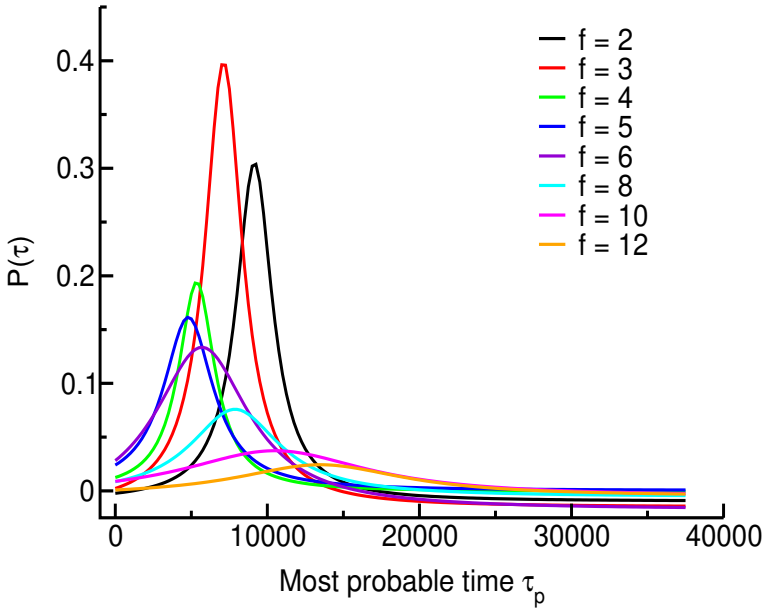

Figure 7.2: A typical probability distribution $P(\tau)$ of translocations for polymers as a function of most probable time τ_p. The wall thickness equals to $w = 1.0$.

Fig. (7.3) describes the variation of $\langle\tau\rangle$ as a function of f for the same set of parameters' values used for the previous case. The result reveals that the exit time exhibits a non-monotonic dependence on f of single-star. For smaller numbers of arms, the mean exit time decreases as the functionality increases. This behaviour continues up until a critical value of the functionality (f_c). Above f_c, the mean translocation time increases with the functionality of star polymer. It is clear that the radius of gyration of the star-shaped polymer decreases as the functionality increases, speeding up the translocation of each arm across the pore as long as the nanopore is large enough not to block the translocation of the backward arms. This is true in the regime of smaller functionalities, where the number of backward arms f_{back} is small enough to be accommodated together

inside the nanopore. But, as f_{back} increases, the concentration of beads inside the pore is such that it leads to a higher arm repulsion resulting in increased opposition of the arms to enter the pore. This corresponds to the regime of higher functionalities, where we observe an increase of the exit time with increasing f. A balance between the pulling force and the opposite force emerging from the crowding effect inside the nanopore results in a minimum of the mean exit time noted in Fig. (7.3) Obviously, the minimum value of the functionality depends on the following parameters: nanopore radius, the magnitude of a pulling force and polymer mass.

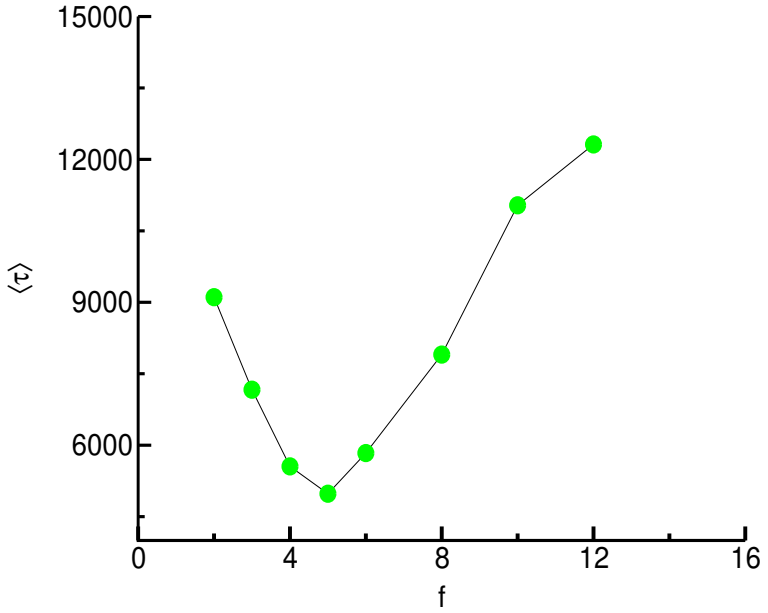

Figure 7.3: Mean translocation versus functionality for the given polymer mass $N = 121$. The values of pulling force, nanopore radius, tube diameter, and wall thickness are also kept constant.

In order to further explore the translocation dynamics, we have investigated how the $\langle\tau\rangle$ is divided between τ of the leading arm τ_f and the trailing arms τ_b respectively. We have illustrated in Fig. (7.4) the ratio of mean translocation time of the trailing arms to the mean translocation of the polymer chain $\langle\tau_b\rangle/\langle\tau\rangle$ as a function of polymer functionality f. Clearly, for linear chains ($f = 2$), the ratio is equal to 0.5 since both half of the chain will take equal time to translocate. As the functionality of star polymers increases,

the ratio increases, the increment being larger in the beginning. For higher functionality, the degree of increment gets smaller, and the trajectory approaches 1 asymptotically. As the chain's functionality becomes significant, the time taken by the trailing arms to exit the tube becomes so important that it is almost equal to the translocation time of the whole chain for higher functionalities. In addition, an inflexion point on the curve is observed around the critical functionality f_c a translocation regime change.

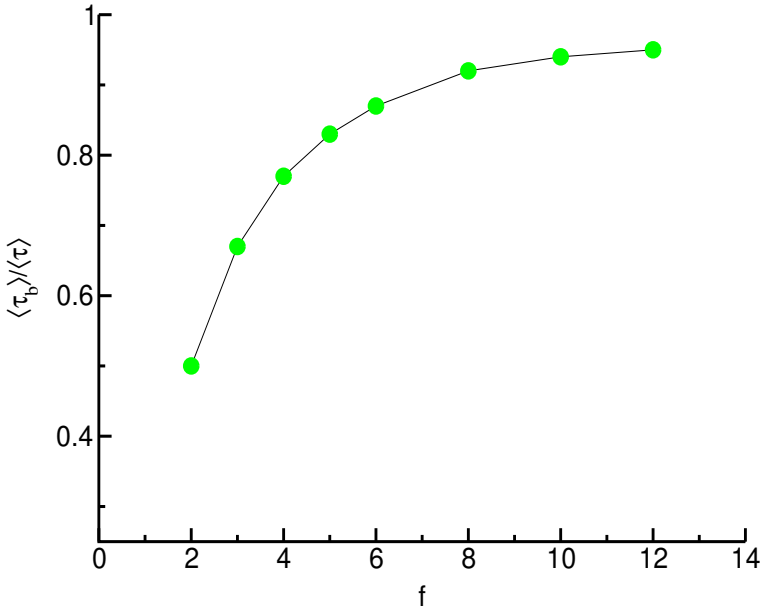

Figure 7.4: The ratio of mean translocation time of the trailing arms to mean translocation of the whole chain $\langle\tau_b\rangle/\langle\tau\rangle$ as a function of f with the same polymer mass $N = 121$. Note: All other parameters used in this numerical result have the same values as the cases mentioned in Figs. (7.2) and (7.3).

7.3.2 Effect of nanopore radius

The crowding effect of trailing arms inside the nanopore is dependent on the pore-size that affects the translocation process of single-star polymers. Figure (7.5) depicts the variation of the mean translocation time in terms of the polymer functionality for different values of the pore radius. First, we note that mean translocation time has a non-monotonic dependence on polymer functionality as already observed in Fig (7.3). The mean exit time increases with the nanopore radius decreasing. However, for the

linear chain ($f = 2$) case, one can note that the time increment due to the nanopore narrowing is negligible, while it becomes significant for higher functionalities. Indeed, for polymers with higher functionalities, the confinement of the trailing arms, when the pore becomes narrower, opposes a resistance to cross the pore due to inter-arms repulsive interactions, which slow the translocation process. Clearly, this is not the case of linear chains for which there is a single backward arm, and that is why the mean exit time is not significantly affected by the pore-size. f_c is dependent on pore-size and increases as the radius of the nanopore increases, as expected. Also, for the given pore size, there exists a cut-off functionality above which no translocation is possible. For instance, when $r = 1.4$, we were not able to register a successful translocation above $f = 4$, although simulations have been run for significantly longer times and with different initial configurations.

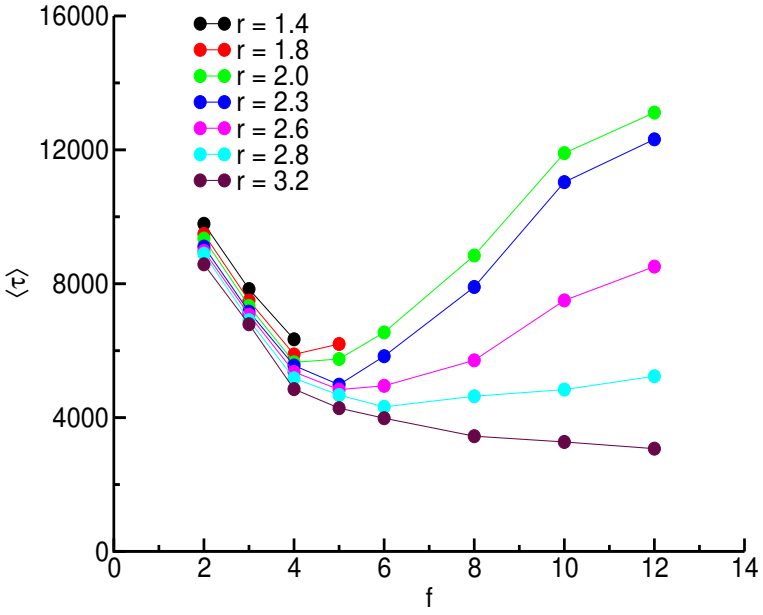

Figure 7.5: Mean translocation time $\langle\tau\rangle$ as a function of star's functionality f of different values $f = 2, 3, 4, 5, 6, 8, 10, 12$ for different nanopore radii (varying from $r = 1.4$ to $r = 3.2$). The cavity length L is changed with f, while nanopore diameter, the total number of monomers, the magnitude of a pulling force, and wall thickness are kept constant, and also used the same values as described in subsection **6.3.1**.

In order to study how sensitive is the mean exit time to the nanopore radius when the functionality of the star polymer is kept fixed in each case, we have depicted in Fig. (7.6a)

and (7.6b) mean exit time $\langle\tau\rangle$ as a function of nanopore radius r for different chain masses with two distinct star-shaped polymer functionalities $f = 4$ and $f = 8$ respectively. As

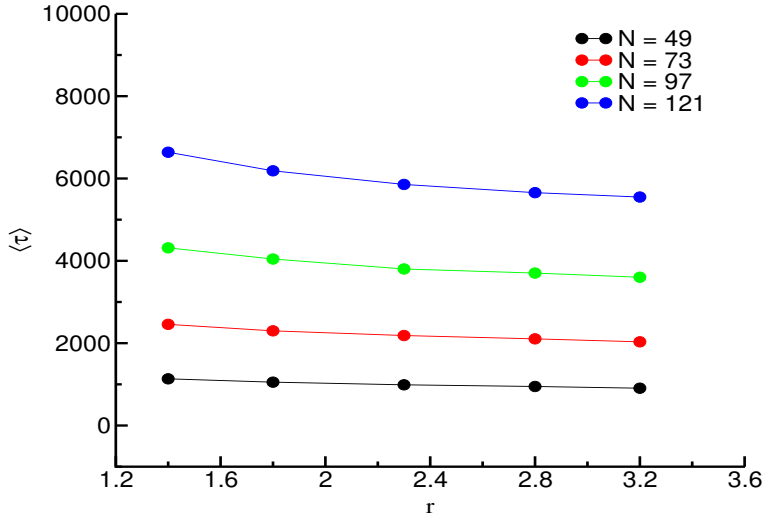

(a) f = 4

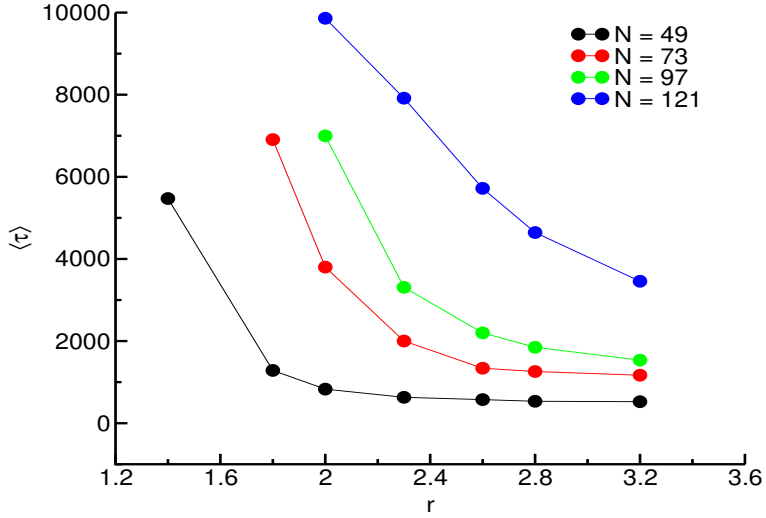

(b) f = 8

Figure 7.6: Mean translocation time against nanopore radius for four different values of polymer masses $N = 49, 73, 97$, and 121. Two different functionlaities are considered, that is, $f = 4(a)$ and $f = 8(b)$. Here, the cavity diameter, the magnitude of a pulling force, and wall thickness are kept constant, as described previously.

shown in Figure (7.6a), for all polymer masses, the same behavior is observed, that is, a small decrease of $\langle\tau\rangle$ as the nanopore radius becomes wider, which means that, for a given polymer mass, the translocation is not significantly affected by the change in nanopore radius. This is true up to $f = 5$, as it was evident in Fig. (7.5). For comparison, the

functionality $f = 8$ for the same polymer masses is displayed in Fig. (7.6b). Here, a high drop in $\langle\tau\rangle$ is observed when increasing r as expected for functionalities greater than 5. Moreover, for relatively longer polymer masses mass and narrower nanopores (that is, $r < 2.0$), star polymers with a higher functionality ($f = 8$) can't cross the nanopore because of the steric constraint, as noted previously.

7.3.3 Dependence of $\langle\tau\rangle$ on the total mass of the chain N

We investigated the effect of the total polymer mass on mean translocation time by considering a given functionality $f = 4$. Figure (7.7) depicts mean exit time $\langle\tau\rangle$ versus chain size N for different values of the nanopore radius while other parameters are kept constant. As expected, for a given polymer total mass the mean translocation time

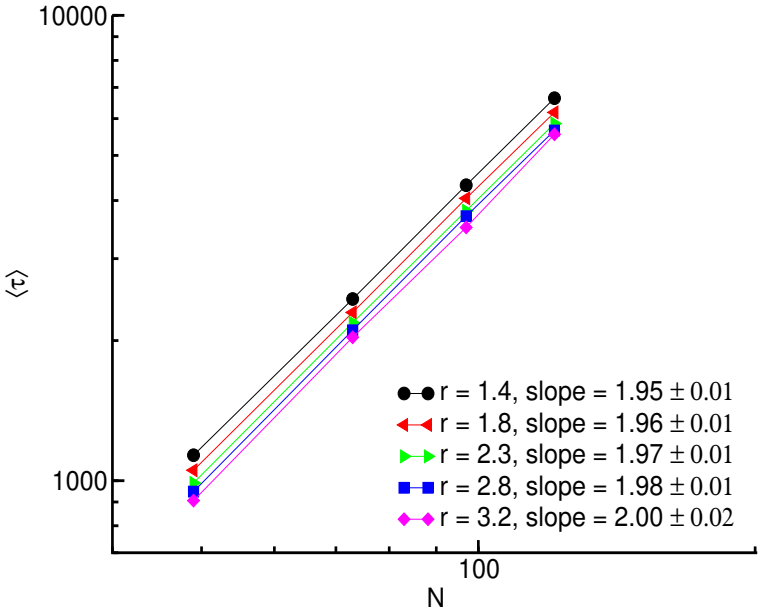

Figure 7.7: A log-log plot of mean translocation time as a function of polymer mass N for a given functionality $f = 4$ with different nanopore radii $r = 1.4, 1, 8, 2.3, 2.8, 3, 2$. The following quantities, such as cavity diameter, wall thickness, and the extent of a pulling force, are kept constant, as was noted earlier.

increases as the nanopore size is decreased. Mainly, the relationship between the mean exit time and the total polymer mass shows a scaling behavior as $\langle\tau\rangle \sim N^{\alpha}$, where the exponent α is close to 2 even though it has a weak dependence on the nanopore radius.

This simulation result is in good agreement with the case of linear polymer propagating under the regime of a strong driving force [134]. Obviously, polymers subjected to a strong localized force do not depend upon their topology as long as the nanopore size does not impede their crossing, that is, in the limit of small functionalities, which is the case here. Clearly, it is a local pulling force that dominates the translocation kinetics.

7.3.4 Dependence of $\langle\tau\rangle$ on the magnitude of pulling force F

The main influence of the driving force is to remove the free energy penalty for translocating the polymer out of the cavity faster. The dependence of the mean translocation time on the applied pulling force for different nanopore radii is displayed in Figure (7.8). The polymer has a total mass of $N = 121$ while its functionality is equal to $f = 4$. As we can see, faster translocation is achieved when the polymer translocates via wider pores for a given pulling force. Moreover, the mean translocation time decreases as the pulling increases, $\langle\tau\rangle \sim F^{-\alpha}$, where $\alpha = 1$. As expected, the higher pulling force corresponds to

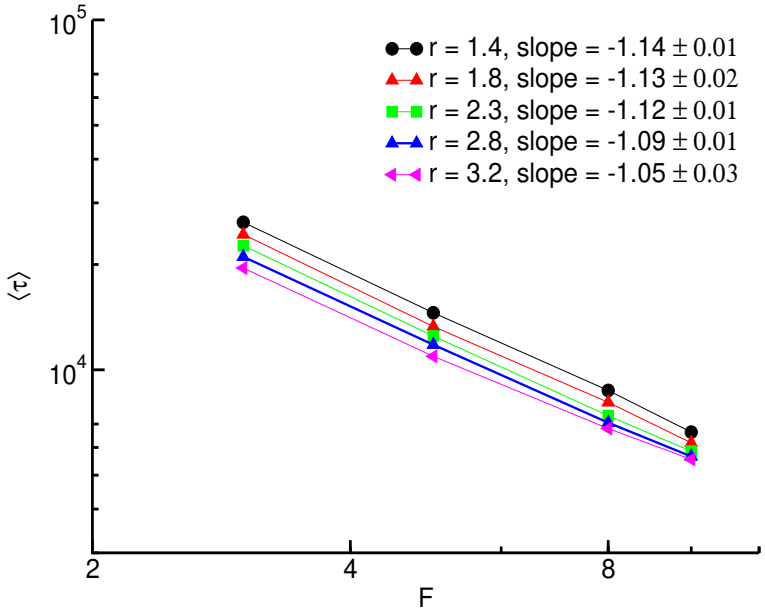

Figure 7.8: A log-log plot of mean translocation time versus the magnitude of the pulling force. Results are shown for five different nanopore radii $r = 1.4, 1.8, 2.3, 2.8,\ 3.2$ and for four various pulling forces $F = 3, 6, 8,\ 10$.

highly deformed polymer conformations throughout the translocation process resulting in a faster rate of translocation, provided that the total polymer mass is held constant for each curve. Hence, the results nearly agreed for most cases in a given chain size on the dependence of translocation time on the magnitude of the pulling force scaling behavior that holds under the restriction of a plane wall for a finite nanopore radius and wall thickness [134].

7.3.5 Dependence of $\langle\tau\rangle$ on the tube length L

The other quantity that affects the process of translocation is the length of a confining cavity. At the beginning of the translocation simulations, the polymer is initially located inside a tube of length large enough to hold a conformation where all arms are straightened out parallel to the tube axis. Next, the branched-chain is equilibrated by fixing the first monomer of the leading arm in the middle of the nanopore. During the equilibration state, the length of the cavity is slowly decreased until it reaches the desired value. The simulation set up is kept the same in the sense that we taken into account a polymer of mass $N = 121$, functionality $f = 4$, nanopore radius $r = 1.4$ and a strong pulling force regime $F = 10$. As previously explained by David Sean and Gary W. Slater for linear polymers, the degree of compression of the chain inside the cavity may minimize its exit time [19]. In this section, we examined the translocation kinetics of single-star polymer by keeping the tube diameter constant while varying its length. We again consider three distinct tube diameters.

Figure (7.9) represents $\langle\tau\rangle$ as a function of L, for three different tube diameters, that are, $D = 6.4, 9.6$ or 12.8. We note that the mean translocation time increases with increasing tube length independently of tube diameter, except for the largest diameter for which an initial increase of the translocation time is observed. A close inspection of the curves reveals that for small values of the cylindrical tube length, we observe a faster translocation for smaller cavity diameter. For larger tube length, however, a reversed

picture of the situation is obtained whereby the mean translocation time is greater for longer tube diameter. For a specific value of channel length at $L = 45.0$, a cross-over of the trajectories characterizing two distinct translocation regimes has occurred. We believe that the position of this particular point depends critically on features of single-star polymer, including the chain size and functionality.

Regarding the smaller cavity lengths, the available volume of the tube is reduced, resulting in polymer axial compression inside the cylindrical tube. The branched-chain compression is even more pronounced in the case of a small cavity diameter, where a reduction of the chain's backward arms conformation in the lateral direction near the core bead may take place. This, in turn, results in the stretching of the backward arms along the longitudinal direction while their free ends are densely packed inducing a severely reduced motion against the opposite wall of the cavity and may be responsible for a faster translocation [19]. We get a different picture for larger channel diameter where the

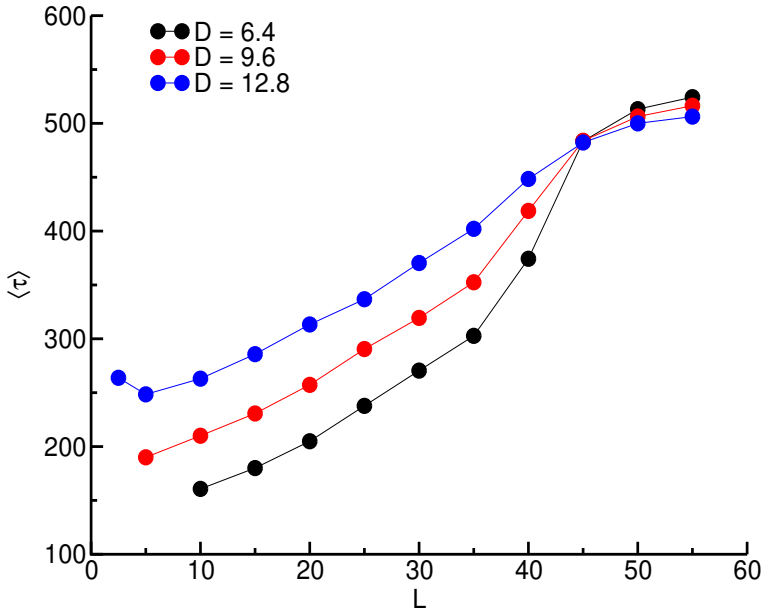

Figure 7.9: Mean translocation time versus tube length for a given functionality $f = 4$ and polymer mass $N = 121$. Here, the length of the constraint (cylindrical cavity) is varied for different constraint diameters, which are $6.4, 9.6$, and 12.8. Also, the length of the cylindrical cavity L is ranging from 2.5 to 55.0. Note: The parameters including pulling force $F = 10.0$, pore length $w = 1.0$, and pore radius $r = 1.4$ are kept fixed. A cross-over of $\langle\tau\rangle$ is observed at $L = 45$.

availability of space enables the backward arms to investigate more conformations in the lateral direction. In this case, we may expect a loss of trailing arms ordering near the core monomer with the formation of hairpin type arms conformations that may slow down the translocation process. On the other hand, in the case of larger cylindrical tube length, the single-star polymer becomes less compressed and its arms are able to explore more conformations in the longitudinal direction, thereby slowing down the translocation.

7.3.6 Dependence of $\langle\tau\rangle$ on aspect ratio a

For further investigation on the geometrical aspect of the cavity, we have examined the influence of aspect ratio, $a = L/D$, upon the mean translocation time $\langle\tau\rangle$ as shown in Fig. (7.10). The confinement volume of cylinder V is kept constant while the aspect ratio is varied. In this part of the simulations, we were performed for three different cavity volumes $V = 750, 1250$, and 1500 while we used the following fixed quantities: $F = 10$, $f = 4$, and $N = 121$, which corresponds to the homogeneous arm length of the chain $N_{arm} = 25$. Besides, the branched-chain is driving under the cylindrical cavity by applying a constant pulling force at one end where the tube is connected to the plane wall with a circular nanopore at the center with the pore radius $r = 1.4$ and the thickness of the wall $w = 1.0$.

A critical aspect ratio a^*, shown by a vertical broken line in Fig. (7.10), is defined as the predicted position where the curves converge closer to the same minimum point. The translocation time is rescaled with τ^* which divides mean translocation time at this critical aspect ratio a^*. Thus, the numerical results in Fig. (7.10) represent the rescaled translocation time as a function of aspect ratio for three different cavity volumes. With this reference, we examined $\langle\tau\rangle$ in terms of a by rescaling $\langle\tau\rangle$ with $\tau^* = \tau(a^*)$ keeping the tube volume remains constant (iso-volume). For these volumes, the mean translocation time decreases with the tube volume (data not shown), and also the critical aspect ratio that minimizes the mean translocation time $\langle\tau\rangle$ and shows the same position

at $a^* = 0.5$. Above the critical aspect ratio a^*, the mean translocation time increases with the aspect ratio when the tube volume is kept constant. This effect is due to the mean distance from monomer to the pore increase as the confined tube length becomes larger as compared with the tube diameter, that is, relatively tube length is higher than the cavity diameter. On the other hand, the translocation time will decrease as we bring the monomer closer to the pore, as stated previously. Furthermore, for an aspect ratio below the critical value a^*, the mean translocation time also increases with the aspect ratio. This observation is not controversial due to, at some point, the tube is importantly a flat disc that radially distributes the monomers further from the pore upon reducing the axial length. To this end, the simulation result of the critical aspect ratio nearly agreed with the theoretical prediction of a linear chain translocation from a confined cylindrical tube, which is concentric with a wall of narrower nanopore radius [19].

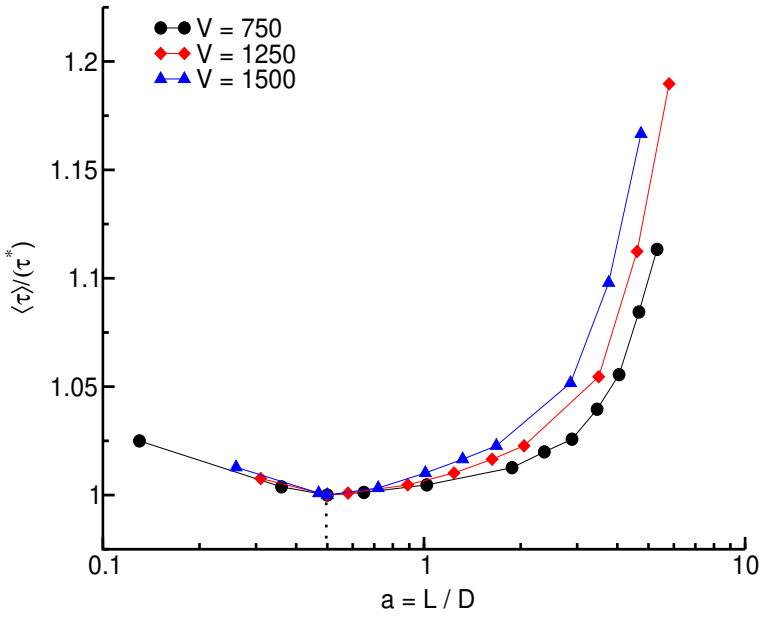

Figure 7.10: Scaled mean translocation time $\langle\tau\rangle/(\tau^*)$ for the three distinct tube volumes as a function of the aspect ratio a. Here the values of functionality, polymer mass, nanopore radius, wall thickness, and pulling force are fixed at $f = 4$, $N = 121$, $r = 1.4$, $w = 1.0$, and $F = 10.0$, respectively, while the tube volume is varied between $V = 750, 1250$, and 1500.

Chapter 8

Summary, conclusions, and future outlook

8.1 Summary

In this dissertation, we have considered two distinct approaches (2D Monte Carlo and 3D Langevin dynamics simulations) to study the problem of multiple arms star polymers translocation in the presence of constraints. In the 3D Langevin dynamics approach, to investigate the properties of star polymer free-diffusion and translocation in the absence and presence of constraints,respectively, we have used the following simulation parameters in LJ units: energy ε , length σ, time $t_{LJ} = (m\sigma^2/\varepsilon)^{1/2}$, time step $dt = 0.001t_{LJ}$, temperature $T = \varepsilon/\kappa_B$, friction coefficient $\gamma = m/t_{LJ}$, thermal noise, pulling force, FENE, and LJ interaction potentials. In the case of Monte Carlo simulation of star polymer free-diffusion and translocation in the absence and presence of nanopore, respectively, using the bond fluctuation algorithm, the excluded volume effect and the bond crossing have been implemented. In the 2D simulation box, the neighbors along the chain (in lattice units) were restricted by the bond distance b_l that vary in the range $2 \leq b_l \leq \sqrt{13}$. The minimum distance that guarantees the excluded volume effect is 2, while the bond crossing is restricted by the value of the upper limit $\sqrt{13}$. The translocation tasks were performed by using two different approaches: i) in the absence of driving force (free translocation), and ii) by applying a pulling force at the end monomer of a leading arm. Besides, we have

invested enough simulation time for the equilibration phase and for the actual simulation runs. Also, sufficient simulation data have been recorded, leading to averaging the results of the simulation over the respective independent simulations runs.

Interestingly, we were concentrated on investigating the effect of star polymers functionality on the translocation dynamics. To arrive at specific conclusions about the role of polymer functionality, we made a systematic comparison between the translocation dynamics of star polymers with varying functionalities but with the same mass of the polymer. Thus, simulating star polymers with an equal mass of the polymer but various structures enabled us to isolate the influence of topology on translocation dynamics. Also, we explored the scaling law of the translocation time versus the polymer mass and the pulling force as well, depending on the nanopore dimensions. The influence of constraints dimensions, temperature, coefficient of friction, and translocation velocity on the translocation time was also examined. Moreover, we investigated the statics features of star polymers in the absence of a nanopore.

8.2 Conclusions

In the first part of this dissertation, we have presented the results from the Monte Carlo simulation of three and four arms star polymers for free diffusion and unforced translocation through a nanopore. Our simulation results that describe both the static and dynamic feature of star-shaped polymers agree with what is expected for constraint-free diffusive motion on the lattice. Specifically, we find that the radius of gyration scales as $R_g \sim N^{\nu}$ with $\nu = 0.75$ being the Flory exponent in 2D, and the self-diffusion coefficient as $D \sim N^{-1}$ for the Rouse model. Furthermore, we see that the size of star polymers increases with the total number of monomers. However, for the given total polymer mass, both the size of star polymers and the rate of diffusion decrease as the functionality increases. This idea suggests that the increase in the functionality of the polymeric materials

leads to having a more compact and denser structure. On the other hand, a good scaling law of $\tau \sim N^{2\nu+1}$ was observed in 2D simulations of undriven translocation of star polymers ($f = 3$ and 4) via a nanopore. This simulation result shows a good agreement with the theoretical prediction for a linear polymer ($f = 2$). Additionally, the translocation time increases with the total polymer mass. Moreover, the possession of final positions for three and four arms star polymers are quite different after translocation: for the four-arm chain, the translocation events are seen either to the left or to the right of the wall with equal probability, which is mainly because the arrangement of the arms is highly symmetric; whereas for the three-arm polymer, we have observed a one-sided (biased) translocation. This fact can be interpreted as the structural arrangement of 3-arms star polymer is exhibited in a dizzy number of branched arms.

As for the second case, we conducted a Langevin dynamics simulation to investigate the kinetics features of star polymers translocation without the external force driving through a pore. In the absence of a nanopore, the radius of gyration of star polymers with the same chain size decreases as the functionality increases. For a relatively larger f, the mean radius of gyration shows a weak dependence on functionality due to the loss of configurational free energy in an open space. Whereas, for the smaller f, we observe that there exists a strong relationship between the mean radius of gyration and functionality during the polymer's free diffusion. Also, we have observed a good scaling law of polymer dimension $R \sim f^{1/2}(f^{-1/2}N)^{\nu}$, where $\nu = 0.6$ in a 3D simulation. These simulation results signified a good agreement with the current analytical prediction. On the other hand, for star polymers translocation dynamics, we explored the effect of star's functionality, coefficient of friction, temperature, and mass of the polymer as well on the translocation time. The influence of star functionality displayed a non-monotonic dependence on the mean translocation time. Additionally, the probability distribution of the mean exit time along with the given functionalities provides a Gaussian distribution for smaller f with a narrower width and symmetric form. However, for higher f, the distribution of mean

exit time displays a broader and asymmetric form with a long tail. We also revealed that the peak values of the probability distribution of the mean exit times are much closer to those obtained for mean translocation time $\langle\tau\rangle$. Concerning the coefficient of frictional force, we observed a gradual increase in the mean exit time for the given values of ξ, which corresponds to above $\xi = 5$. While below $\xi = 5$, the mean escape time showed a weak dependence on the coefficient of friction. We have also examined how $\langle\tau\rangle$ depends on the temperature, indicating that the translocation time decreases as the temperature increases up to $T = 1.0$ while at $T > 1.0$, the mean exit time is independent of the temperature. Moreover, the power-law dependence of the mean exit time on the total polymer mass was observed, depending on the functionality f and a nanopore radius r. Using the log-log curve fitting and for the values of f and r under consideration, the Flory scaling exponent is close to $\nu = 0.6$, which nearly agrees with the analytical argument. At $r = 2.3$ with a given N, the mean escape time first decreases as the functionality increases until the minimum point and then $\langle\tau\rangle$ increases with f, which causes an increase in the resistance to enter the nanometric pore due to a more powerful inter-arms interaction. As the nanopore radius increases ($r = 3.2$), the translocation time decreases monotonically with f. This idea is because the resistance of the arms to enter the pore gets weaker as a nanopore can hold all the arms at the same time.

Next, we have performed a 3D Langevin dynamics simulation to study the dynamics of multiple arms homogeneous star polymer translocation into a circular nanochannel. The translocation process is driven by a localized end-pulled force, in which it is acted on the first monomer. The influence of channel length and the functionality of star polymers as well on the translocation time was focused. Besides, we have examined various factors that affect the translocation dynamics such as the total polymer mass, the magnitude of the pulling force, a nanopore diameter, and the translocation velocity. We observed that increasing the channel length at a fixed nanopore diameter increases the mean escape time across the channel. Both the total polymer mass and a pulling force also play a vital role

in translocation dynamics. In the given intervals of channel length, the chain size N and the driving force F displayed the power-law dependence on τ as $\tau \sim N^2$ and $\tau \sim F^{-1}$, respectively. These results confirmed that under the constraint of the plane wall for a nano-scaled pore of limited diameter and different channel length, it is much simpler for the branched-chain to become fully tightened and hence retains the scaling behavior. On the other hand, the distribution profile of the exit times was broader for longer f and had a long tail for smaller f. We also verified that the mean average escape time and the most probable time scales were almost similar, indicating that the mean translocation time was well stated. The effect of the star's functionality on the mean escape time showed a non-monotonic dependence. Also, the minimum point was noticed whereby the pulling force and the entropic barrier of the system attain a state of balance. However, τ is highly sensitive to the lower limit nanopore diameter and the higher functionality; this is corresponding to the cutoff functionality to be recognized, which seizes the central role on the entire translocation dynamics that the polymer translocation is prohibited. Regarding the dependence of chain size on the translocation velocity v, we found a scaling relationship between v and N in a regime of strong pulling force as $v \sim N^{-1}$ (in the logarithmic scale). Consequently, in the limit of longer polymers, there was a high density of segments near the pore exit that retarded the translocation process, noting that the rate change of chain conformation was significantly slow.

Finally, we have studied star polymers translocation out of a cylindrical cavity under a constant pulling force using a Langevin dynamics simulation. By this reference, we examined the influence of star's functionality, a nanopore radius, polymer chain size, the magnitude of the pulling force as well as the confining geometry agents (such as cavity length and aspect ratio) on the translocation time. Here we have focused on the dependence of the translocation time on the functionality of the star polymers. We could also take into account the nanopore radius that allows us to describe the translocation dynamics for polymer molecules of the same size. We found that the strong non-monotonic

dependence of mean escape time on the functionality of star polymer for the given N, corresponding to the wider range of star's functionality. Remarkably, mean exit time decreases as the functionality increases until it reaches the critical value. Above f_c, the exit time increases with f. These results provide a fundamental promotion in understanding the structural effects on star polymers. For the multiple arms of star-shaped polymers, various conformations are observed; the rate of translocation is significantly faster in star's conformation with lower backward arms than the higher ones. We also proved that the mean exit time of the polymer approaches to the mean exit time of the trailing arms as the functionality increases, that is, $\langle\tau_b\rangle/\langle\tau\rangle \longrightarrow 1$. Besides, the probability distributions of mean exit time would distinguish between star polymers of varying functionalities. We also verified that the mean translocation time that associates with the total number of monomers as $\tau \sim N^2$, for the given intervals of nanopore radius in the regime of a strong driving force. Furthermore, a slower rate of translocation was observed as the chain propagates through a narrower nanopore. Our result of average translocation time in terms of the magnitude of the pulling force obeyed the scaling behavior $\tau \sim F^{-1}$. The above scaling laws suggested the fact that the mean translocation time behaves like $\tau \sim N^2/F$. Additionally, we examined the non-monotonic dependence of translocation time on both cavity dimensions and aspect ratio. As noted, there was a reduction of mean translocation time due to the squeezing of cavity length at a constant tube diameter, leading to faster translocation. Likewise, the exit time was reduced in the lowest cylindrical cavity volume. Also, there was overlying in the mean escape times at the critical value of aspect ratio ($a^* = 0.5$) for the given intervals of confinement volumes.

8.3 Future outlook

Future work on this project should include a field-driven translocation of multiple arms star polymer through a nanopore using in 2D and 3D Monte Carlo simulation by

considering the influence of constraints geometrical factors (such as pore radius and pore thickness), electric field, functionality, spring constant and total chain mass upon the translocation dynamics. It is conceivable that star polymers with arm lengths of the order of hundreds could be simulated by using such a simulation approach. Additionally, the simulation results could be compared with the one that has already been used in this dissertation, the so-called Langevin dynamics simulation. Further to the multiple arms of star polymer using Langevin dynamics simulation, future work could include the influence of translocation dynamics using a spherical confining cavity with many extended arms where the total number of monomers of the chain is kept constant. Thus, the results could be compared with the one that we found for a cylindrical cavity. In addition, the conformation-dependent forced translocation of the star-shaped polymer through a nanopore as well as a nanochannel could be performed using the Langevin dynamics approach. Moreover, a possible avenue for further investigation is to examine the dependence of the translocation dynamics upon the tube dimensions by extending a smaller number of arms to a larger set of functionalities.

Bibliography

[1] Aloorkar *et al. Star Polymers: An Overview.* International Journal of Pharmaceutical Sciences and Nanotechnology, **5**:1675–1684 (2012).

[2] Jing M. Ren, *et al. Star Polymers.* Chem. Rev., **116**:6743–6836 (2016).

[3] Bhagath GP. *et al. Star Polymers: An Overview.* International Journal of Biological and Pharmaceutical Researchs, **4**:76–79 (2013).

[4] Grzegorz Lapienis. *Star-shaped Polymers having Polyethylene Oxide Arms.* Progress in Polymer Science, **34**:852–892 (2009).

[5] C.Branca *et al. Star Polymer/Water Solutions: New Experimental Findings.* Condensed Matter Physics, **5**:275–284 (2002).

[6] Junfang Wang *et al. Dynamics of Polymer Translocation through Kinked Nanopores.* J. Chem. Phys., **142**:084901 (2015).

[7] Ramesh Adhikari and Aniket Bhattacharya. *Driven Translocation of a Semiflexible Chain through a Nanopore: A Brownian Dynamics Simulation Study in Two Dimensions.* J. Chem. Phys., **138**:204909 (2013).

[8] Elena Slonkina *et al. Polymer Translocation through a Long Nanopore.* J. Chem. Phys., **118**:7112–7118 (2003).

[9] Stanislav Kotsev *et al. Effect of Orientation in Translocation of Polymers through Nanopores.* J. Chem. Phys., **125**:084906 (2006).

[10] Huopaniemi *et al. Langevin Dynamics Simulations of Polymer Translocation through Nanopores.* J. Chem. Phys., **125**:124901 (2006).

[11] Ilkka Huopaniemi *et al. Polymer Translocation through a Nanopore under a Pulling Force.* Physical Review E, **75**:061912 (2007).

[12] S.T.T. Ollila *et al. Polymer Translocation in a Double-force Arrangement.* Eur. Phys. J. E, **28**:385–393 (2009).

[13] Clement Chatelain *et al. Probability Distributions for Polymer Translocation.* Physical Review E, **78**:021129 (2008).

[14] K. Luo *et al. Driven Polymer Translocation through Nanopores: Slow-vs.-Fast Dynamics.* A Letters Journal Exploring the Frontiers of Physics, **88**:68006 (2009).

[15] Kaifu Luo and Ralf Metzler. *The Chain Sucker: Translocation Dynamics of a Polymer Chain into a Long Narrow Channel Driven by Longitudinal Flow.* J. Chem. Phys., **134**:135102 (2011).

[16] Zhu Liu *et al. Conformation-dependent Translocation of a Star Polymer through a Nanochannel.* Biomicrofluidics, **8**:054107 (2014).

[17] H. H. Katkar and M. Muthukumar. *Single Molecule Electrophoresis of Star Polymers through Nanopores: Simulations.* J. Chem. Phys., **149**:163306 (2018).

[18] H. Ge *et al. How does a Star Chain (Nanooctopus) Crawl through a Nanopore?.* Polymer Chem., **2**:1071–1076 (2011).

[19] David Sean *et al. Translocation of a Polymer through a Nanopore Starting from a Confining Nanotube.* Electrophoresis, **36**:682–691 (2015).

[20] W. Reisner *et al. Statics and Dynamics of Single DNA Molecules Confined in Nanochannels.* Phys. Rev. Lett., **94**:196101 (2005).

[21] M. Muthukumar. *Polymer Escape through a Nanopore.* J. Chem. Phys., **118**:5174 (2003).

[22] M. Muthukumar. *Translocation of a Confined Polymer through a Hole.* Phys. Rev. Lett., **86**:3188 (2001).

[23] W. Reisner, J. Pedersen and R. Austin. *DNA Confinement in Nanochannels: Physics and Biological Applications.* Rep. Prog. Phys., **75**:106601 (2012).

[24] E. Luijten and A. Cacciuto. *Translocation of polymers out of confined geometries.* Comp. Phys. Comm., **177**:150 (2007).

[25] M. Alizadehheidari *et al. Nanoconfined Circular and Linear DNA: Equilibrium Conformations and Unfolding Kinetics.* Macromolecules, **48**:871–878 (2015).

[26] R. Metzler and K. Luo. *Polymer Translocation through Nanopores: Parking lot Problems, Scaling Laws and their Breakdown.* Eur. Phys. J. Special Topics, **189**:119–134 (2010).

[27] Wong and Muthukumar. *Scaling Theory of Polymer Translocation into Confined Regions.* Biophysical Journal, **95**:3619–3627 (2008).

[28] Jalal Sarabadani *et al. Dynamics of End-pulled Polymer Translocation through a Nanopore.* A Letters Journal Exploring the Frontiers of Physics, **120**:38004 (2017).

[29] Huopaniemi *et al. Polymer Translocation through a Nanopore under a Pulling Force.* Physical Review E, **75**:061912 (2007).

[30] H.J. Limbach *et al. ESPResSo -an Extensible Simulation Package for Research on Soft Matter Systems.* Computer Physics Communications, **174**:704–727 (2006).

[31] Hima Bindu Kolli and K.P.N.Murthy. *Phase Transition in a Bond Fluctuating Lattice Polymer.* arXiv:1204.2691v2 (2012).

[32] Rubinstein, M. and Colby, R. *Polymer Physics.* Oxford University Press (2003). ISBN 9781613449431.

[33] David I. Bower. *An Introduction to Polymer Physics.* Cambridge University Press (2002). ISBN 9780521631372.

[34] H. Gao and K. Matyjaszewski. *Synthesis of Functional Polymers with Controlled Architecture by CRP of Monomers in the Presence of Rross-linkers: From Stars to Gels.* Progress in Polymer Science , **34**:317–350 (2009).

[35] Christopher Barner-Kowollik *et al. Synthesis of Star Polymers using RAFT Polymerization: What is Possible?.* Aust. J. Chem., **59**:719–727 (2006).

[36] Teraoka, I. *Polymer Solutions: An Introduction to Physical Properties.* Wiley (2002). ISBN 9780471389293.

[37] Flory *et al. Synthesis of Multichain Polymers and Investigation of their Viscosities.* J. Am. Chem. Soc., **241**:2709–2718 (1948).

[38] Morton *et al. Preparation and Properties of Monodisperse Branched Polystyrene.* Journal of Polymer Science Part A: Polymer Chemistry, **57**:471–482 (1962).

[39] Wenger *et al. Dilute Solution Properties of Branched Polymers. Polystyrene Trifunctional Star Molecules.* The Journal of Physical Chemistry, **67**:566–575 (1963).

[40] Mayer *et al. Organized Structures in Amorphous Styrene/cw-1,4-Isoprene Block Copolymers: Low Angle X-ray Scattering and Electron Microscopy.* Polymer, **15**:137–145 (1974).

[41] D. Decker and P. Rempp. *Star and Hyperbranched Polymers.* CR Acad Sci, **261**:1965 (1977).

[42] R. Milkovich and P. J. Flory. *Polymers.* Polymer Letters, **3**:71–79 (1965).

[43] E. Helmut and B. Walther. *Star Polymers from Styrene and Divinylbenzene.* Polymer, **16**:180–184 (1975).

[44] Zelinski *et al. Synthesis of Trichain and Tetrachain Radial Polybutadienes.* Journal of Polymer Science: Part A, **3**:93–103 (1965).

[45] Sunil P. Singh *et al. Hydrodynamic Correlations and Diffusion Coefficient of Star Polymers in Solution.* J. Chem. Phys., **141**:084901 (2014).

[46] Alexandros Chremos *et al. Adsorption of Star Polymers: Computer Simulations.* Soft Matter, **6**:1483–1493 (2010).

[47] K. Solc and W. H. Stockmayer. *Shape of a Random-Flight Chain.* J. Chem. Phys., **54**:2756–2757 (1971).

[48] M. Daoud and J. P. Cotton. *Star Shaped Polymers: A model for the Conformation and its Concentration Dependence.* J. Phys. (France), **43**:531–538 (1982).

[49] T. M. Birshtein and E. B. Zhulina. *Conformations of Sar-branched Macromolecules.* Polymer, **25**:1453–1461 (1984).

[50] T. M. Birshtein *et al. Temperature-concentration Diagram for a Solution of Star-branched Macromolecules.* Polymer, **27**:1078–1086 (1986).

[51] Sioula *et al. Direct Evidence for Confinement of Junctionsto Lines in an 3-miktoarm Star Terpolymer Microdomain Structure.* Macromolecules, **31**:8429-8432 (1998).

[52] Jingquan Liu *et al. An Approach to Biodegradable Star Polymeric Architectures using Disulfide Coupling.* Chem. Commun., **10**:6582–6584 (2008).

[53] D. Vlassopoulos *et al. Ordering and Viscoelastic Relaxation in Multiarm Star Polymer Melts.* Europhys. Lett., **39**:617–622 (1997).

[54] G. Foffi *et al. Structural Arrest in Dense Star-Polymer Solutions.* Phys. Rev. Lett., **90**:238301 (2003).

[55] G. Haifeng and M. Krzysztof. *Synthesis of Low-Polydispersity Miktoarm Star Copolymers via a Simple "Arm-First " Method: Macromonomers as Arm Precursors.* Macromolecules, **41**:4250–4257 (2008).

[56] Andreas Heise *et al. Star Polymers with Alternating Arms from Miktofunctional μ-Initiators Using Consecutive Atom Transfer Radical Polymerization and Ring-Opening Polymerization.* Macromolecules, **34**:2798–2804 (2001).

[57] G. Haifeng and M. Krzysztof. *Synthesis of Star Polymers by a Combination of ATRP and the "Click " Coupling Method.* Macromolecules, **39**:4960–4965 (2006).

[58] Shchetnikava *et al. A Comparison of Tube Model Predictions of the Linear Viscoelastic Behavior of Symmetric Star Polymer Melts.* Macromolecules, **47**:3350–3361 (2014).

[59] Goh *et al. Synthesis and Characterization of Core Cross-Linked Star Clusters by Conventional Free-Radical Polymerization.* Macromolecules, **40**:7819–7826 (2007).

[60] Park *et al. Morphology and Microphase Separation of Star Copolymers.* J. Polym. Sci., Part B: Polym. Phys., **53**:1–21 (2015).

[61] Matsushita *et al. Morphologies from Abc Star-Shaped Terpolymers.* J. Phys.: Condens. Matter, **23**:284111 (2011).

[62] Li *et al. Peo-Based Star Copolymers as Stabilizers for Water-in-Oil or Oil-in-Water Emulsions.* Macromolecules, **45**:9419–9426 (2012).

[63] Binks *et al. Emulsions Stabilized by Monodisperse Latex Particles: Effects of Particle Size.* Langmuir, **17**:4540–4547 (2001).

[64] Grigsby *et al. Balancing Protection and Release of DNA: Tools to Address a Bottleneck of Non-Viral Gene Delivery.* J. R. Soc., Interface (Suppl 1), **7**:S67–S82 (2010).

[65] Payne and C. K. *Imaging Gene Delivery with Fluorescence Microscopy.* Nanomedicine, **2**:847–860 (2007).

[66] Georgiou *et al. Nanoscopic Cationic Methacrylate Star Homopolymers: Synthesis by Group Transfer Polymerization, Characterization and Evaluation as Transfection Reagents.* Biomacromolecules, **5**:2221–2229 (2004).

[67] Han *et al. Development of Biomaterials for Gene Therapy.* Mol. Ther., **2**302–317 (2000).

[68] Torchilin and V. P. *Micellar Nanocarriers: Pharmaceutical Perspectives.* Pharm. Res., **24**:1–16 (2006).

[69] Wang *et al. Approaches for the Preparation of Non-Linear Amphiphilic Polymers and Their Applications to Drug Delivery.* Adv. Drug Delivery Rev., **64**:852–865 (2012).

[70] Liu *et al. Synthesis of Functional Core, Star Polymers Via Raft Polymerization for Drug Delivery Applications.* Macromol. Rapid Commun., **33**:760–766 (2012).

[71] Khor *et al. The Pharmacokinetics and Biodistribution of a 64 Kda Polypeg Star Polymer after Subcutaneous and Pulmonary Administration to Rats.* J. Pharm. Sci., **105**:293–300 (2016).

[72] Adkins *et al. High Relaxivity Mri Imaging Reagents from Bimodal Star Polymers.* Polym. Chem., **3**:390–398 (2012).

[73] G. Allegra, E. Colombo, and F. Ganazzoli. *Linear and regular star polymer in a good solvent.* Macromolecules, **26**:330 (1993).

[74] A. Miyake and K. F. Freed *Excluded Volume in Star Polymers: Chain Conformation Space Renormalization Group.* Macromolecules, **16**:1228 (1983).

[75] A.Y. Grosberg and A.R. Khokhlov. *Statistical Physics of Macromolecules.* AIP Press, 1994.

[76] J. Paturej *et al. Star polymers Confined in a Nanoslit: A Simulation Test of Scaling and Self-Consistent Field Theories.* Soft Matter, **9**: 10522–10531 (2013).

[77] Debabrata Panja and Gerard T. Barkema. *Rouse Modes of Self-avoiding Flexible Polymers.* J. Chem. Phys., **13**:154903 (2009).

[78] Rick Keesman *et al. Dynamical Eigenmodes of Star and Tadpole Polymers.* arXiv:1210.0774v2 (2013).

[79] S. Brown and G. Szamel. *Computer Simulation of Three-arm Star Polymers.* Macromol. Theory Simul., **9**:1419 (2000).

[80] Johan T. Padding. *Theory of Polymer Dynamics.* Cambridge University Press (2005).

[81] Kehong Zhang and Kaifu Luo. *Polymer Translocation into a Confined Space: Influence of the Chain Stiffness and the Shape of the Confinement.* J. Chem. Phys., **140**:094902 (2014).

[82] Pu, Jiang, and Hou. *Polymer Translocation through Nanopore into Active Bath.* J. Chem. Phys., **145**:174902 (2016).

[83] David Sean and Gary W. Slater. *Highly Driven Polymer Translocation from a Cylindrical Cavity with a Finite Length.* University of Ottawa (2016).

[84] David Sean, Hendrick W. de Haan and Gary W. Slater. *Translocation of a Polymer through a Nanopore Starting from a Confining Nanotube.* Electrophoresis, **36**:682–691 (2015).

[85] P. G. Kadam and S. Mhaske. *Synthesis of Star-Shaped Polymers.* Des. Monomers Polym., **14**:515–540 (2011).

[86] J. Sabli, M. Praprotnik and R. Delgado-Buscalioni. *Deciphering the Dynamics of Star Molecules in Shear Flow.* Soft Matter, **13**:4971–4987 (2017).

[87] J. M. Ren *et al. Star Polymers.* Chem. Rev., **116**:6743–6836 (2016).

[88] Karthik Nagarajan and Shing Bor Chen. *Flow-Induced Translocation of Star Polymers through a Nanopore.* J. Phys. Chem. B, **123**:7919–7925 (2019).

[89] M. Muthukumar, C. Plesa, and C. Dekker. *Single-molecule Sensing with Nanopores.* Physics Today, **68**:40–46 (2015).

[90] S. M. Bezrukov, I. Vodyanoy, and V. A. Parsegian. *Counting Polymers Moving through a Single Ion Channel.* Nature, **370**:279–281 (1994).

[91] A. Meller *et al. Rapid Nanopore Discrimination Between Single Polynucleotide Molecules.* Porc. Natl. Acad. Sci. U.S.A., **97**:1079–1084 (2000).

[92] M. Wanunu. *Nanopores: A journey towards DNA Sequencing.* Physics of Life Reviews, **9**:125–158 (2012).

[93] L. Song *et al. Structure of Staphylococcal* $\alpha-$*hemolysin, a Heptameric Transmembrane Pore.* Science, **274**:1859–1865 (1996).

[94] Vladimir V. *et al. Polymer Translocation: The First Two Decades and the Recent Diversification.* Soft Matter, **10**:9016 (2014).

[95] M. Faller, M. Niederweis, and G. E. Schulz. *The Structure of a Mycobacterial Outer-membrane Channel.* Science, **303**:1189–1192 (2004).

[96] J. Li *et al. DNA Molecules and Configurations in a Solid-state Nanopore Microscope.* Nat. Materials, **2**:611$\alpha-$615 (2003).

[97] Golovchenko *et al. Ion-beam Sculpting at Nanometer Length Scales.* Nature, **412**:166–169 (2001).

[98] A. R. Hall *et al. Hybrid Pore Formation by Directed Insertion of $\alpha-$haemolysin into Solid-state Nanopores.* Nature Nanotech., **5**:874$\alpha-$877 (2010).

[99] T. Gilboa and A. Meller. *Optical Sensing and Analyte Manipulation in Solid-state Nanopores.* Analyst (2015).

[100] Timothe Menais *.Polymer Translocation under a Pulling Force: Scaling Arguments and Threshold Forces.* Physicsl Review E, **97**:022501 (2018).

[101] Takahiro Sakaue. *Dynamics of Polymer Translocation: A Short Review with an Introduction of Weakly-Driven Regime.* Polymers, **8**:424 (2016).

[102] Timothe Menais *et al. Polymer Translocation through Nano-pores in Vibrating Thin Membranes.* Scientific Reports, **6**:38558 (2016).

[103] Murugappan Muthukumar. *Mechanism of DNA Transport Through Pores.* Annu. Rev. Biophys. Biomol. Struct., **36**:435–450 (2007).

[104] Yacov Kantor and Mehran Kardar. *Anomalous Dynamics of Forced Translocation.* Phys. Rev. E, **69**:021806 (2004).

[105] Alberts *et al. Molecular Biology of the Cell.* 4 ed. Garland Science (2002).

[106] D. Panja and I. J. Molineux. *Dynamics of Bacteriophage Genome Ejection.* Phys. Biol., **7**:045006 (2010).

[107] K. Luo *et al. Adsorption and Self-assembly of Linear Polymers on Smooth Surfaces.* Soft Matter Phys., **80**:021907 (2009).

[108] J. Shenga and K. Luo. *Ejection Dynamics of a Ring Polymer out of a Nanochannel.* Soft Matter, **8**:367–374 2012.

[109] I. Ali, D. Marenduzzo and J. M. Yeomans. *Polymer Packaging and Ejection in Viral Capsids: Shape Matters.* Phys. Rev. Lett., **96**:208102 (2006).

[110] T. S. Baker, N. H. Olson and S. D. Fuller. *Adding the Third Dimension to Virus Life Cycles: 3D Reconstruction of Icosahedral Viruses from Cryo-electron Micrographs.* Microbiol. Mol. Biol. Rev., **63**862–922 (1999).

[111] Viovy, J. L. *Electrophoresis of DNA and other Polyelectrolytes: Physical Mechanisms.* Rev. Mod. Phys., **72**:813–872 (2000).

[112] J. Han *et al. Entropic Trapping and Escape of Long DNA Molecules at Submicron Size Constriction.* Phys. Rev. Lett., **83**:1688–1691 (1999).

[113] D. Stein *et al. Pressure-driven Transport of Confined DNA Polymers in Fluidic Channels.* Proc. Natl. Acad. Sci. U. S. A., **103**:15853–15858 (2006).

[114] L. Q. Gu *et al. Prolonged Residence Time of a Noncovalent Molecular Adapter, Beta-cyclodextrin, within the Lumen of Mutant α-hemolysin Pores.* J. Gen. Physiol., **118**:481–493 (2001).

[115] K. Zhang and K. Luo. *Dynamics of Polymer Translocation into a Circular Nanocontainer through a Nanopore.* J. Chem. Phys., **136**:185103 (2012).

[116] K. Zhang and K. Luo. *Dynamics of Polymer Translocation into an Anisotropic Confinement.* Soft Matter, **9**:2069–2075 (2013).

[117] S. M. Simon, C. S. Peskin and G. F. Oster. *What drives the Translocation of Proteins?.* Proc. Natl. Acad. Sci. U. S. A., **89**:3770–3774 (1992).

[118] S. M. Bezrukov *Ounting Polymers Moving through a Single Ion Channel.* Nature, **370**:279–281 (1994).

[119] Kasianowicz *et al. Characterization of Individual Polynucleotide Molecules using a Membrane Channel.* Proceedings of the National Academy of Sciences, **93**:13770–13773 (1996).

[120] J. Li *et al. DNA Molecules and Configurations in a Solid-state Nanopore Microscope.* Nat. Materials, **2**:611–615 (2003).

[121] A. Storm *et al. Fast DNA Translocation through a Solid-state Nanopore.* Nanoletters, **5**:1193–1197 (2005).

[122] U. F. Keyser *et al. Direct Force Measurements on DNA in a Solid-state Nanopore.* Nature, **2**473–477 (2006).

[123] M. M. Mohammad *et al. Controlling a Single Protein in a Nanopore through Electrostatic Traps.* J. Ame. Chem. Soc., **130**:4081–4088 (2008).

[124] D. Pedone *et al. Fabrication and Electrical Characterization of a Porecavitypore Device.* J. Phys. Condens. Matter, **22**:454115 (2010).

[125] A. R. Hall *et al. Hybrid Pore Formation by Directed Insertion of α-haemolysin into Solid-state Nanopores.* Nature Nanotech., **5**:874–877 (2010).

[126] W. Guo *et al. Target Specific 3D DNA Gatekeepers for Biomimetic Nanopores.* Advanced Materials, **27**:2090–2095 (2015).

[127] H. Ge, S. Pispas, and C. Wu. *How Does a Star Chain (Nanooctopus) Crawl through a Nanopore.* Polym. Chem., **2**:1071–1076 (2011).

[128] W. Sung and P. Park. *Polymer Translocation through a Pore in a Membrane.* Phys. Rev. Lett., **77**:783–786 (1996).

[129] M. Muthukumar. *Polymer Translocation through a Hole.* J. Chem. Phys., **111**:10371–10374 (1999).

[130] J. Chuang, Y. Kantor, and M. Kardar. *Anomalous Dynamics of Translocation.* Phys. Rev. E, **65**011802 (2002).

[131] Pai-Yi Hsiao. *Polyelectrolyte Threading through a Nanopore.* Polymers, **8**:73 (2016).

[132] Wei *et al. Unforced Translocation of a Polymer Chain through a Nanopore: The Solvent Effect.* J. Chem. Phys., **126**:204901 (2007).

[133] Debabrata Panja and Gerard T. Barkema. *Passage Times for Polymer Translocation Pulled through a Narrow Pore.* Biophysical Journal, **94**:1630–1637 (2008).

[134] Ilkka Huopaniemi *et al. Polymer Translocation through a Nanopore under a Pulling Force.* Phys. Rev. E, **75**:061912 (2007).

[135] Karthik Nagarajan and Shing Bor Chen. *Flow-Induced Translocation of Star Polymers through a Nanopore.* J. Phys. Chem. B, textbf123:7919–7925 (2019).

[136] Ryan Bradley and Ravi Radhakrishnan. *Coarse-Grained Models for Protein-Cell Membrane Interactions.* Polymers, **5**:890–936 (2013).

[137] J. Baschnagel *et al. Monte Carlo Simulation of Polymers: Coarse-Grained Models.* Computational Soft Matter, **23**:83–140 (2004).

[138] E. W. Montroll. *Markoff Chains and Excluded Volume Effects in Polymer Chains* J. Chem. Phys., **18**:734 (1950).

[139] P. Grassberger. *Pruned-enriched Rosenbluth Method: Simulations of Polymers of Chain Length up to 1 000 000.* Phys. Rev. E, **56**:3682 (1997).

[140] P. H. Verdier and W. H. Stockmayer. *Monte Carlo Calculations on the Dynamics of Polymers in Dilute Solution.* J. Chem. Phys., **36**:227 (1962).

[141] I. Carmesin and K. Kremer. *The bond Fluctuation Method: A New Effective Algorithm for the Dynamics of Polymers in All Spatial Dimensions.* Macromolecules, **21**:2819 (1988).

[142] I. Carmesin and K. Kremer. *Static and Dynamic Properties of Two-dimensional Polymer Melts.* J. Phys. France, **51**:915 (1990).

[143] H. P. Deutsch and K. Binder. *Inter-diffusion and Self-diffusion in Polymer Mixtures: A Monte Carlo Study.* J. Chem. Phys., **94**:2294 (1991).

[144] I. Carmesin and K. Kremer. *The Bond Fluctuation Method: A New Effective Algorithm for the Dynamics of Polymers in All Spatial Dimensions.* Macromolecules, **21**:2819 (1988).

[145] K. Kremer and G. S. Grest. *Dynamics of Entangled Linear Polymer Melts: A molecular-dynamics Simulation.* J. Chem. Phys., **92**:5057 (1990).

[146] R. Keesman. *Dynamical Eigenmodes of Various Bead-spring Systems.* arXiv:1212.1024v1 (2013).

[147] Aniket Bhattacharya. *How Local Factors Affect the Exponents of Forced Polymer Translocation through a Nanopore.* Physics Procedia, **3**:1411–1416 (2010).

[148] A. Bhattacharya *et al. Scaling Exponents of Forced Polymer Translocation through a Nanopore.* Eur. Phys. J. E, **5**:10495 (2009).

[149] Kaifu Luo *et al. Translocation Dynamics with Attractive Nanopore-polymer Interactions.* Phys. Rev. E, **78**:061918 (2008).

[150] Wims Briels. *Theory of Polymer Dynamics.* Lecture note, 1998.

[151] J. Baschnagel, J. P. Wittmer, and H. Meyer. *Monte Carlo Simulation of Polymers: Coarse-Grained Models.* J. France, **6**:67083 (2004).

[152] Scott Brown and Grzegorz Szamel. *Computer Simulation of Three-arm Star Polymers.* Macromol. Theory Simul., **9**:14–19 (2000).

[153] Meng-Bo Luo, Dessalegne A Tsehay, and Li-Zhen Sun. *Temperature Dependence of the Translocation Time of Polymer through Repulsive Nanopores.* J. Chem Phys, **147**:034901 (2017).

DECLARATION

I hereby declare that this Ph.D. dissertation is my original work and has not been presented for a degree in any other university. All sources of material used for the Ph.D. dissertation have been duly acknowledged.

Name: **Mesay Tilahun Abebe**

Signature:– – – – – – – – – – – –

Place and time of submission: Addis Ababa University, November 2020

This Ph.D. dissertation has been submitted for examination with my approval as University advisor.

Name: **Dr. Tatek Yergou**

Signature:– – – – – – – – – ––